DEPARTMENT OF COMMERCE
SINCLAIR WEEKS, Secretary

WEATHER BUREAU
F. W. REICHELDERFER, Chief

MONTHLY WEATHER REVIEW

JAMES E. CASKEY, JR., Editor

Volume 84
Number 2

FEBRUARY 1956

Closed April 15, 1956
Issued May 15, 1956

AREAS OF HURRICANE DEVELOPMENT

GORDON E. DUNN

Weather Bureau Office, Miami, Fla.

[Manuscript received November 14, 1955; revised January 16, 1956]

The phrase "area of development" with respect to hurricane formation needs further definition. Obviously this area is not a point, yet the concept is meaningless if it is expanded to encompass the entire known existence of the wave prior to the attainment of hurricane intensity. Namias and C. Dunn [3] in discussing the formation of hurricane Connie (1955) state: "While hurricane Connie was first reported on August 4 at about 16.6°N. and 48.0° W., there is some indication that it developed off North Africa some time earlier." Connie was scouted thoroughly by hurricane reconnaissance planes and it is quite definite that it did not reach hurricane intensity until more than 1,700 miles west of the Cape Verdes. And Connie continued to develop in intensity for another 700 miles or more. Just where should it be said that this hurricane developed?

The hurricane tracks of Mitchell [1] and Tannehill [2] apparently were constructed by tracing each storm as far back as any evidence of circulation or strong winds could be found, although the criteria used by them are not fully described. In some cases the track apparently begins where a full-fledged hurricane was discovered and in others where ship reports merely indicated the existence of an unstable wave with mildly squally weather or somewhat abnormal winds.

It is not the purpose of this paper to define "area of development". However there is an arbitrary point in the development—where the tropical storm reaches hurricane intensity—that can be located within a reasonable degree of accuracy. It is believed this particular hurricane statistic may be of some value.

All hurricanes from 1901 to 1955 have been studied and the location where they attained hurricane intensity plotted, if sufficient information permitted reasonable accuracy. Considerable reliance has been placed on articles and other information appearing in the *Monthly Weather Review* during this period. With plane reconnaissance during the past decade, positions can usually be estimated very closely. Many tropical storms are first encountered by ships on the New York to Capetown route and frequently several ships may send in reports on the day of discovery. Inferences can be made from the lowest pressure, wind velocities, and wind shifts concerning the maturity and intensity of the storm and consequently the probable position where it reached hurricane intensity. In the area west of long. 60° W., it is believed the point where the tropical storm reaches hurricane intensity can be located accurately, within 150 miles, approximately 85 percent of the time. The area of greatest uncertainty is southeast of Bermuda. East of long. 60° W., the positions become more questionable as the data become scarcer. In this area, the errors have a bias and in almost all cases the position, if in error, should be farther to the east than plotted. Hurricane positions during the first decade and a half are less reliable than positions since 1915.

Of the 242 hurricanes from 1901–55 used in this study, approximately 40 developed in perturbations moving away from the intertropical convergence zone (ITC) in the Panama region, although almost all of the major developments occurred a considerable distance away from the ITC. Most of the remaining hurricanes (202) developed in easterly waves. The origin of easterly waves is obscure but some develop as a result of a fracture of polar troughs and many others enter our field of observations, which here in Miami begins in the vicinity of the Cape Verde Islands, from the east. It is evident that the great majority of the Atlantic hurricanes do not develop in the "doldrums",

379802—56——1

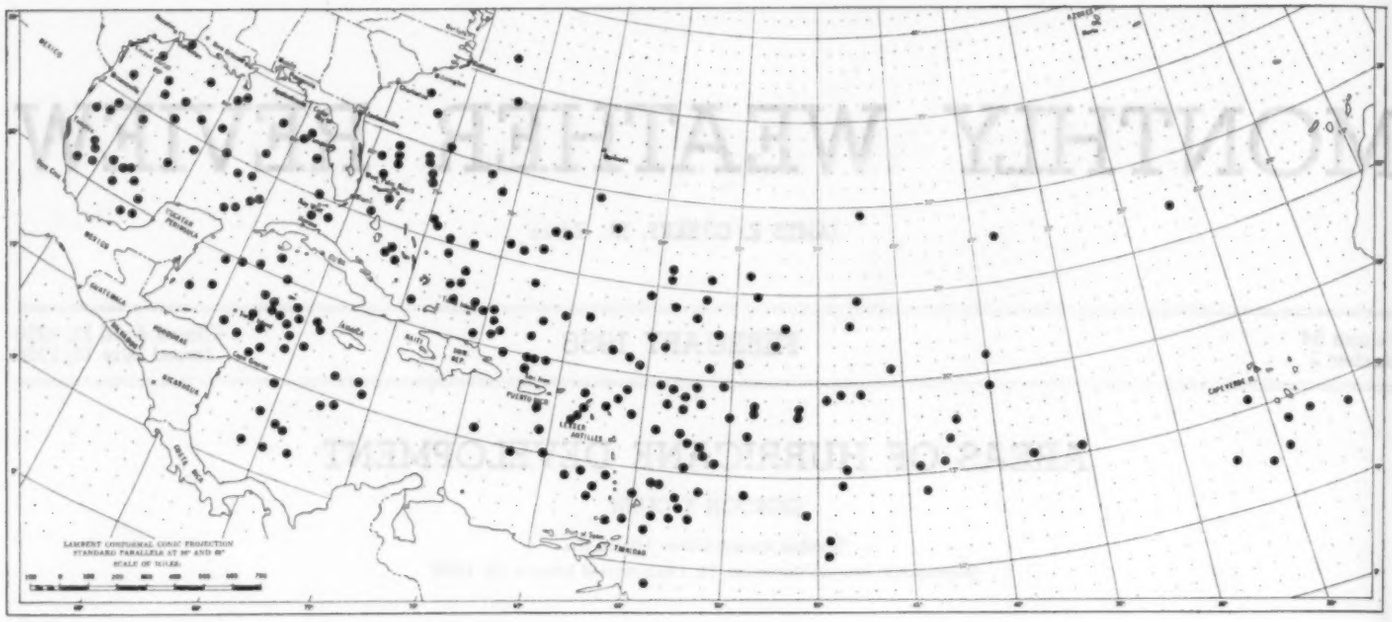

FIGURE 1.—Locations where tropical storms reached hurricane intensity, 1901–55.

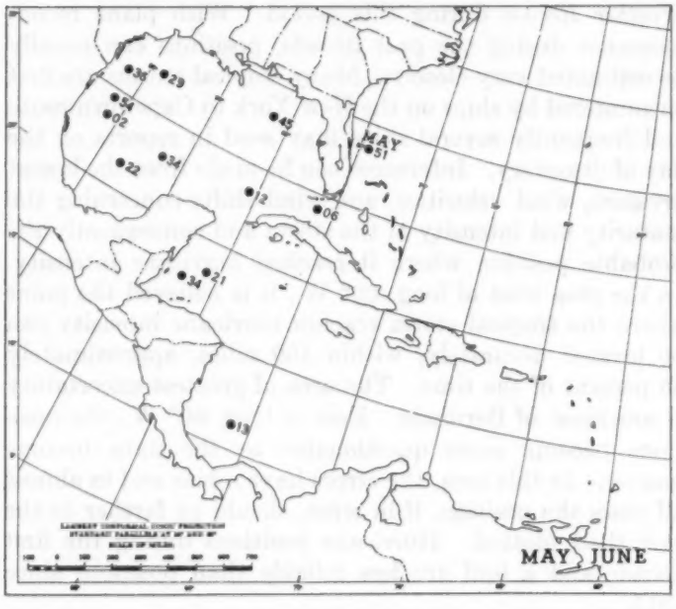

FIGURE 2.—Locations where tropical storms reached hurricane intensity, May and June, 1901–55. The two-digit number at each location indicates the year.

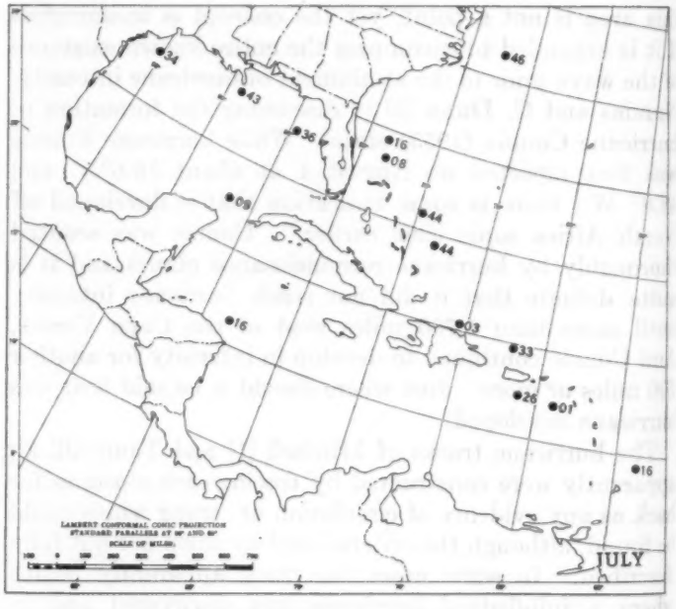

FIGURE 3.—Locations where tropical storms reached hurricane intensity, July, 1901–55. The two-digit number at each location indicates the year.

which to many of the earlier authors was synonymous with what is now termed the ITC, but rather in the trade wind current. Indeed a comparison of the areas of hurricane formation in the Atlantic with the Atlas of Climatic Charts of the Ocean [4] would indicate many of the tropical storms undergo their major and most rapid development in the region where the constancy and strength of the trades is the greatest and frequency of calms the least (fig. 4).

In the comparatively few cases where tropical storms reach full hurricane intensity in or near the ITC, development usually takes place slowly, sometimes requiring as long as 6 days from the time the wave can be described as unstable until it reaches hurricane intensity. On the other hand, intensification in easterly waves is more rapid, perhaps averaging about 3 days.

The positions where all 242 of the tropical cyclones are estimated or known to have reached hurricane intensity are plotted in figure 1. A concentration just to the east of Swan Island and another just to the east of the Leeward and Windward Islands can be noted. The only 5° squares west of long. 35° W. where none developed are the two between western Hispaniola and Venezuela. Mitchell [1]

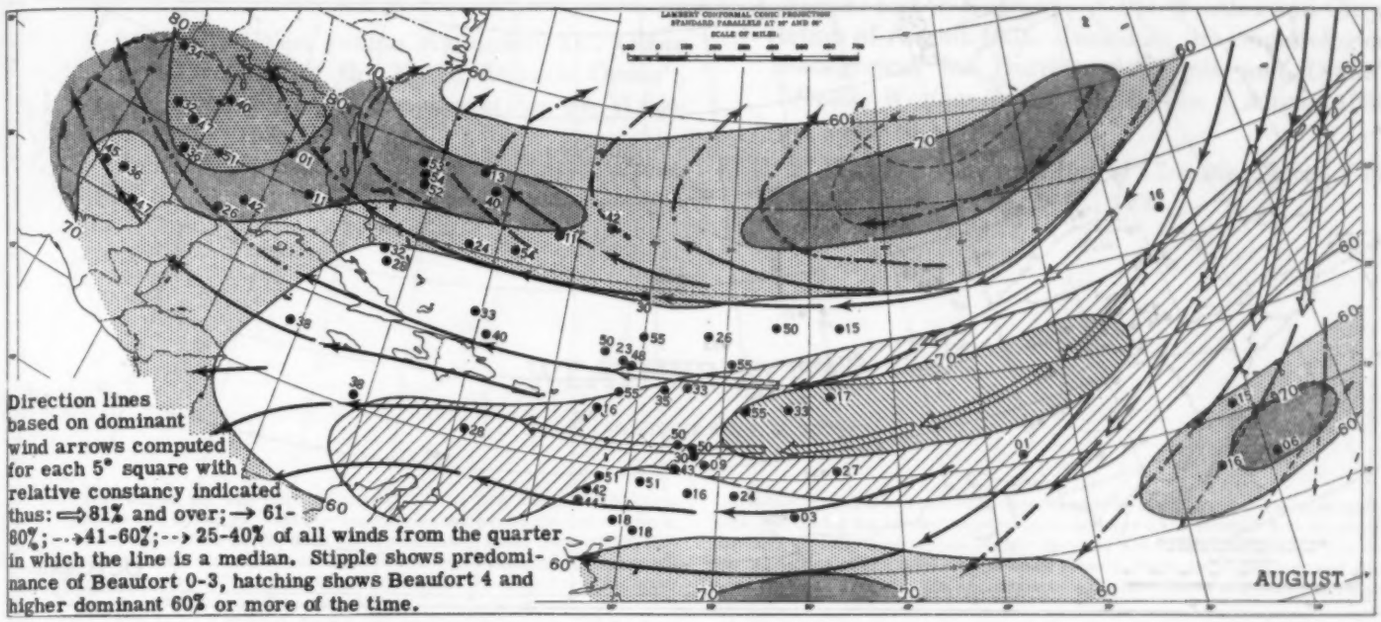
Direction lines based on dominant wind arrows computed for each 5° square with relative constancy indicated thus: ⟹81% and over; → 61-80%; -·→41-60%; --→ 25-40% of all winds from the quarter in which the line is a median. Stipple shows predominance of Beaufort 0-3, hatching shows Beaufort 4 and higher dominant 60% or more of the time.
AUGUST

FIGURE 4.—Locations where tropical storms reached hurricane intensity, August 1901–55. The two digit number at each location indicates the year. Predominant wind direction and constancy are indicated by the arrows and predominant wind force by the stippling (see explanation inset on chart).

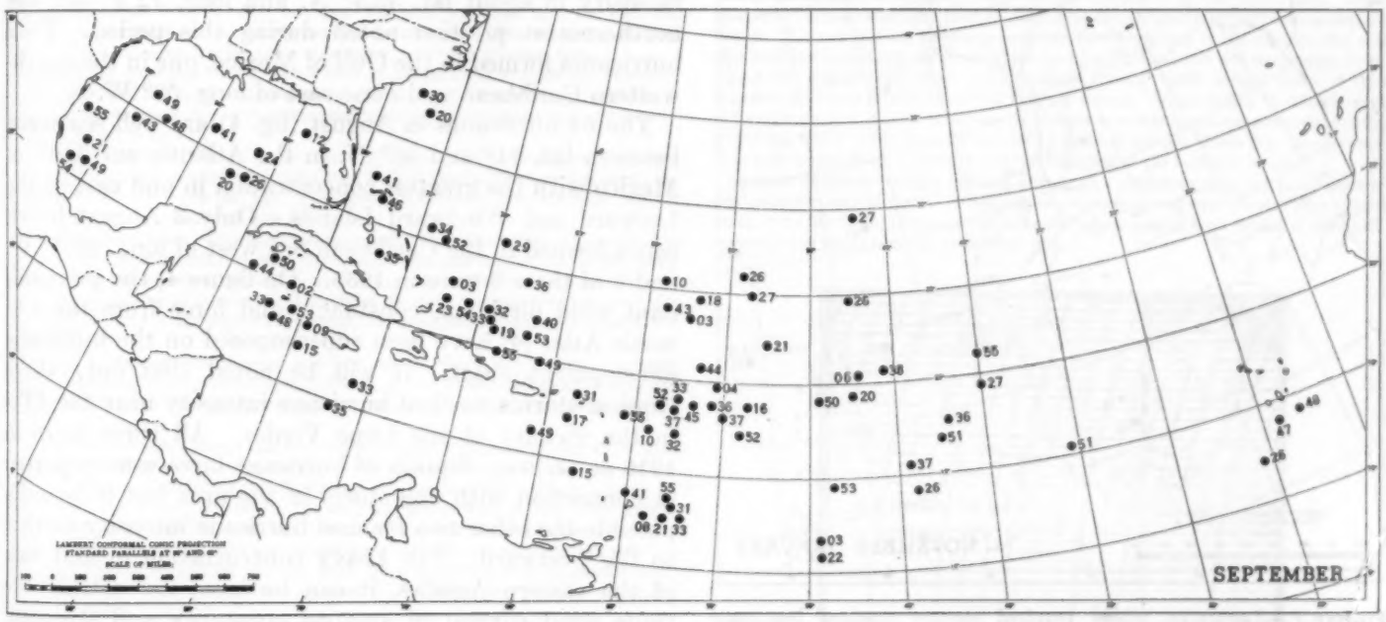

FIGURE 5.—Locations where tropical storms reached hurricane intensity, September, 1901–55. The two-digit number at each location indicates the year.

stated, "In every instance the *first evidence* of storm development, although rather obscure in some cases, was found either over the western third of the Caribbean Sea (west of long. 78° W.) or to the east of the eastern limits of the Caribbean Sea." This statement has been misquoted by others to the effect that hurricanes do not develop in the eastern and central portions of the Caribbean. Certainly comparatively few storms reach hurricane intensity in this area, particularly between longitudes 67° and 75°, perhaps due to the significant divergence in the lower tropospheric easterly flow as the easterly trade is diverted into the heat Low over the Amazon Valley. On the other hand, two recent severe hurricanes—Hazel 1954 and Janet 1955—attained great intensity in this area although both were comparatively weak hurricanes when they entered the Caribbean.

Seven hurricane developments have been placed in the Cape Verde area. These positions are largely based on the works of earlier investigators. In the majority of cases the evidence available to the author, indicated only that

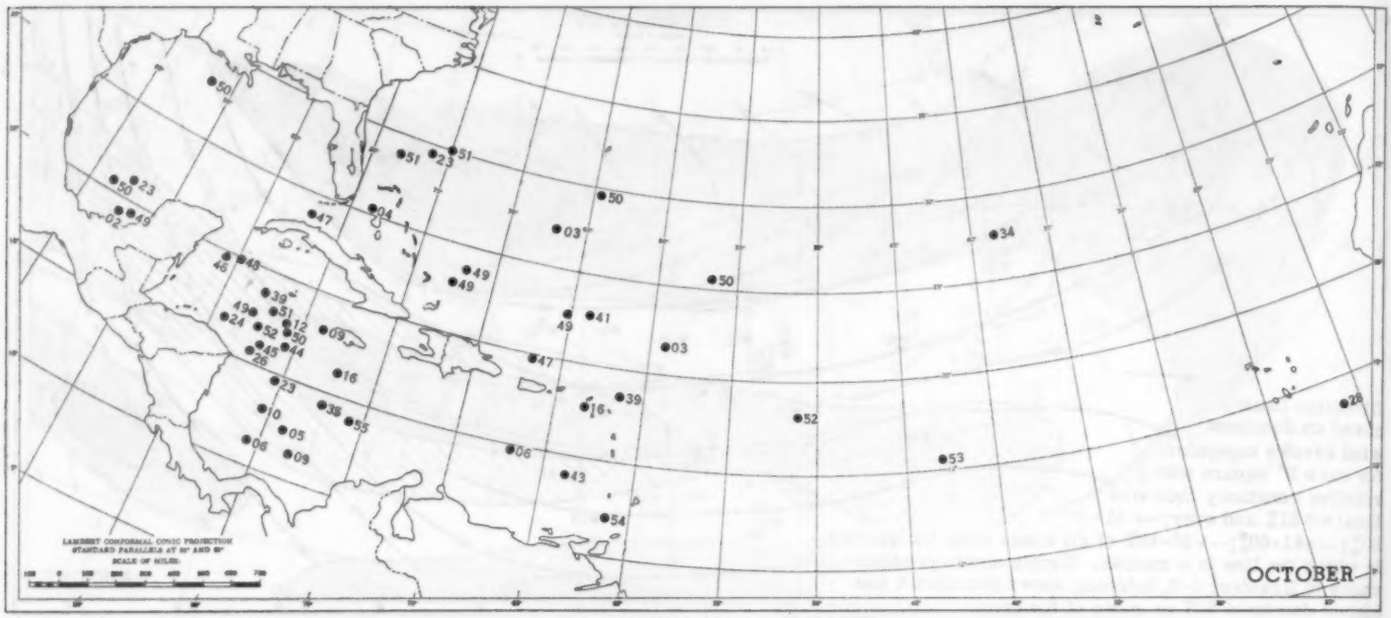

FIGURE 6.—Locations where tropical storms reached hurricane intensity, October, 1901–55. The two-digit number at each location indicates the year.

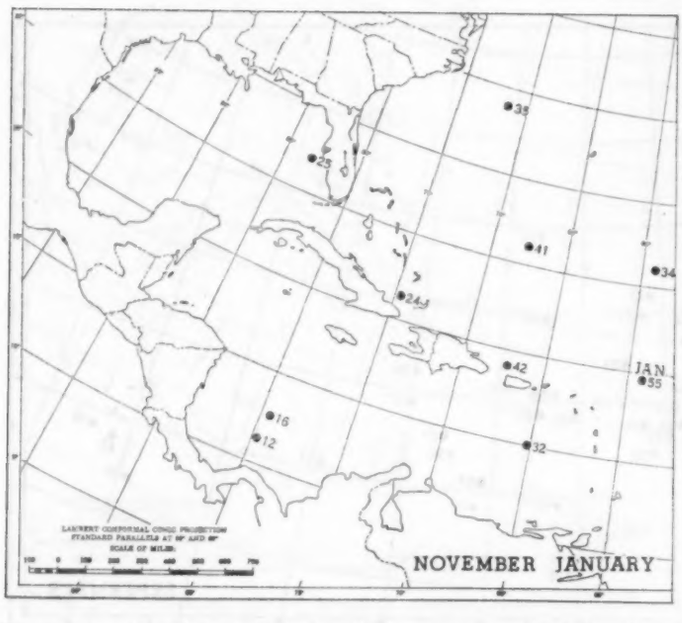

FIGURE 7.—Locations where tropical storms reached hurricane intensity, November and January, 1901–55. The two-digit number at each location indicates the year.

an unstable wave passed through the islands and that the hurricane intensity was actually reached some 10° to 15° to the westward.

The only May hurricane developed off the east coast of Florida (fig. 2). Hurricane formation in June (13 storms) (fig. 2) is confined to the extreme western Caribbean and Gulf of Mexico, as is well known.

July hurricane positions are plotted on figure 3. Nine of the 15 reached hurricane intensity along a narrow band from northeast of Barbados northwestward to a point off the Florida east coast. One in 1946 reached hurricane intensity in about lat. 36.5° N. and long. 72.5° W., the northernmost position noted during this period. Four hurricanes formed in the Gulf of Mexico, one in the northwestern Caribbean and none east of long. 58° W.

The 64 hurricanes in August (fig. 4) are well scattered between lat. 11° and 30° N. in the Atlantic and Gulf of Mexico with the greatest concentration in and east of the Leeward and Windward Islands. Only 3 August hurricanes formed in the Caribbean Sea west of long. 62.5° W. and 2 of these 3 were in 1938. On figure 4, the predominant wind direction, constancy, and force from the Climatic Atlas [4] have been superimposed on the hurricane development chart. It will be noted that only three tropical storms reached hurricane intensity near the ITC in the vicinity of the Cape Verdes. All three were in 1916 or earlier. Squalls of hurricane force were reported in connection with one storm in the area but it is quite possible the other two reached hurricane intensity farther to the westward. The heavy concentration in and east of the eastern Antilles, it can be seen, lies astride the trade wind current of greatest constancy and strength.

September's 90 hurricanes (fig. 5) are spaced rather similarly to August's except for a significant number forming in the northwestern Caribbean Sea and close to the Mexican coast in the Gulf of Mexico.

The principal concentration in October, figure 6, is in the northwestern Caribbean with marked diminution in all other sections. Formation in the Gulf of Mexico was largely confined to the Bay of Campeche.

The nine storms in November and the one in January developed between long. 59° and 80° W. except for the one off the southwest coast of Florida in late November in 1925 (fig. 7). These late season storms are few and unimportant.

REFERENCES

1. C. L. Mitchell, "West Indian Hurricanes and Other Tropical Cyclones of the North Atlantic Ocean", *Monthly Weather Review, Supplement* No. 24, Washington, D. C., 1924, 47 pp.
2. I. R. Tannehill, *Hurricanes*, Princeton University Press, 1945.
3. J. Namias and C. R. Dunn. "The Weather and Circulation of August 1955—Including the Climatological Background for Hurricanes Connie and Diane", *Monthly Weather Review*, vol. 83, No. 8, August 1955, pp. 163–170. (See p. 164.)
4. U. S. Weather Bureau, *Atlas of Climatic Charts of the Oceans*, Washington, D. C., 1938.

WEATHER NOTES

A NEW ONE-MINUTE RAINFALL RECORD

Introduction.—During the early morning hours of July 10, 1955, heavy thunderstorm activity occurred over an area embracing several counties just west of the center of Iowa. Associated with one of these storms there was a particularly heavy burst of rain that established a new United States record and possibly a new world's record for the heaviest recorded 1-minute rainfall. Over a period of 1.4 minutes the rate of fall was 0.69 inch per minute. For some shorter periods the rate was considerably greater.

At Opid's Camp, Calif., a storm on April 5, 1926, produced heavy rain that has been evaluated at 0.65 inch per minute [1]. A rainfall of 0.82 inch per minute was reported from Porto Bello, Panama, on November 29, 1911, but the nature of the record leaves considerable doubt about its reliability [2]. Other heavy rainfall records for various periods are listed in reference [3].

The new record rainfall was collected in a 9-inch, single-traverse, unshielded, Universal recording gage that was the property of the U. S. Weather Bureau, but on loan to the Iowa Natural Resources Council. Mr. Lawrence Nahnsen, on whose farm the gage was located, was serving as rainfall observer and operator of the gage for the Resources Council. The farm is 11 miles north of the town of Jefferson, in Greene County, Iowa.

The exposure of the gage is good. A few trees are located about 80 feet north of the gage. Shrubs to the west and south of the gage are at a distance of 32 feet and 24 feet, respectively. The house is 100 feet or more away, in a northwesterly direction, and the barn is even farther removed to the east.

The U. S. Geological Survey has a recording stream gage and sediment measuring station about 5 miles downstream on the East Fork of Hardin Creek, which drains the area over which the heavy rain fell. That agency obtained a very interesting trace of the stream rise associated with this storm.

Evaluation of the Record.—The chart had been on the drum for a period of nearly 10 days before the heavy rainfall was recorded. It was some time after the storm before the heavy rate of fall came to our attention, and by that time it was not possible to reconstruct some of the details relating to the storm. A study of the trace indicates that the clock was running at the time of the heavy rain, although the drum did not appear to be set to the correct time.

From interviews with the observer, and with others living in the vicinity, it appears that the heaviest rain probably fell around 2 or 3 a. m. The trace ends about an hour and a half after the storm. This would suggest that probably the clock had stopped before the chart was changed.

A study of the chart indicates that rain was still falling at an excessive rate at the time the pen was lifted off the chart by the clip holding the chart on the drum. The pen line reappeared on the other side of the clip some 20 minutes later and 0.29 inch higher. At the time the line was lost on the clip, the trace was approaching the clip at an angle of about 11°, showing that the drum was turning. There was nothing in the trace to indicate that the drum movement was restricted as a result of contact of the pen with the clip. The trace developed on previous days, when there had been no precipitation, indicates that the chart was properly mounted on the drum, with the edge uniformly against the flange.

The precise evaluation of so small a record chart with such a steep trace is difficult, and there is a strong probability that there is some error in the values developed by this study. However, every possible precaution has been taken to avoid misinterpretation and to keep the errors of measurement and computation as small as possible.

In order to obtain sufficient enlargement to permit careful study of the record, a Kodachrome slide was prepared of that part of the chart that was of particular interest. (Figure 1 is an enlargement from the slide.) The image of the slide was then projected onto a large sheet of stiff paper that was firmly fastened to the wall at the end of a long hall. On the enlargement the time scale measured 0.43 inch per minute, and the precipitation scale was 35.44 inches per inch of rain. A sharp line was traced through the middle of each appropriate line on the projected image, being particularly careful to follow any minor variations that were apparent in the trace.

A calibration of the gage shortly after the record was established indicated that 1.00 inch of precipitation in the range involved showed an increment of 1.01 inch on the chart. Therefore, a measurement of the ordinate distance of 1.01 inches of rain (35.80 inches) was divided by 100 to obtain the proper spacing for the 0.01 intervals, and rainfall amounts were measured on this basis.

The distances between 20-minute time arcs both prior to and following the heavy precipitation were averaged in computing the mean 1-minute distance, and a scale was prepared showing 0.10-minute intervals.

Readings of vertical and horizontal distance from the starting point were made on the large-scale tracing (to hundredths of an inch) for every 0.10 (corrected) inch of rainfall. Readings were also made, independently for every 0.10 minute (6 seconds). The two sets of readings were plotted on coordinate paper to check for consistency, and were found to agree very well. The measurements were then reduced to amounts and times (table 1).

A two-way table was then prepared showing, for each interval, the elapsed time and the increment of precipitation, as well as the rate of fall per minute for that interval. From this table, it was possible to determine readily the greatest rate of precipitation indicated for any given interval of time.

A plot of cumulative rainfall against time indicates that although heavy precipitation was continuous through the period in question there were two separate intervals during which rainfall was substantially heavier than it was during the rest of the time. Beginning at 0.10 minute after time zero and continuing for 0.20 minute rainfall was particularly heavy. The rate was less for nearly 1 minute, then beginning at 1.30 minutes after time zero another heavy burst occurred, which lasted until the record was terminated by the spring clip 0.20 minutes later. Any 60-second period which utilizes either of these intervals of heavier rainfall shows 0.67 inch per minute. By extending the time interval to 1.4 minutes, it is possible to include both of these periods in one computation to obtain an average rate of 0.69 inch per minute for a 1.4 minute period. Since this rate was maintained for longer than 1 minute, it has been adopted as the 1-minute record.

Synoptic Situation.—On the morning of July 10, a stationary front lay in an east-west line across northern Missouri. There was considerable shower and thunderstorm activity north of the front, and numerous reporting stations measured total rainfall of from 1 to 3 inches during the 48 hours of the 9th and 10th.

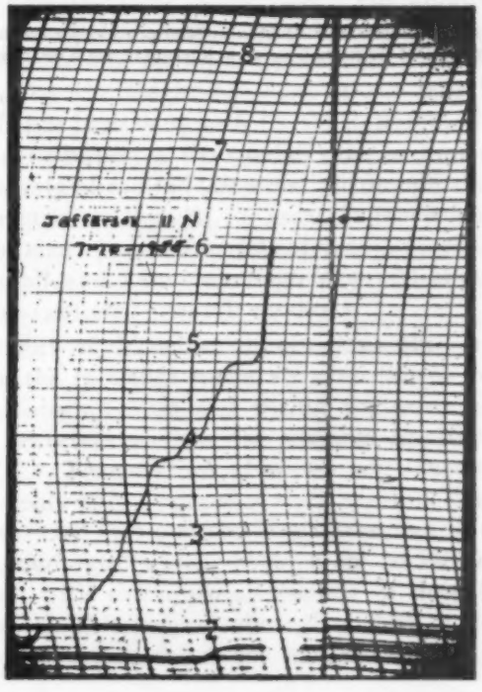

FIGURE 1.—Reproduction of hydrograph record during storm of July 10, 1955.

TABLE 1.—*Rainfall and elapsed-time measurements made from large-scale tracing of precipitation record*

Ordinate [1] (inches)	Abscissa [2] (inches)	Precipitation amount (inches)	Elapsed time (minutes)
0	0	0	0
1.43	.043	.04	.10
3.58	.07	.10	.16
6.45	.086	.18	.20
7.18	.09	.20	.21
10.82	.12	.30	.28
11.20	.129	.31	.30
12.82	.172	.36	.40
14.38	.215	.40	.50
15.45	.258	.43	.60
16.41	.300	.46	.70
17.51	.344	.49	.80
17.90	.35	.50	.82
19.99	.386	.56	.90
21.50	.40	.60	.93
22.84	.430	.64	1.00
25.11	.46	.70	1.07
25.42	.473	.71	1.10
26.86	.516	.75	1.20
28.24	.558	.79	1.30
28.64	.57	.80	1.32
31.80	.602	.89	1.40
32.23	.61	.90	1.42
35.80	.64	1.00	1.49

[1] Measured from 4.99-inch line.
[2] Measured from 7 a. m. line plus 0.520 inches.

Precipitation began about 3 hours before the heavy burst of rain, and accumulated during that time at the rate of approximately 1 inch per hour. It was following this 3-inch fall that the additional inch fell within less than a minute and a half. The storm ended about 20 minutes after the heavy burst of rain.

Although considerable time had elapsed before it was possible for us to make detailed inquiry, an attempt was made to determine the total rainfall measured at nearby points. Best indications are that the storm total increased in an eastward direction to a maximum of over 6 inches in the vicinity of Boxholm, about 12 miles east of the Nahnsen farm. It should be emphasized that these amounts are approximate and are based, in most cases, upon values taken from the memory of farmers living in the area. Only a few written notations were located; in all cases, however, these written records fitted into the pattern described.

Radar Indications.—Radar was in operation during the period of the heavy shower. The equipment was located at the Des Moines airport, about 55 miles southeast of the point where the heavy rain was recorded. The radar showed almost continuous echoes in the Jefferson area from 11 p. m. on the 9th to 2 a. m. on the 10th. Strong echoes between Des Moines and Jefferson after that may have prevented reception of echoes from the Jefferson area. At midnight the tops of echoes in the area were measured at 50,000 feet. Figure 2 is a map of western Iowa upon which is plotted the distribution of radar echoes in the Jefferson area at 11:30 p. m. of the 9th, at 12:30 a. m. of the 10th, and at 1:30 a. m. of the 10th.

Summary.—Although there is some doubt about the exact time at which the heavy rain fell, indications are that the record is correct as it relates to rate of fall, except for the 1-percent correction applied to the amount of precipitation in the interval over which the rainfall was recorded. Correcting for this 1-percent error, the average of 0.69 inch per minute maintained for well over 1 minute establishes a new record 1-minute rainfall for the United States, and a new world's record, if the Porto Bello record cannot be substantiated.

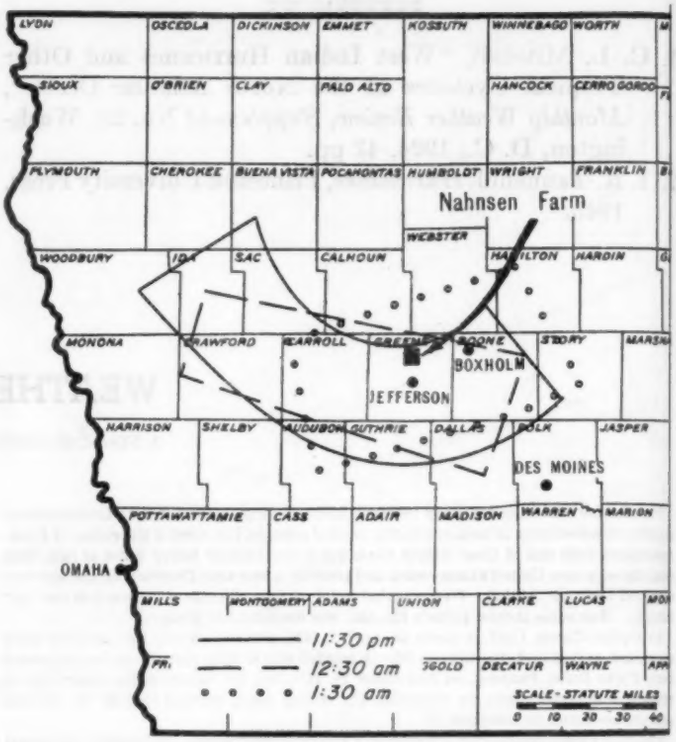

FIGURE 2.—Map of western Iowa showing location of Nahnsen farm and the distribution of radar echoes as seen on the Des Moines radar.

References.—1. G. N. Brancato and W. E. Remmele, *Record One-Minute Rainfall at Opid's Camp, Calif.*, U. S. Weather Bureau, 1946. 2. Benjamin C. Kadel, "The Most Intense Rainfall on Record," *Monthly Weather Review*, vol. 48, No. 5, May 1920, pp. 274–276. 3. Arthur H. Jennings, "World's Greatest Observed Point Rainfalls," *Monthly Weather Review*, vol. 78, No. 1, Jan. 1950 pp. 4–5.

C. R. Elford, Climatologist, WBO, Des Moines, Iowa.

QUANTITATIVE ANALYSIS AND FORECASTING OF WINTER RAINFALL PATTERNS

W. W. SWAYNE

Hydrometeorological Section, U. S. Weather Bureau, Washington, D. C.

[Manuscript received November 29, 1955; revised March 9, 1956]

ABSTRACT

A method is given for analysis of current rainfall intensity distribution and for preparation of short-period quantitative rainfall distribution forecasts using practical synoptic techniques. The analysis procedure is justified by a formulation which gives the condensation rate associated with the horizontal transport of saturated air through a stationary temperature field. The forecast procedure in addition utilizes (1) short-period extrapolations of the fields of moisture, motion, and temperature, (2) volumetric inflow of moisture in depth northward across a fixed boundary near the Gulf Coast as an approximation of the total rainfall during the forecast period, or when this is not applicable, the volume indicated by the moisture-depletion formulation, (3) envelopment of the initial and terminal period boundaries of moisture depletion to define the boundaries of the forecast pattern, (4) position of the maximum moisture advection to forecast the rainfall center, and (5) isohyetal analogues to fill in details of the pattern, particularly the orographic details which have not been treated otherwise in the present application. The results of a systematic test of forecasts using these ideas are also presented.

1. INTRODUCTION

One of the basic problems in hydrometeorology is the quantitative definition of rainfall distribution in terms of other meteorological parameters. Good correspondence between observed and computed rainfall patterns has been obtained by simultaneous treatment of the fields of motion, moisture, and temperature for each sub-layer of a multi-layered atmosphere. Thompson and Collins [1] used the vertical velocities obtained by divergence computations at 50-mb. intervals to compute the precipitation rate. Spar [2] also used 50-mb. intervals to obtain "integrated moisture transport vectors" for computing the rainfall rate. An approach suitable for high-speed numerical computations has been reported by Smagorinsky and Collins [3]; it was applied to a 3-level model of the atmosphere.

Another approach is to relate the rainfall rate directly to the transport of moisture through a single deep layer. This has been done analytically for the case of high orographic barriers in [4], [5] and other reports. Benton and Estoque [6] in a climatological-hydrologic study of water-vapor transport in the 1,000- to 400-mb. layer for the calendar year 1949 show a good relationship between monthly and seasonal transport patterns and precipitation.

The feasibility of simple dynamic treatment of moisture in depth for estimating the volume rate of rainfall for short-time periods was demonstrated by an experiment conducted in the Hydrometeorological Section in 1954 [7]. The instantaneous rate of northward mass transport of water vapor between the surface and 400 mb. across the Gulf Coast was computed once daily for two winter months. Assuming the instantaneous transport rate to persist for 24 hours, the 24-hour moisture transport for high inflow rates was found to be about equal to the observed 24-hour volume of rainfall measured over the area downwind from the inflow boundary the next day (fig. 1).

The present study was initiated in an effort to forecast the pattern and area of occurrence of the rainfall volume indicated by the Gulf inflow rate. The approach is to treat the precipitable water and thickness fields through a single deep layer in the lower troposphere with the motion indicated by the height contours at the middle of the layer. It has been used both for the determination of the current distribution of the rainfall rate, and for quantitative forecasts of rainfall patterns. Although the method is more restrictive than [3], for example, it seems especially useful for short-period forecasts of heavy, general, winter-type rainfall, and is simple enough for practical day-to-day use by conventional synoptic methods.

The point of departure in attacking this problem is given by the fact that warm air advection is very often observed upwind from and within the areas of general rainfall occurrence. (See, for example Appleby [8] and Means [9].) Temperature advection will concern us here, however, only as it is related to the horizontal advection of moisture. Our first purpose is to determine whether the condensation rate, which would seem to be necessarily associated with the apparent cooling of deep layers of saturated air in transport through a field of decreasing temperature, is reflected in the rainfall intensity distribution.

In section 2 of this paper a formulation relating hori-

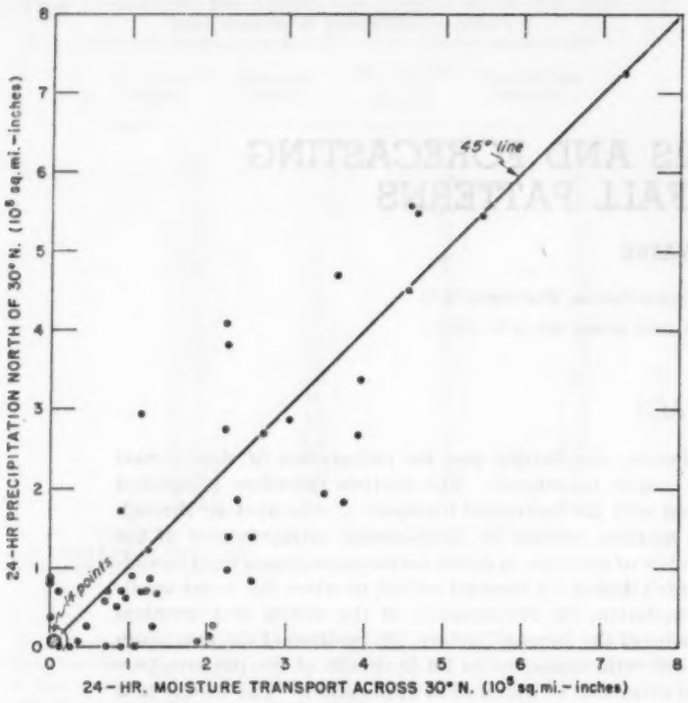

FIGURE 1.—Transport of moisture across 30° N. between longitudes of Tallahassee, Fla., and San Antonio, Tex., from surface to 400-mb. level (assuming 1500 GMT rate is maintained 24 hours) plotted against observed precipitation, during 24 hours beginning at 0630 CST of day moisture-transport measurement was made, measured downwind from the San Antonio-Tallahassee baseline.

zontal moisture transport to the rainfall rate is developed from simple physical and synoptic ideas. For practical synoptic application certain simplifying approximations and assumptions are required. These have not been tested intensively; instead, their validity as a set has been evaluated by the preparation of a series of rainfall rate analyses (section 3) and short-period forecasts (section 4).

2. MOISTURE TRANSPORT RELATED TO RAINFALL RATE

The distribution of rainfall is basically dependent on the transport and condensation of moisture. Thus, for a comprehensive treatment of rainfall it is necessary to relate moisture, temperature, pressure, and motion, at all levels in the atmosphere. A less comprehensive but still useful treatment is possible under certain simplifying assumptions.

ASSUMPTIONS

The rainfall rate can be related to moisture transport in a simple and convenient way with the following assumptions:

(1) To circumvent the difficulty of treating moisture layer by layer, precipitable water through a single deep layer in the lower troposphere is assumed to be an appropriate moisture variable. Moisture in depth (precipitable water) as related to rainfall intensity, is discussed extensively by Showalter [10], [11], [12], [13] and in reports of the Hydrometeorological Section [14], [15]. The selection of precipitable water as the moisture variable in this study has the further advantage that the horizontal distribution of precipitable water may be conveniently expressed in terms of thickness, the use of which is already well established in synoptic practice. The precipitable water is related to the thickness (mean virtual temperature of a layer between isobaric surfaces) by conversion to "saturation thickness". This is defined as the thickness between the specified constant pressure surfaces of a saturated pseudoadiabatic column having the same precipitable water value as the observed column. Tables 2 and 6 of "Tables of Precipitable Water" [16] provide the required values; table 2 gives the integrated values and increments of precipitable water for the various pressure intervals and height intervals, while table 6 gives the pressure-height values for a saturated atmosphere. Since the formulas on which the tables are based are simple and well-known [17, 18], we shall omit the thermodynamic theory and use the tabular values directly.

The relationship between saturation thickness and precipitable water for a saturated layer between 1,000 and 700 mb. is shown in table 1.

(2) An area of general, heavy, winter-type rainfall is assumed to occur within an area overlain by a deep saturated layer, that is, a layer whose observed thickness is approximately equal to the saturation thickness.

(3) Thickness lines in saturated areas are assumed to be fixed over the area for the duration of general rainfall. In a preliminary experiment, the 12-hour thickness change at all radiosonde stations where rainfall was continuous between soundings was tabulated for two winter months. In these cases it was found that despite strong warm advection, the average thickness change was about what would be expected from the standard observational error. Spar [2] and Locklear [19] also made this assumption for the computation of the rainfall rate.

(4) The transport of moisture through the deep layer is proportional to the geostrophic wind at the middle of the layer. In synoptic practice it is often assumed that the vector mean value of the horizontal motion at the base plus that at the top of an isobaric layer gives the mid-layer motion—the basis of differential analysis methods for interpolating a mid-layer surface contour field. Conversely,

TABLE 1.—*Thickness as a function of precipitable water in a saturated pseudoadiabatic column between 1,000 mb. and 700 mb. (Smoothed values). (Computed from tables 2 and 6 [16].)*

Precipitable water (inches)	Saturation-thickness (feet)	Precipitable water (inches)	Saturation-thickness (feet)
2.032	10,100	.499	9,300
1.734	10,000	.406	9,200
1.474	9,900	.328	9,100
1.248	9,800	.263	9,000
1.052	9,700	.211	8,900
.882	9,600	.171	8,800
.735	9,500	.142	8,700
.608	9,400		

it may be assumed that the mid-layer motion approximates the net motion of air through the layer. We are more concerned, however, with the approximation for moisture transport through a layer. A test was performed with data from the Gulf water vapor transport study. The following ratio was obtained for the northward component of moisture transport between two radiosonde stations: the sum of the moisture transport for the 1,000- to 700-mb. and the 700- to 400-mb. layers, divided by the product of the average precipitable water 1,000- to 400-mb. and the transport at 700 mb. The ratio was found to be close to unity for the higher transport values.

(5) Vertical moisture transport, other than that implied by the nonmovement of thickness lines in the rain areas (see assumption 3), is ignored in this formulation. Investigations of the local intensification of the vertical motion and associated rainfall by differential temperature advection, have been reported by Gilman [20], Appleby [8], and Miller [21].

(6) For convenience the variation of the Coriolis parameter and the effect of changes in spacing of contours of the mid-layer pressure surface will be neglected. These simplifications will not introduce appreciable error so long as actual computations are made for small increments of area.

Under the above assumptions a simple expression for the moisture transport can now be derived and related to the rainfall rate.

MOISTURE TRANSPORT

Consider the case of a saturated layer, stationary temperature field, and horizontal geostrophic motion. Since, as table 1 shows, the thickness specifies the precipitable water value, the instantaneous moisture transport across a boundary in the saturated area is specified, under our assumptions, by superimposing the thickness field and the pressure contours at the middle of the layer. Thus, the moisture transport M across the segment of a thickness line Z that is intercepted by two adjacent contours of geopotential ϕ_1 and ϕ_2, with a spacing Δn, is given by

$$M=V_g W \Delta n \tag{1}$$

where W is the precipitable water defined by the saturation thickness Z, and V_g is the geostrophic wind speed

$$V_g=\frac{1}{f}\frac{\phi_2-\phi_1}{\Delta n} \tag{2}$$

Equations (1) and (2) therefore give the following simple expression for the moisture transport:

$$M=\frac{1}{f}(\phi_2-\phi_1)\,W \tag{3}$$

The moisture transport as given by equation (3), though indicating the volume rate of rainfall (e. g., fig. 1), does not by itself specify the location or size of the area of rainfall occurrence. However, equation (3) can be used to obtain a convenient expression for moisture advection, which under the assumptions of this paper is proportional to rainfall rate.

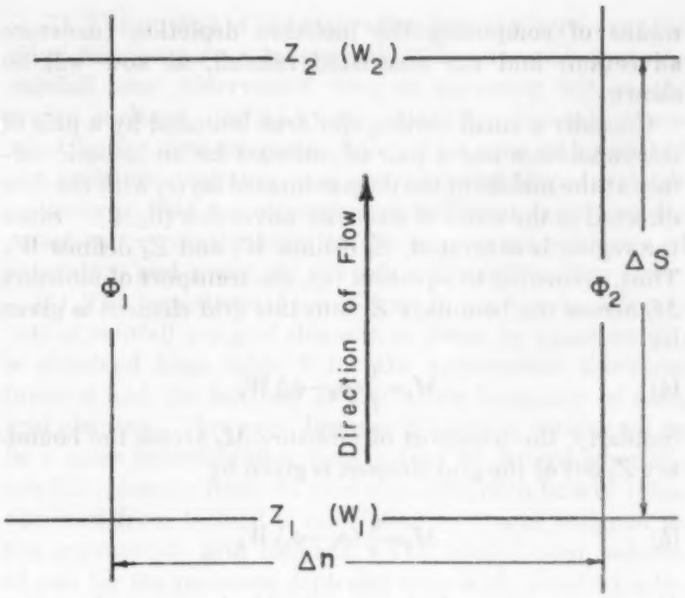

FIGURE 2.—Grid element of thickness and height contours in a saturated region. Z_1, W_1 and Z_2, W_2 are thickness and precipitable-water values at the inflow and outflow boundaries of the element, respectively. The geopotential heights, ϕ_1 and ϕ_2, are the geopotential height contours bounding the grid element. Since the region is saturated, Z defines the value of W. The symbols Δs and Δn are the distances between the thickness lines and the height contours, respectively. Also $\phi_2 > \phi_1$ and $Z_1 > Z_2$, conditions for condensation of moisture by horizontal advection (assuming no supersaturation).

RAINFALL RATE

Consider the condensation process for the limiting case of a saturated layer, stationary temperature field, and horizontal geostrophic motion. The difference between the moisture transport at suitably selected inflow and outflow boundaries, that is the moisture advection, is determined by the temperature advection. Where initially saturated air columns are moving into regions of lower temperature, water vapor must be condensed out (assuming no supersaturation); and where they are moving into warmer regions, the water-vapor capacity of the columns is increasing, thereby inhibiting the condensation process. This study is chiefly concerned with moisture depletion, that is, with moisture advection in saturated air associated with warm temperature advection.

In general, measurement of the moisture advection is not a simple computation. (See e. g., Spar. [2].) For the special case of saturated air with geostrophic motion, however, the indicated warm temperature advection pattern represented by the superposition of the thickness field and height contours at the middle of the layer gives a ready

379802—56——2

means of computing the moisture depletion (moisture advection) and the associated rainfall, as now will be shown.

Consider a small rectangular area bounded by a pair of thickness lines and a pair of contours for an isobaric surface at the middle of the deep saturated layer, with the flow directed in the sense of warm air advection (fig. 2). Since the region is saturated, Z_1 defines W_1 and Z_2 defines W_2. Thus, according to equation (3), the transport of moisture M_1 across the boundary Z_1 into this grid element is given by

$$M_1=\frac{1}{f}(\phi_2-\phi_1)W_1 \tag{4}$$

Similarly, the transport of moisture M_2 across the boundary Z_2 out of the grid element is given by

$$M_2=\frac{1}{f}(\phi_2-\phi_1)W_2 \tag{5}$$

Now the moisture depletion rate M_c due to condensation over the area of the grid element is M_1-M_2, which from (4) and (5) is given by

$$M_c=\frac{1}{f}(\phi_2-\phi_1)(W_1-W_2) \tag{6}$$

The author is indebted to a reviewer for pointing out that equation (6) follows immediately from Spar's [2] expression for precipitation intensity as a function of the "vapor transport vector" when one uses the mean geostrophic wind V_g for the layer and makes the assumptions that $\frac{\partial W}{\partial t}=0$ and $\frac{\partial V_g}{\partial s}=0$, as was done in the present paper.

The factor $W_c\equiv W_1-W_2$ represents the amount of water which would be condensed out by cooling a saturated column at the pseudoadiabatic lapse rate through the thickness interval Z_1-Z_2. Table 2 gives values of this factor for cooling through various thickness intervals. These values can be used to approximate the rate of condensation of water vapor within an isobaric layer, required by the apparent advection of saturated columns from higher to lower thickness values (neglecting vertical motion).

In equation (6), the factor $\frac{1}{f}(\phi_2-\phi_1)$ is the familiar geostrophic transport term, giving the area transported between height contours on a constant pressure surface at a given latitude per unit time. This factor has been calculated using the Smithsonian wind tables [18]. With use of this factor and values of W_c from table 2, values of M_c have been calculated from equation (6) for the 1,000–700-mb. layer. Values of M_c are given in table 3.

The average rainfall rate (R) over the area of the grid element, if all the condensed water falls out, is proportional to the moisture advection and is given by

$$R=\frac{M_c}{(\Delta s)(\Delta n)} \tag{7}$$

It can further be shown that

$$W=K\sum_{p(\text{base})}^{p(\text{top})}(\rho^* T^*)(\Delta p), \tag{8}$$

where $K=\frac{R_d}{g\rho_w\bar{p}}$, ρ^* is absolute humidity, T^* the virtual temperature, Δp the pressure interval between the top and bottom of an isobaric layer, ρ_w the density of liquid water, $\bar{p}$ the average pressure in the column, and R_d is the gas constant for dry air. Then the rate of condensation of moisture is given by

$$M_c=\left[\frac{1}{f}(\phi_2-\phi_1)\right]\left[K\sum_{p(\text{base})}^{p(\text{top})}(\rho_{w_1}T_1^*-\rho_{w_2}T_2^*)(\Delta p)\right]. \tag{9}$$

This is the relation between the transport, the absolute humidity, the virtual temperature, and the condensation rate.

More comprehensive treatment of the moisture continuity considerations will be found in two recent papers [2] and [3] in the *Monthly Weather Review* to which the reader is referred for discussion of assumptions. In their paper, Smagorinsky and Collins [3] proceed from the requirement for continuity of the mixing ratio r, given by

$$\frac{dr}{dt}=\frac{\partial r}{\partial t}+\mathbf{V}\cdot\nabla r+\omega\frac{\partial r}{\partial p}$$

TABLE 2.—*Amount of precipitable water condensed by cooling a saturated column through specified thickness intervals (prepared from data in table 1)*

Change in saturation thickness (feet)	Change in precipitable water (inches)	Change in saturation thickness (feet)	Change in precipitable water (inches)
10,100–10,000	0.298	9,400–9,300	0.109
10,000–9,900	.260	9,300–9,200	.093
9,900–9,800	.226	9,200–9,100	.078
9,800–9,700	.196	9,100–9,000	.065
9,700–9,600	.170	9,000–8,900	.052
9,600–9,500	.147	8,900–8,800	.040
9,500–9,400	.127	8,800–8,700	.029

TABLE 3.—*Hourly rate of condensation per thickness-contour grid element in the 1,000- to 700-mb. layer for various latitudes and thickness value intervals (in inch-square-miles per grid element, 100-ft. contour and thickness intervals)*

Thickness interval (feet)	Latitude ° N.						
	25	30	35	40	45	50	55
10,100–10,000	2,010	1,700	1,480	1,320	1,200	1,110	1,040
10,000–9,900	1,750	1,480	1,300	1,150	1,050	970	900
9,900–9,800	1,520	1,290	1,130	1,000	910	840	780
9,800–9,700	1,320	1,120	980	870	790	730	680
9,700–9,600	1,140	970	850	750	680	630	590
9,600–9,500	990	840	730	650	590	550	510
9,500–9,400	860	720	630	560	510	470	440
9,400–9,300	730	620	540	480	440	410	380
9,300–9,200	630	530	466	410	370	350	320
9,200–9,100	530	440	390	350	310	290	270
9,100–9,000	440	370	320	290	260	240	220
9,000–8,900	350	300	260	230	210	190	180
8,900–8,800	270	230	200	180	160	150	140
8,800–8,700	200	170	140	130	120	110	100

where $\mathbf{V}$ is the horizontal wind vector, $\omega = dp/dt$, and ∇ is the horizontal vector gradient operator. In a personal communication these investigators demonstrate that equation (9) in the text above can be obtained directly from their work [3] by essentially one approximation. They state:

. . . it is merely necessary to make the approximation that the non-conservation of the mixing ratio is given to a sufficiently good approximation by the horizontal advection of the mixing ratio $\left[\text{i. e., } \frac{dr}{dt} \approx \mathbf{V}\cdot\nabla r\right]$. This implies that the local change in the mixing ratio $[\partial r/\partial t]$ is for the most part balanced by the vertical advection $\left[\omega \frac{\partial r}{\partial p}\right]$. We know that especially in moist tongues there is at least a tendency for compensation in sign. However, from our own work we know that during the condensation process $\frac{\partial r}{\partial t}$, $\mathbf{V}\cdot\nabla r$, and $\omega \frac{\partial r}{\partial p}$ tend to be of the same magnitude, so one would expect situations where there is not adequate compensation between $\frac{\partial r}{\partial t}$ and $\omega \frac{\partial r}{\partial p}$.

3. ANALYSIS OF RAINFALL

ANALYSIS PROCEDURE

Details of the actual operations in analyzing the motion, thickness, and moisture fields for a specified isobaric layer will now be explained utilizing the observed 1,000- to 700-mb. thickness and precipitable-water fields and the 850-mb. contours. The 850-mb. contours give the geostrophic field of motion of the layer, the 1,000- to 700-mb. thickness pattern gives the temperature field, and the precipitable-water pattern gives the distribution of moisture in depth.

Thickness and contour lines were spaced at 100-ft. intervals. A finer grid would have been desirable, but the average error of observation [22, 23] would not seem to justify it. The scale is set by the grid interval. Even in the moisture-depletion areas associated with the heaviest winter rains, 100-ft. x 100-ft. grid elements are seldom smaller than perhaps 15,000 or 20,000 square miles. The aim is to define the average depth of rainfall by areas as large as or larger than this. It is not expected that the grid elements would represent intensity for time periods much shorter than 3 hours and it has been assumed that a 6-hour period is not too long.

The analysis steps are:

(1) The temperature advection pattern is obtained by superimposing the 850-mb. contours on the 1,000–700-mb. thickness pattern.

(2) A zero-advection line is then drawn on the superimposed field to separate the areas of warm- and cold-air advection.

(3) The isopleths of saturation thickness are drawn by converting the precipitable-water pattern to saturation thickness, using the conversion given in table 1.

(4) The 1,000- to 700-mb. observed thickness pattern is superimposed on the saturation thickness pattern. Those areas where the saturation thickness is within 100 feet of the observed thickness are outlined. This latitude is required because the humidity observations are known to be consistently low.

(5) The outline of the saturation area is placed over the advection pattern. In general, it is expected that the rainfall near observation time is occurring within the region enclosed upwind by the saturation line and downwind by the zero-advection line. This area is designated the moisture-depletion area, because the procedural hypothesis is that a necessary and sufficient condition for water-vapor condensation is the concurrent existence of saturation and warm air advection through a deep layer.

(6) The hypothetical lower limit to the hourly volume-rate of rainfall per grid element, as given by equation (6), is obtained from table 3 for the appropriate thickness interval and the latitude at the inflow boundary of each grid element. However, because 6 hours is considered to be a more representative time period for determining the rainfall intensity from the grid elements, each hourly value obtained from table 3 is multiplied by 6 and assigned to the appropriate grid element. The total 6-hour volume of rain for the moisture depletion area is obtained by adding the values for the grid elements.

In the application of the above procedure, it is of course well to keep in mind the limitations imposed by the underlying assumptions. The instantaneous rainfall pattern is visualized as a system of many moving cells, forming and dissolving in the general flow, the instantaneous intensities heavy over only a small part, and light over a much larger part, of the rain area.

The analysis, of course, neglects the contribution of ageostrophic motions and non-advective processes to the rainfall production. For example, the rainfall volume associated with gravitational displacement of warm by cold air at a steep, rapidly moving, cold front is not assessed. In general winter rains it is thought that this is small compared to the volume of the advective contribution. However, experience shows that the thickness-moisture analysis will generally differentiate the "wet" and "dry" sections of such a front.

The centers of heavy winter rainfall patterns are very often located in strongly orographic regions. In the present application the orographic contribution has not been treated; however warm moisture advection seems always to be present at the time of important rainfall occurrences over such regions.

One or both of two processes might end the rain at a given point during the 6-hour period. If the inflow moisture decreases, the upwind boundary of the rainfall area must move toward lower thickness values. (In such a case, the saturation line could conceivably move downwind out of the warm-advection area, and the rainfall area would vanish.) In the second process, layer motion may shift relative to the thickness lines in such a way that the net moisture advection vanishes or is directed toward greater thickness.

ANALYZED SERIES—JANUARY 1954

The procedure described above has been followed in analyzing the 6-hour rainfall rate centered at the 0300 GMT and 1500 GMT upper-air observations for January

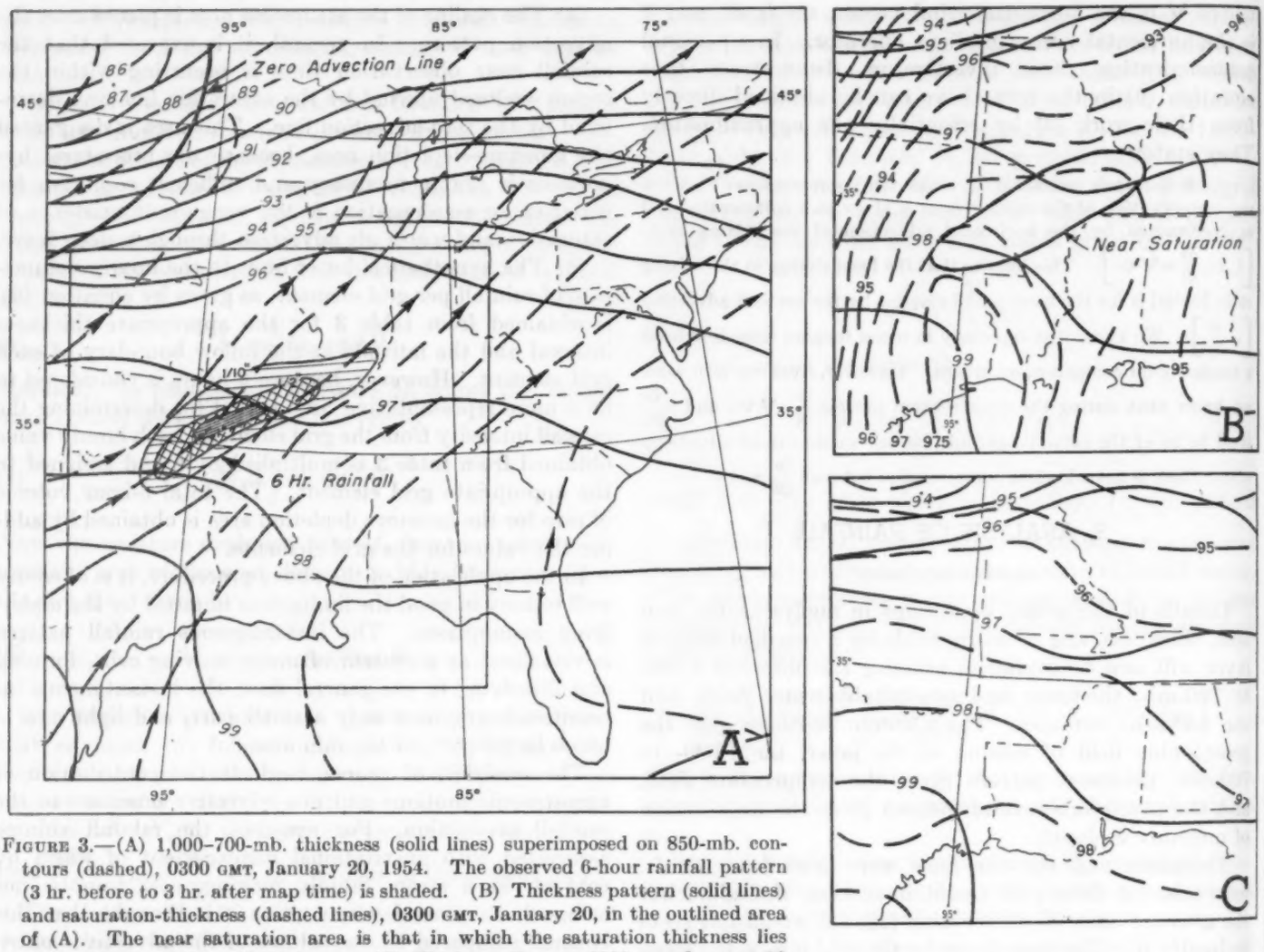

FIGURE 3.—(A) 1,000–700-mb. thickness (solid lines) superimposed on 850-mb. contours (dashed), 0300 GMT, January 20, 1954. The observed 6-hour rainfall pattern (3 hr. before to 3 hr. after map time) is shaded. (B) Thickness pattern (solid lines) and saturation-thickness (dashed lines), 0300 GMT, January 20, in the outlined area of (A). The near saturation area is that in which the saturation thickness lies within 100 ft. of the real thickness. (C) Thickness lines at 0300 GMT January 20 (solid) and 1500 GMT, January 19 (dashed) in the outlined area of (A).

1954. To make the analyzed series compatible with the forecast series (described in section 4), the analyses utilize the 850-mb. contours and the 1,000- to 700-mb. thickness. Some other constant level surface, and/or thickness interval might well have been used for indicating the moisture advection. However, daily forecasts (section 4) were an essential part of the procedure in this experiment; therefore, practical considerations determined the choice of thickness interval.*

Thermal winds were computed for every point where wind observations were available, using the approximation recently adopted by the National Weather Analysis Center that the thermal wind is the vector difference between the observed wind at the top of the layer and the sea level geostrophic wind. These were used as an aid in the analysis of the thickness pattern. Due weight was given to the observed winds in analyzing the 850-mb. contours.

No such guide as the geostrophic spacing is available in analyzing the moisture pattern; advecting it with the speed of the mid-layer wind from map to map appears to be the best way of keeping track of it in the sparse sounding network. This has been done with the analyzed examples.

The analysis procedure was that described previously, with the exception that the precipitable-water values between the surface and 700 mb. were used to construct the saturation thickness field.

Examples from an analyzed series are shown in figures 3 to 5. Three charts are shown for each date and time of observation. Chart A is the contour-thickness grid, with the zero-advection line indicated. The isohyetal pattern, based on a fairly dense network of recording gages, is also shown. Chart B shows the saturation-thickness field superimposed on the real thickness and an outline of the area over which the saturation thickness lies within 100 feet of the real thickness. That portion of the

* The National Weather Analysis Center prepares a mid-layer contour chart for the 1,000- to 700-mb. interval; time was not available for preparation of mid-layer contours for the 1,000- to 500-mb. interval in the daily forecast procedure.

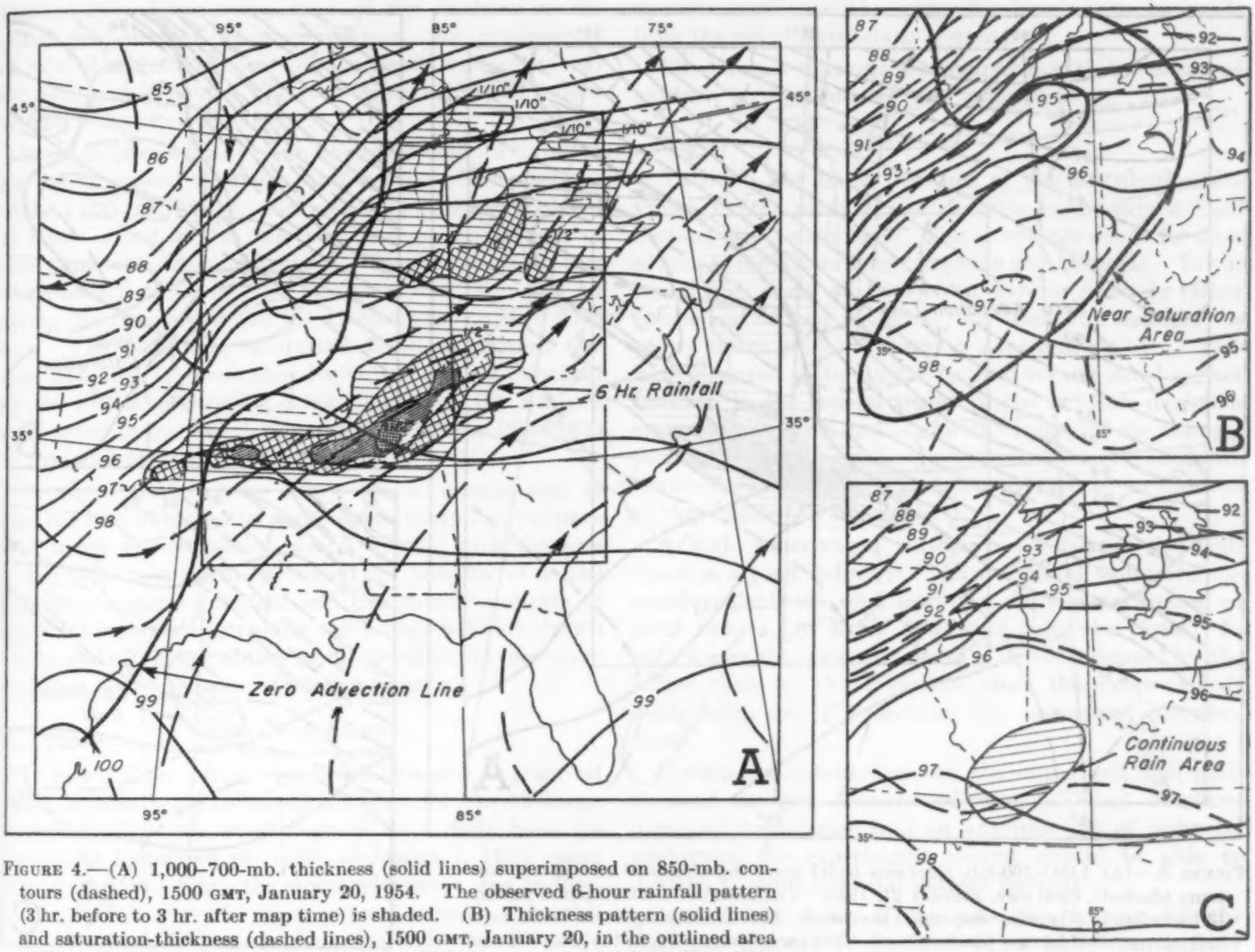

FIGURE 4.—(A) 1,000–700-mb. thickness (solid lines) superimposed on 850-mb. contours (dashed), 1500 GMT, January 20, 1954. The observed 6-hour rainfall pattern (3 hr. before to 3 hr. after map time) is shaded. (B) Thickness pattern (solid lines) and saturation-thickness (dashed lines), 1500 GMT, January 20, in the outlined area of (A). The near saturation area is that in which the saturation thickness lies within 100 ft. of the real thickness. (C) Thickness lines at 1500 GMT (solid) and 0300 GMT (dashed), January 20, 1954 in the outlined area of (A).

area of saturation that lies in a warm advection region is termed the moisture-depletion area. Chart C compares the position of the thickness lines at the time of observation with the position 12 hours earlier. From the figures it can be seen that the boundaries of the observed 6-hour rainfall patterns (3 hours preceding and 3 hours following the upper-air soundings) correspond well with the position of the moisture-depletion area. Furthermore, the higher rainfall values appear to be associated with the grids of smaller size. It will also be noted that in those areas continuously within the moisture-depletion area between observations the indicated thickness change is very small.

A day-to-day comparison of the current day moisture-depletion and rainfall patterns for more than a year substantiates the usefulness of these techniques; it appears that the heavier, general, winter-type precipitation patterns are especially well defined by the moisture-depletion pattern technique.

4. SHORT-PERIOD FORECASTS

An obvious but important inference from the results of the analysis of moisture depletion areas is this: A forecast of the moisture and thickness field, and of the contours of the middle pressure surface, defines a first approximation of the rainfall-intensity pattern at the time of forecast. A forecast experiment will be discussed later in this section, but first it is necessary to consider the transport and advection of moisture in unsaturated areas, attention thus far having been limited to saturated layers.

TRANSPORT OF MOISTURE IN UNSATURATED AREAS

It is clear that the horizontal moisture advection alone will not result in condensation until saturation is reached, whatever the rate of moisture transport. Therefore consideration of rate of change of moisture storage as related to the change in the water-vapor capacity of an un-

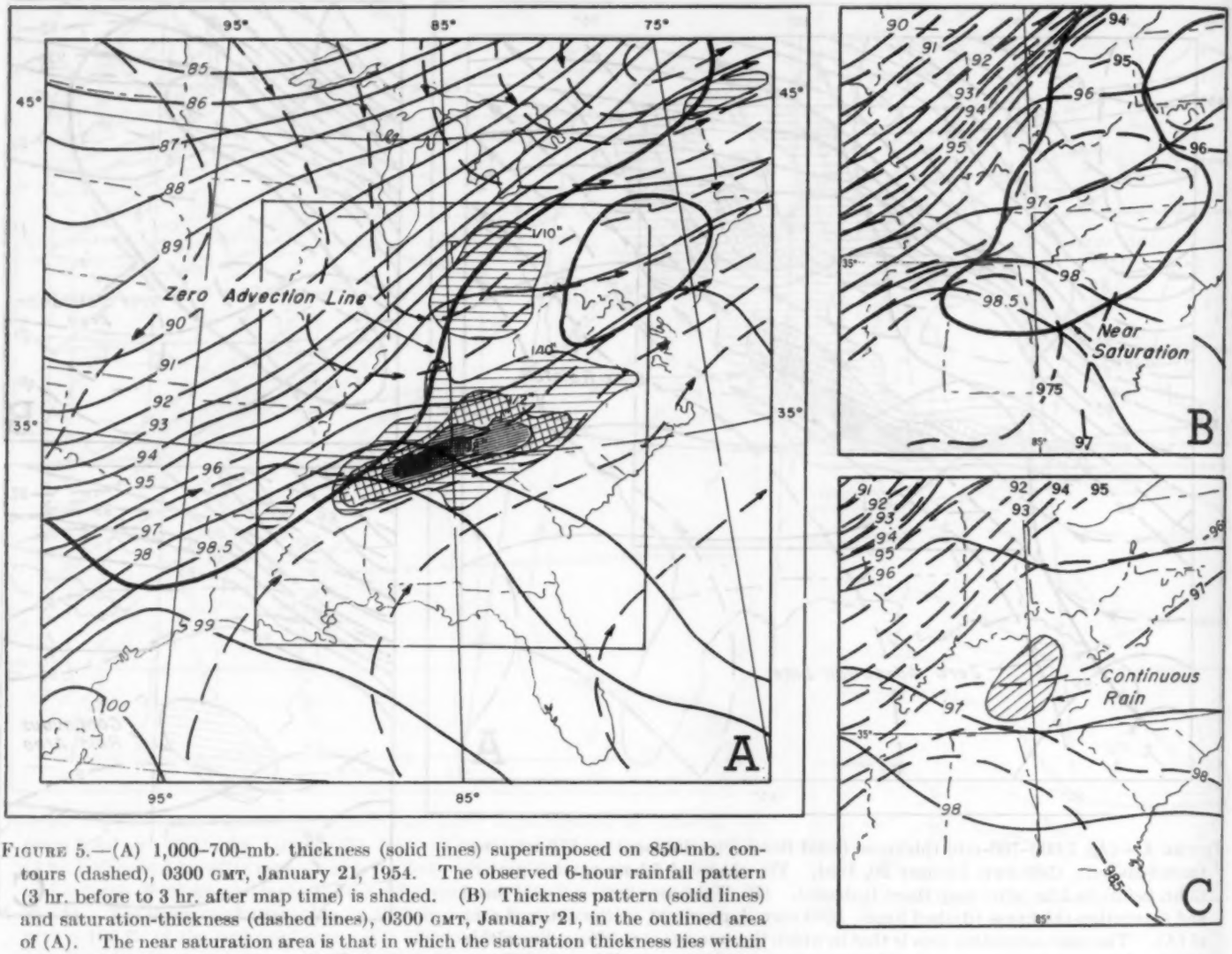

FIGURE 5.—(A) 1,000–700-mb. thickness (solid lines) superimposed on 850-mb. contours (dashed), 0300 GMT, January 21, 1954. The observed 6-hour rainfall pattern (3 hr. before to 3 hr. after map time) is shaded. (B) Thickness pattern (solid lines) and saturation-thickness (dashed lines), 0300 GMT, January 21, in the outlined area of (A). The near saturation area is that in which the saturation thickness lies within 100 ft. of the real thickness. (C) Thickness lines at 0300 GMT, January 21 (solid) and 1500 GMT, January 20 (dashed) in the outlined area of (A).

saturated layer is an important consideration in a rainfall forecast.

In general, the thickness lines move more slowly than the saturation thickness field, and this is especially true in warm-advection areas. Craddock [24] in a study of advective changes in the 1,000- to 700-mb., and 700- to 500-mb. thickness patterns, states that the effect of advection in modifying the thermal field appears to be offset by other processes, the resultant change being a residual with a correlation of about 0.6 with the advective component.

In a crude preliminary experiment, the precipitable-water field at 0300 GMT was moved with the streamline motion at mid-layer to the saturation position, assuming no later motion of the thickness lines. The placement of the saturation line found in this way often corresponded rather well with the position of the upwind boundary of the 24-hour rainfall pattern beginning 9 hours later. In any case, a forecast of the position of the upwind boundaries of general winter rains requires a quantitative appraisal of the rate at which the saturation thickness is overtaking the real thickness pattern; with a good forecast of the thickness pattern, the time of initiation and the placement of the upwind rainfall boundary should be usefully defined. (This paper is chiefly concerned with the treatment of moisture in depth, and discussion of techniques of forecasting development of thickness and contour patterns is outside its scope.)

With these considerations taken into account, a forecast procedure will now be developed for use in a short-period forecast experiment.

FORECAST PROCEDURE

The procedure for forecasting the rainfall pattern has two main steps: First, analysis of the current thickness-contour grid, and second, preparation and analysis of a forecast of the grid near the end of the rainfall forecast period. The analysis procedure has already been described

(section 3). Upon completion of the analysis of the initial grid-element moisture pattern, the volume-rate of rainfall and the 6-hour average depth were estimated for each grid element. The total 0630–1230 GMT, 6-hour volume was then calculated.

For step two, a primitive method was used for developing the forecasted thickness-contour grids. The positions of the 1,000- to 700-mb. thickness lines were extrapolated 12 hours ahead of the 0300 GMT position at the rate of their previous 24-hour motion. Next, the 1500 GMT configuration of the 850-mb. contours was estimated by noting the changes during the 12 hours previous to 0300 GMT. The 0300 GMT saturation thickness pattern was then advected 12 hours ahead with the motion indicated by the initial geostrophic streamlines, and the analysis was carried through as in step one to obtain the 1230–1830 GMT rainfall pattern.

Finally a pattern was drawn whose volume was as near the sum of the initial and forecast computed volumes as a quick eye-estimation would permit, with the axis of heaviest rain drawn between the position of initial and forecast-period centers and the outside isohyets of appreciable rainfall (generally the ¼-inch isohyet) drawn within and of a shape similar to the swath of the successive positions of the moisture-depletion areas.

FORECAST EXPERIMENT

To test the forecast procedure and to assess its practical value, forecasts of rainfall distribution for the 12 hours beginning 0630 GMT were prepared on a daily basis for the period December 28, 1954, to March 1, 1955, using 0300 GMT data. Since the primary interest was in forecasting distribution of intense general rains, it was arbitrarily decided to prepare forecasts only for the days when the rate of water-vapor transport across the Gulf Coast exceeded 50,000 square-mile-inches per 12 hours. The implicit forecast for the other days is "less than 50,000 square-mile-inches, distribution not defined."

The basic working materials were the 0300 GMT charts of the National Weather Analysis Center for the 850-mb. level, and the 1,000- to 700-mb. thickness. (The 1,000- to 500-mb. thickness was used with the 850-mb. contours for the first two weeks.) The 0630 GMT Daily Weather Map and the 1500 GMT constant pressure charts of the previous day were also available, but little use was made of any but the 850-mb., 1500 GMT chart.

The strictures of a practical forecast situation were observed in every respect. The forecast preparation was begun as soon as the charts were available, and no later data were used. By the "rules of the game" no corrections were allowed after the forecast pattern was presented to a disinterested "referee" although a few obvious mistakes were discovered later. A rigidly standardized forecast scheme would have been desirable in many respects, but certain changes in emphasis and modifications in technique were strongly indicated as the experiment progressed. These are not fundamental and do not in our opinion invalidate the general inferences to be made from the set of forecasts as a whole.

The forecast patterns are compared with the observed patterns for each forecast day in figure 6.

CLIMATOLOGICAL AIDS

Although the larger features of the distribution are shown by the analysis, the detail is not clearly defined because the "model scale" defines average depth for sizes of area as large as or larger than the grid elements. In our experience nearly all heavy winter rains occur in rather simple and definite patterns. An "isohyetal analogue" is a convenient guide for drawing a forecast pattern. This is an observed pattern with the total volume equal to that forecast, in the general region of the moisture-depletion area, of its general outline, for the length of the forecast period. The analogue integrates two unassessed contributions—the orographic effect and convergence—in addition to that implied by our model.

A high water-vapor transport rate across the Gulf Coast is a good indicator of future rainfall volume if the moisture-depletion area lies over the Central States no more than a few hours downwind from the Coast. In such a case the forecast volume is better indicated by the inflow than by the depletion, since the inflow-rainfall relationship (see [7]) includes the unassessed contributions.

Having the volume-forecast, the initial and final positions of the grid elements of least size, and moisture-depletion boundaries, and an adequate file of isohyetal analogues, the experienced analyst should be able to develop a useful isohyetal pattern forecast.

In the first group of forecasts (fig. 6, page 62) the emphasis was on the "climatological aids," particularly the moisture inflow rate. Precipitable-water values were computed only for stations near the Gulf Coast. Later, the moisture-depletion computation was used in regions far downwind from the Gulf Coast where the inflow rate was not adequately defining the volume of rainfall. It was, of course, necessary to prepare the saturation thickness field for the entire area in using this method.

5. CONCLUDING REMARKS

The results of the forecast series indicate that the assumptions and approximations of the model are useful; and they may suggest that the most important of the processes contributing to general, heavy, winter-type rainfall is the ascending motion implied by the non-motion of the thickness contours. Methods for treating the orographic contribution are of course implicit in the model formulation, and work is underway on this aspect. Combined with adequate methods for treating the development, and perhaps other contributions to the vertical motion, the short period forecasts of rainfall would very likely be improved, and the period of the forecasts considerably extended. Whatever success was attained in

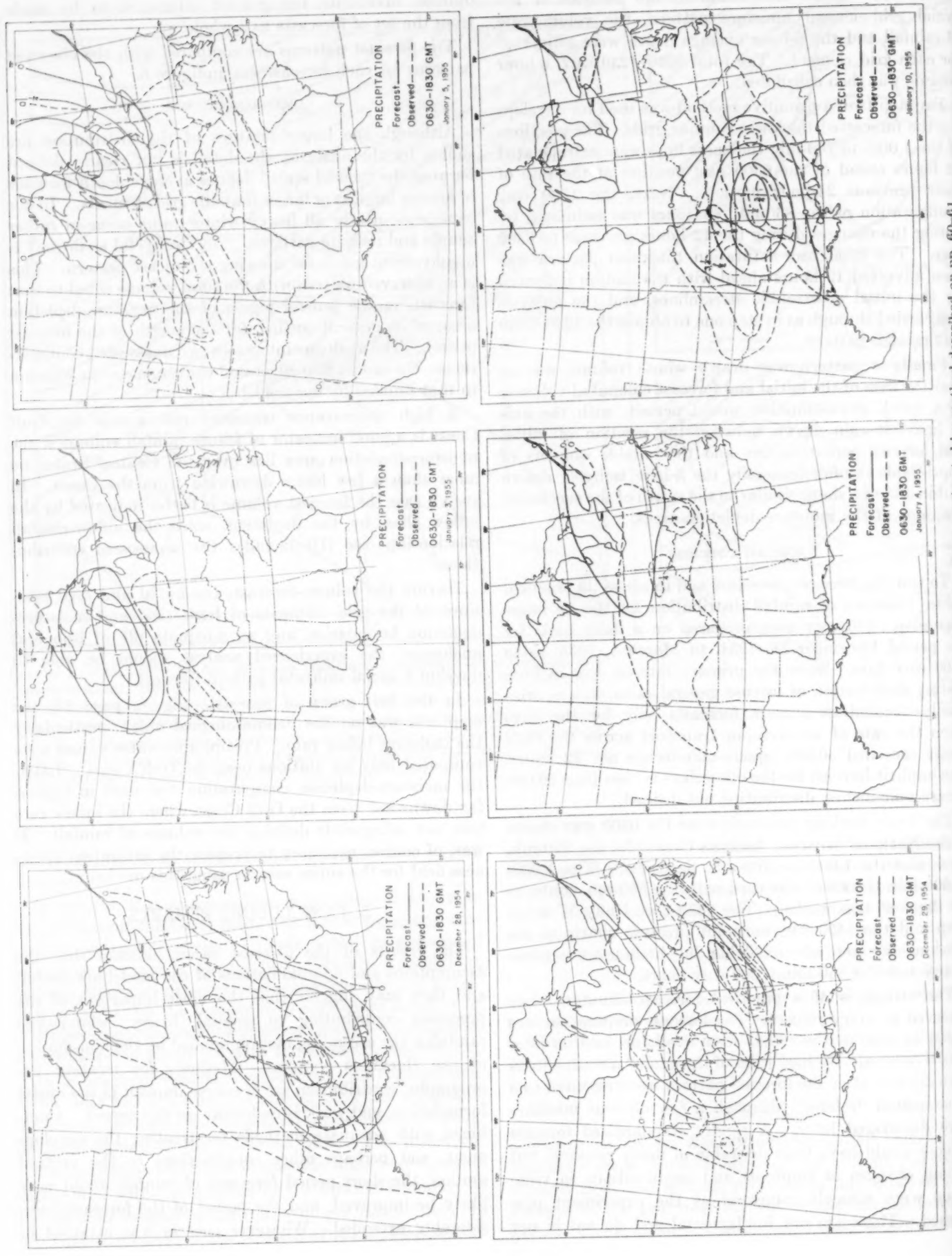

FIGURE 6.—Observed rainfall pattern superimposed on forecast pattern constructed by method described on pp. 60–61.

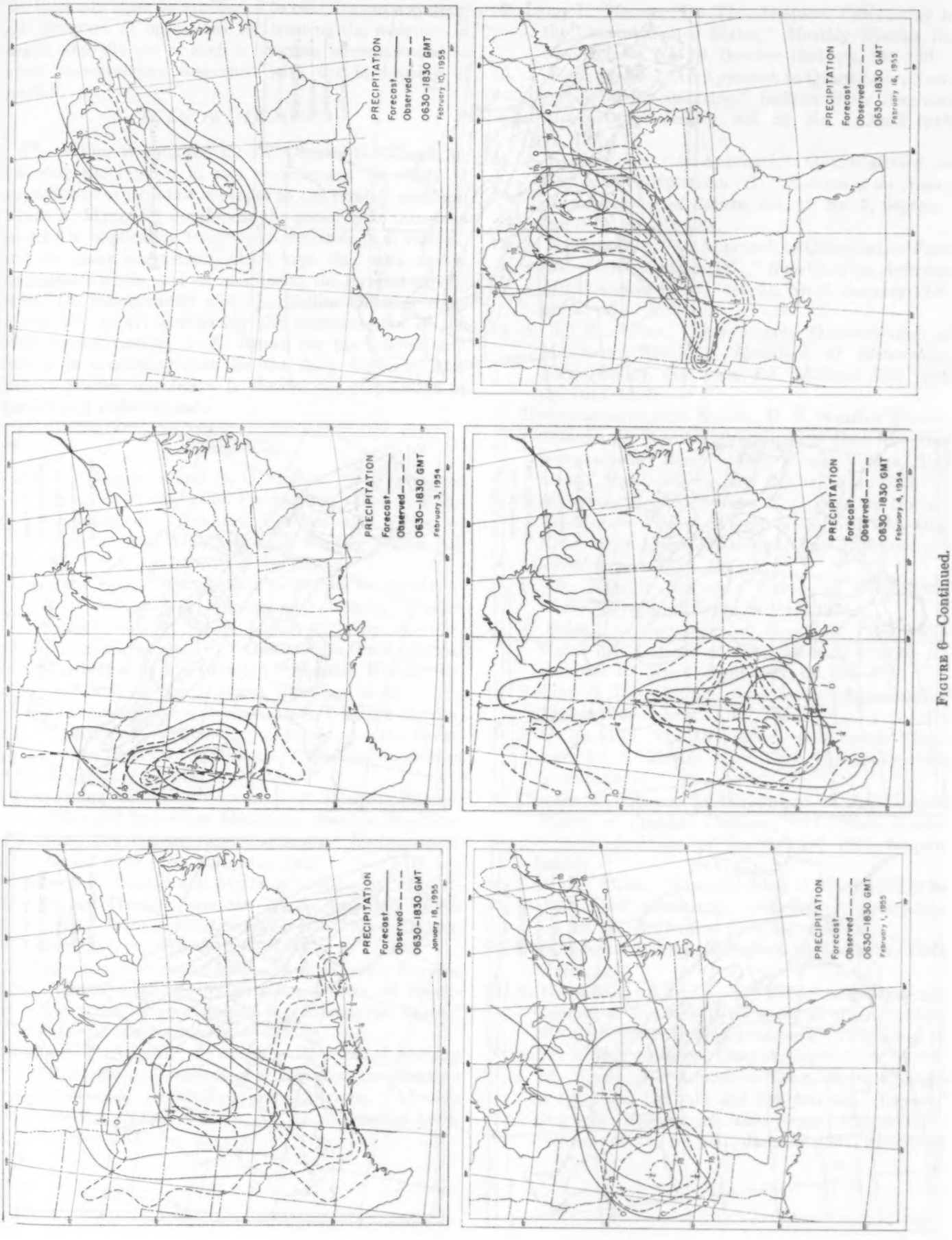

FIGURE 6.—Observed rainfall pattern superimposed on forecast pattern constructed by method described on pp. 60–61.

FIGURE 6—Continued.

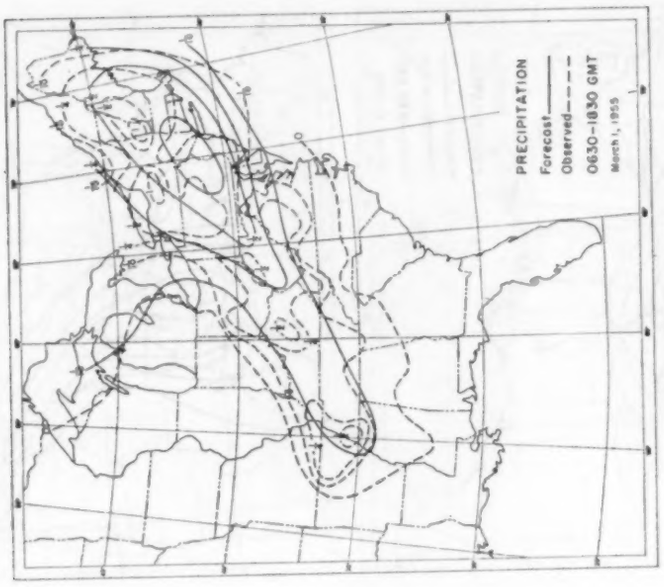

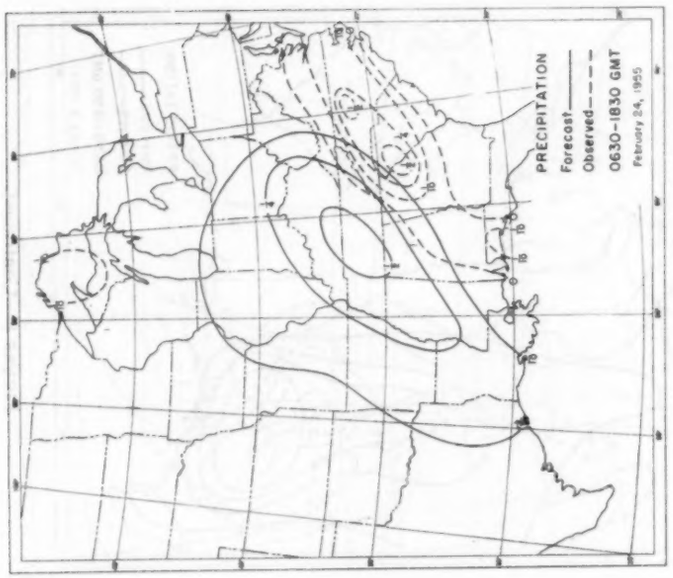

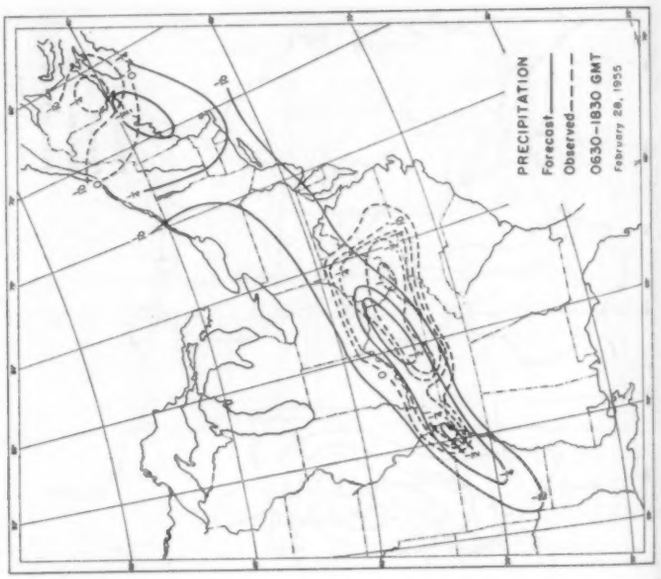

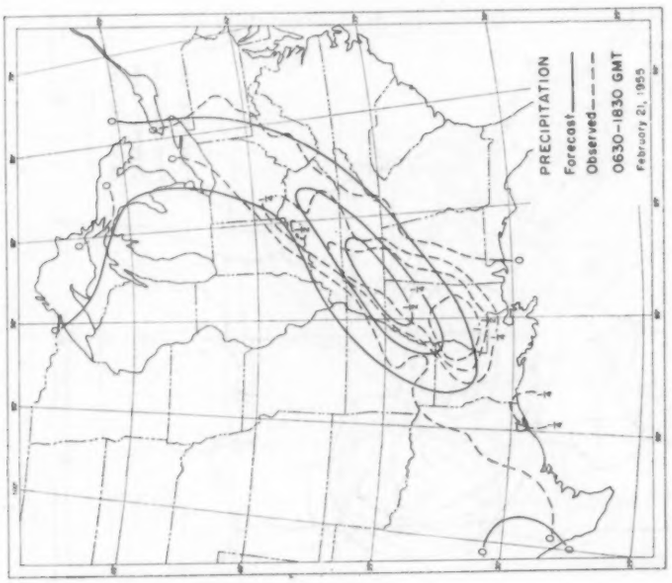

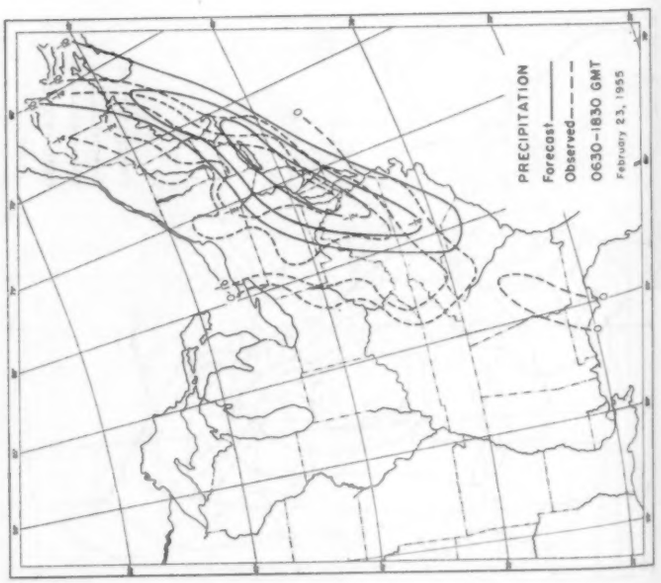

FIGURE 6—Continued.

the forecasts must be attributed to carrying out a systematic program of operations for treating the moisture in depth, and the use of such a program is commended to every meteorologist concerned with the forecasting of rainfall.

ACKNOWLEDGMENTS

The author is indebted to: Dr. Charles S. Gilman for fostering the interest in and environment for study of applications of dynamic concepts to the rainfall problem; Vance A. Myers for developing the geostrophic transport concept in application to synoptic climatology of rainfall, and for many suggestions which kept this work within manageable limits, and for monitoring the forecast experiment; Dr. Smagorinsky and Mr. Collins for their comments (see p. 57) elucidating the interpretation of the experimental results; A. E. Brown for his interest and facility in processing data for the daily forecasts; also Robert Frazier and James L. Keister for preparation of rainfall and moisture data.

REFERENCES

1. J. C. Thompson and G. O. Collins, "A Generalized Study of Precipitation Forecasting. Part 1: Computation of Precipitation From the Fields of Moisture and Wind," *Monthly Weather Review*, vol. 81, No. 4, April 1953, pp. 91–100.
2. Jerome Spar, "A Suggested Technique for Quantitative Precipitation Forecasting," *Monthly Weather Review*, vol. 81, No. 8, August 1953, pp. 217–221.
3. J. Smagorinsky and G. O. Collins, "On the Numerical Prediction of Precipitation," *Monthly Weather Review*, vol. 83, No. 3, March 1955, pp. 53–68.
4. Hydrometeorological Section, U. S. Weather Bureau, "Maximum Possible Precipitation over the Sacramento Basin of California," *Hydrometeorological Report* No. 3, 1943.
5. Hydrometeorological Section, U. S. Weather Bureau, "Revised Report on Maximum Possible Precipitation, Los Angeles Area, California," *Hydrometeorological Report* No. 21B, May 1945.
6. George S. Benton and Mariano A. Estoque, "Water-Vapor Transfer over the North American Continent," *Journal of Meteorology*, vol. 11, No. 6, December 1954, pp. 462–477.
7. Hydrometeorological Section, U. S. Weather Bureau, "Meteorology of Precipitation Storms of Flood-Producing Proportions in the Mississippi Basin," *Hydrometeorological Report* No. 34, 1956.
8. James F. Appleby, "Trajectory Method of Making Short Range Forecasts of Differential Temperature Advection, Instability, and Moisture," *Monthly Weather Review*, vol. 82, No. 11, November 1954, pp. 320–334.
9. Lynn L. Means, "On Thunderstorm Forecasting in the Central United States," *Monthly Weather Review*, vol. 80, No. 10, October 1952, pp. 165–189.
10. A. K. Showalter, "An Approach to Quantitative Forecasting of Precipitation," *Bulletin of the American Meteorological Society*, vol. 25, No. 4, April 1944, pp. 137–142.
11. A. K. Showalter, "An Approach to Quantitative Forecasting of Precipitation (II)," *Bulletin of the American Meteorological Society*, vol. 25, No. 7, September 1944, pp. 276–288.
12. A. K. Showalter, "An Approach to Quantitative Forecast of Precipitation (III)," *Bulletin of the American Meteorological Society*, vol. 31, No. 1, January 1950, pp. 23–25.
13. A. K. Showalter, "Quantitative Determination of Maximum Rainfall," *Handbook of Meteorology*, Berry, Bollay, and Beers, Ed., McGraw-Hill, 1945, pp. 1015–1027.
14. Hydrometeorological Section, U. S. Weather Bureau, "Maximum Possible Precipitation Over the Ompompanoosuc River above Union Village, Vermont," *Hydrometeorological Report* No. 1, 1943.
15. Hydrometeorological Section, U. S. Weather Bureau, "Maximum Possible Precipitation over the Ohio River Basin above Pittsburgh, Pa." *Hydrometeorological Report* No. 2, 1942.
16. U. S. Weather Bureau, "Tables of Precipitable Water," *Technical Paper*, No. 14, 1951.
17. S. Solot, "Computation of Depth of Precipitable Water in a Column of Air," *Monthly Weather Review*, vol. 67, No. 4, April 1939, pp. 100–103.
18. Robert J. List, Editor, *Smithsonian Meteorological Tables*, Washington, D. C., 1951.
19. J. Q. Locklear, The Divergence of Moisture Transport, M. S. Thesis, New York University, 1952 (unpublished).
20. Charles S. Gilman, An Expansion of the Thermal Theory of Pressure Changes, ScD Thesis, Massachusetts Institute of Technology, 1949 (unpublished).
21. James E. Miller, "Intensification of Precipitation by Differential Advection", *Journal of Meteorology*, vol. 12, No. 5, October 1955, pp. 472–477.
22. U. S. Weather Bureau, *Radiosonde Compatibility Tests*, March 1952.
23. E. Hovmöller, "A Comparison Between Observed and Computed Winds with Respect to their Applicability for Vorticity Computations," *Tellus*, vol. 4, No. 2, May 1952, pp. 126–134.
24. J. M. Craddock, "Advective Temperature Changes in the 1,000–700 mb. and 700–500 mb. Layers," *Quarterly Journal of the Royal Meteorological Society*, vol. 77, No. 331, January 1951, pp. 51–60.

THE WEATHER AND CIRCULATION OF FEBRUARY 1956[1]

Including a Discussion of Persistent Blocking and Severe Weather in Europe

JAMES F. ANDREWS

Extended Forecast Section, U. S. Weather Bureau, Washington, D. C.

1. THE REVERSAL FROM EARLY WINTER

From December 1955 to January 1956 the large-scale circulation patterns over North America were remarkably persistent [1, 2]. In both months the controlling features were two deep troughs, one in the eastern Pacific, the other just off the Atlantic Coast. In February an abrupt reversal occurred as these troughs filled rapidly at middle and low latitudes, thus lengthening the wavelength and resulting in formation of a new trough in the central United States. The monthly mean 700-mb. chart (fig. 1) shows the first trough as only a relatively minor feature in the Gulf of Alaska, the second extending from middle latitudes of the western Atlantic into eastern Canada, and the new trough as a major feature from the Missouri Valley southwestward through Lower California.

The change in 700-mb. height anomalies associated with this transition in circulation pattern was very striking, as can be seen in figure 2 by noting the large areas of positive anomalous height change in the eastern Pacific and western Atlantic, separated by a band of negative change in the central United States. The magnitude of this circulation reversal is expressed statistically in table 1, which shows that the correlation coefficient between the height anomaly patterns in the area from 30° N. to 50° N. and 70° W. to 130° W. was negative from January to February, but positive from December to January.

Closely related to the circulation reversal was an abrupt change in weather from the regime of December and January to that of February. In the West mild, excessively rainy weather was replaced by cold, relatively dry weather; while the East experienced a change from cold, dry conditions to a mild and rainy regime. This can best be seen by comparing figures 3 and 4, which show the observed temperature and precipitation anomaly classes for the months of January and February 1956. In table 1 is given a summary of statistical measures of this reversal. From a count of 100 stations evenly distributed around the country it was found that 48 did not change by more than one class in temperature, while only 27 remained in the same precipitation class. These values

TABLE 1.—*Persistence measures of monthly mean anomalies in the United States during 1955–56 winter*

	Jan.-Feb.	Normal (1942–60)	Chance	Dec.-Jan.
700-mb. height (lag correlation)	−.52	.26	0	.42
Temperature (0 or 1 class change, percent)	48	71	59	82
Precipitation (0 class change, percent)	27	37	33	48

are appreciably less than expected by chance or the normal amount of persistence from January to February as found by Namias [3]. Especially striking is the contrast with the marked persistence from December to January as given in the last column of table 1 [1].

2. WEATHER AND CIRCULATION IN THE UNITED STATES

Temperatures in the western portion of the United States averaged below normal during February, with greatest departures in the eastern halves of Washington and Oregon (fig. 3A and Chart I-B). The source region for much of this cold air was Alaska and northwest Canada, where mean temperatures in the layer from the surface to 700 mb. averaged as low as 8° C. below normal for the month (fig. 5). This cold pool has been a persistent feature of this fall and winter; in fact, portions of Alaska have had below normal temperatures each month since February 1955. Stronger than normal northwesterly flow at 700 mb. between a deep subpolar Low and a strong mid-Pacific ridge (fig. 1), brought repeated outbreaks of this cold polar air into the West. Note the existence of northwesterly anomalous flow components in the lower troposphere from Alaska to Texas (figs. 1 and 6B) The coldest weather was observed during the first half of the month, occurring at a time when the mean ridge reached its strongest development off the Pacific Coast. During the period January 29-February 5, temperatures averaged 21° F. below normal in parts of eastern Washington, Oregon, and Idaho, and 18° F. below normal in western Texas [4].

The subnormal temperatures throughout the West produced few records. It was, however, the coldest February ever observed at Fresno, Calif., and the second

[1] See Charts I–XV following p. 85 for analyzed climatological data for the month.

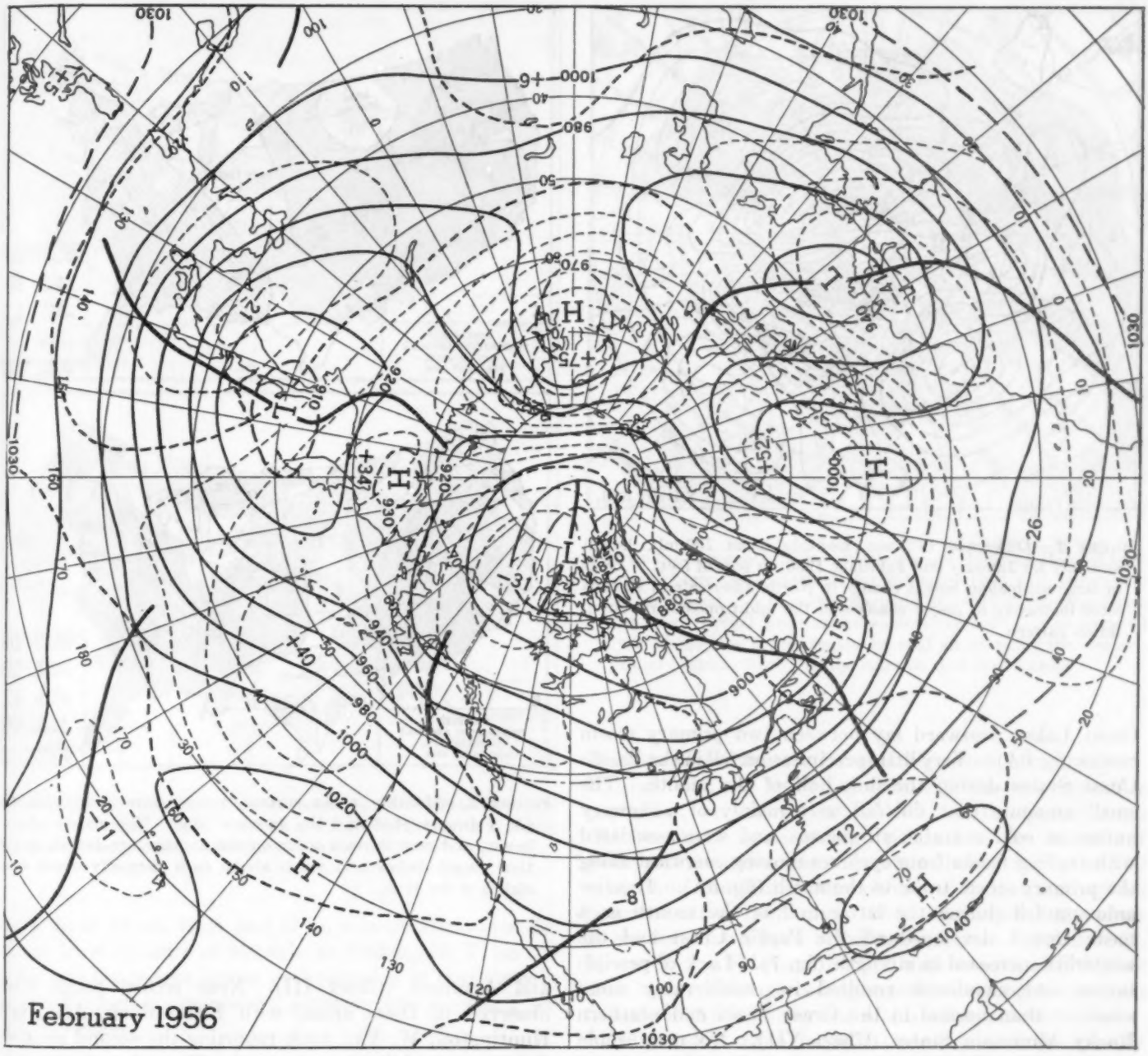

FIGURE 1.—Mean 700-mb. height contours (solid) and departures from normal (dashed) (both in tens of feet) for February 1956. Extensive bands of positive anomaly at higher latitudes and negative anomaly at lower latitudes were typical of a low index circulation pattern. Stong blocks were located in the North Atlantic and Eurasia.

coldest at Reno, Nev. New daily minimum temperature records were set during the month in parts of Oregon, Washington, and in eastern portions of the Dakotas and Colorado. At Yuma, Ariz., the monthly mean minimum temperature was the second lowest in 77 Februarys.

Mild weather with above normal temperatures prevailed in the eastern half of the United States (fig. 3A and Chart I-B) as a result of southwesterly flow at 700 mb. ahead of the trough in the central part of the country. Note especially the southerly anomalous flow at both 700 mb. (fig. 1) and sea level (fig. 6B). Greatest temperature departures were observed in the Southeast where the thickness anomaly (fig. 5) was also largest. Miami, Fla., had the warmest February day it has ever experienced with 85° F. on the 28th, while Augusta, Ga., reported a new high of 82° F. on the 19th.

The precipitation anomaly pattern in the West was rather chaotic, but in general subnormal amounts were observed (fig. 4A and Chart III). This resulted largely from lack of an adequate moisture source in northwesterly flow aloft to the rear of the mean trough in the central United States. In addition, the area from the

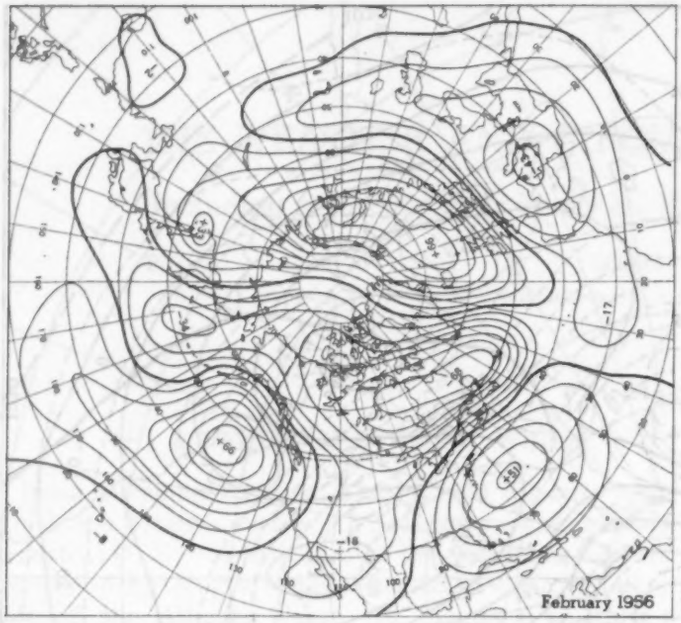

FIGURE 2.—Difference between monthly mean 700-mb. height anomaly for January and February 1956 (in tens of feet). Areas of large anomalous height change in North America and Eurasia were indicative of major changes in the mid-tropospheric circulation pattern.

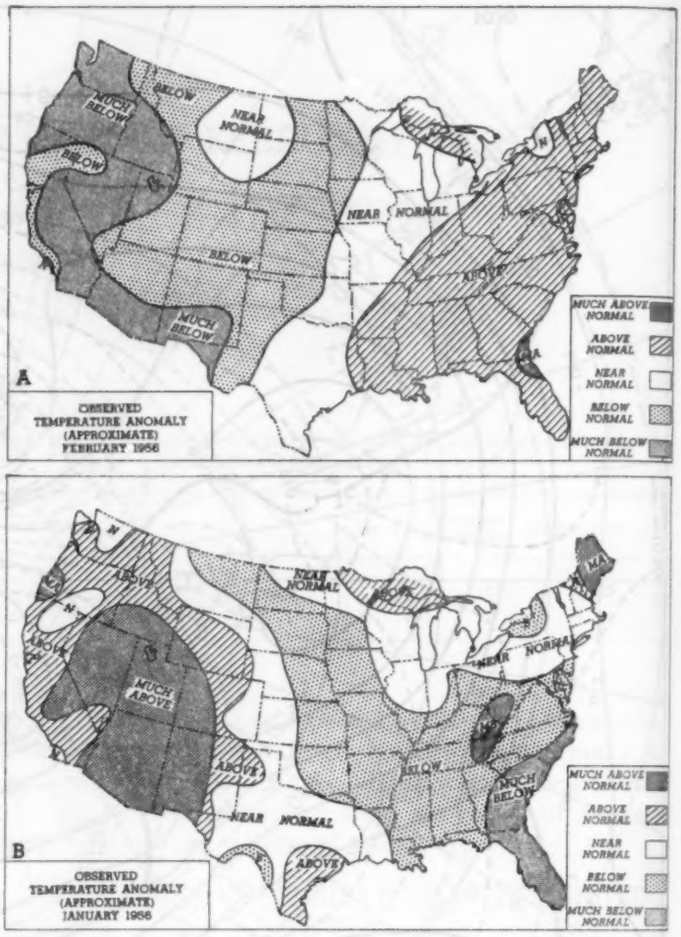

FIGURE 3.—Monthly mean surface temperature anomalies for (A) February 1956 and (B) January 1956. The classes above, below, and near normal occur on the average one-fourth of the time; much below and much above each normally occur one-eighth of the time.

Great Lakes westward lay between two primary storm tracks (fig. 6A). Very little precipitation fell in the Pacific Coast States during the first half of the month. The small amounts that did fall were mainly of a showery nature in cold unstable air masses, and were associated with trailing fronts from cyclones moving eastward along the primary storm track to the north (fig. 6A). Heavier amounts fell during the latter half of the month as a mean trough developed off the Pacific Coast and the westerlies increased in strength (fig. 7). Lack of precipitation and cloudiness resulted in considerably more sunshine than normal in the Great Basin and northern Rocky Mountain States (Chart VII). No measurable precipitation fell during the month at Las Vegas, Nev., the fourth such February in the last twenty.

Greater than normal amounts of precipitation in eastern Arizona, New Mexico, and the Texas Panhandle (Chart III and fig. 4A) were accompanied by a center of negative 700-mb. height anomaly in the mean trough (fig. 1). Most of this precipitation fell during a severe snowstorm from the 1st to the 5th, with as much as 15 inches in portions of southeastern New Mexico and the Texas Panhandle. Further details of this storm will be found elsewhere in this issue in an article by Brown and Brintzenhofe [5]. The total snowfall for the month (8.9 inches) at El Paso, Tex. was the greatest for any month of record.

From the Lower Mississippi Valley to New England precipitation was generally heavy (fig. 4A), with twice the normal amount falling in the Ohio Valley, Tennessee, and Arkansas (Chart III). Near record totals were observed in these areas, with Little Rock, Ark., and Huntington, W. Va., both reporting the second greatest February precipitation of record. These heavy amounts were related to southwesterly flow aloft east of the mean trough, and to southerly anomalous flow components advecting Gulf moisture northeastward. The primary storm track (fig. 6A) was close to the axis of heaviest precipitation and just to the north of the 700-mb. jet stream (fig. 8) in the area of maximum cyclonic shear.

What proved to be the worst storm of the month first entered the North Pacific States on the 22d. This storm system deepened rapidly as it swept eastward, bringing with it a variety of weather: a severe dust storm in the Southern Plains States, tornadoes and associated thunderstorms and hail in Missouri, Illinois, and Indiana, and freezing drizzle in Minnesota and Wisconsin. Winds of gale force and near record speeds in some areas accompanied the storm from the Rockies to the Atlantic Coast, with gusts reaching 88 m. p. h. at Amarillo, Tex., 84

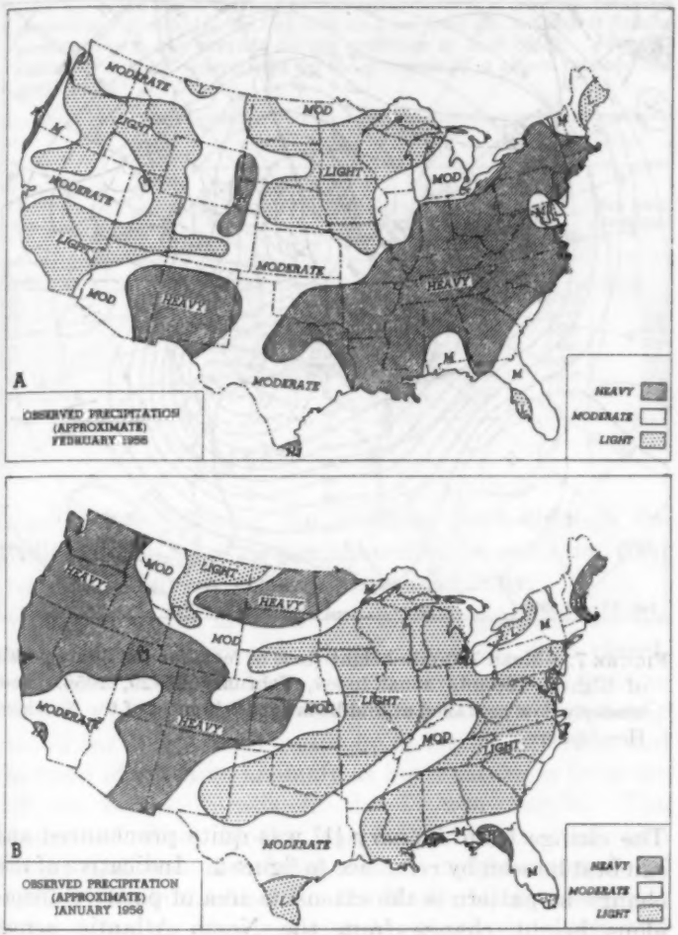

FIGURE 4.—Monthly precipitation anomalies for (A) February 1956 and (B) January 1956. The classes light, moderate, and heavy each normally occur one-third of the time.

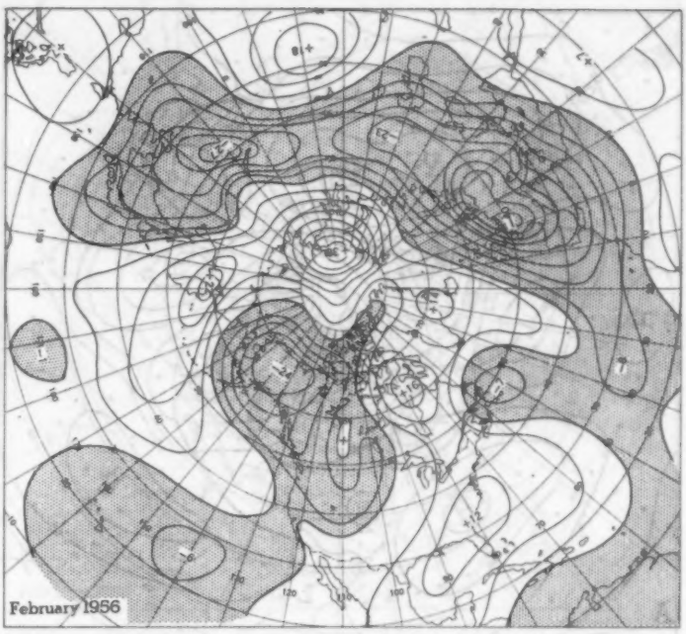

FIGURE 5.—Departure from normal of mean thickness (tens of feet) for the layer 700–1,000 mb. for February 1956 with subnormal values shaded. A thickness anomaly of −240 ft. corresponding to a mean virtual temperature anomaly of −8° C. was centered over Alaska, the source region for cold air invading the western United States. Note also the extreme cold over Europe.

m. p. h. at Akron, Ohio, and 87 m. p. h. at Allentown, Pa. A sea level pressure of 972 mb. at Buffalo, N. Y. on the 25th was the second lowest ever recorded at that station, while Rochester's minimum pressure was a record for any February.

3. INDEX TRENDS

The unusual behavior of the zonal index has been the subject of considerable discussion in the past few articles of this series [1, 2, 6, 7]. This index is a measure of the mean geostrophic west wind speed, expressed in meters per second, between latitudes 35° N. and 55° N. for the Western Hemisphere. Its monthly mean values at both 700 mb. and sea level, together with the corresponding anomalies, are shown in table 2 for the period from October 1955 to February 1956. For the month of February the index was 1.2 m. p. s. below normal at 700 mb., thus continuing the period of subnormal values observed since November 1955. Corresponding values at sea level have been below normal since October 1955. However, the February indices were considerably higher than those of the preceding month as strong blocking in Canada and the Bering Sea almost disappeared.

TABLE 2.—*Monthly zonal indices and departures from normal (m. p. s.). Negative indices represent net east-west flow*

	Western Hemisphere				Eastern Hemisphere			
	700 mb.	Anomaly	Sea level	Anomaly	700 mb.	Anomaly	Sea level	Anomaly
October	9.8	+0.3	3.3	−0.2	6.2	−0.2	−0.9	−1.1
November	8.9	−1.6	2.1	−2.0	8.2	+.4	.1	−.4
December	10.1	−1.2	2.9	−1.4	10.9	+2.9	1.8	+1.6
January	6.6	−5.2	0.0	−4.1	7.3	+.1	−1.1	−.8
February	9.0	−1.2	1.9	−1.5	5.3	−1.8	−4.1	−3.3

On a 5-day mean basis the zonal index rose rapidly after mid-month, reaching a value of 10.2 m. p. s. at 700 mb. for the period February 22–26, 1956. This was the first 5-day mean index above normal since October 22–26, 1955. The index continued to rise rapidly during the following week to a peak value of 14.4 m. p. s. (4.8 m. p. s. above normal) during the period February 29–March 4, 1956. The principal contribution to increasing westerlies at this time was relaxation of blocking in the North Atlantic. This is well illustrated by the 700-mb. chart for the period February 25–29 shown in figure 7.

The preceding has pertained to the Western Hemisphere index only. Similar values computed for the Eastern Hemisphere evidence quite a different trend. Table 2 shows that during November, December, and January subnormal values of the 700-mb. zonal index in the Western Hemisphere were accompanied by above normal values in the Eastern Hemisphere. Furthermore, from

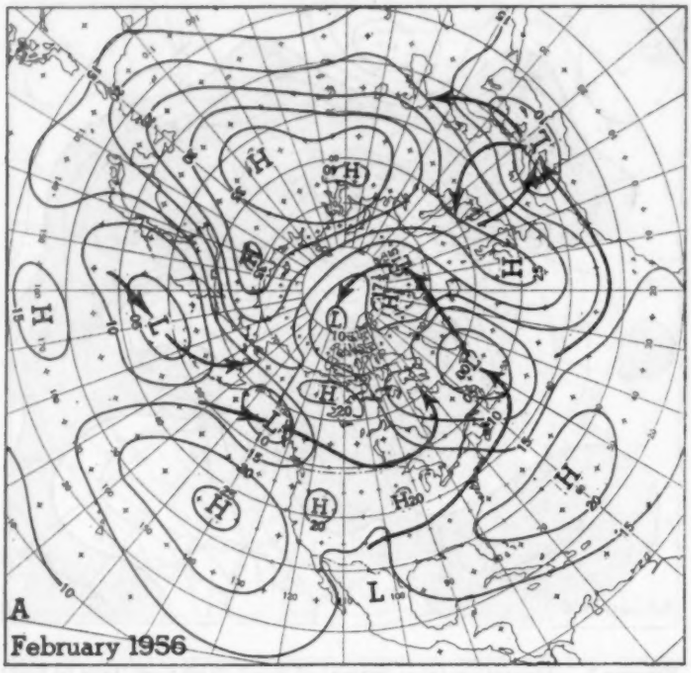

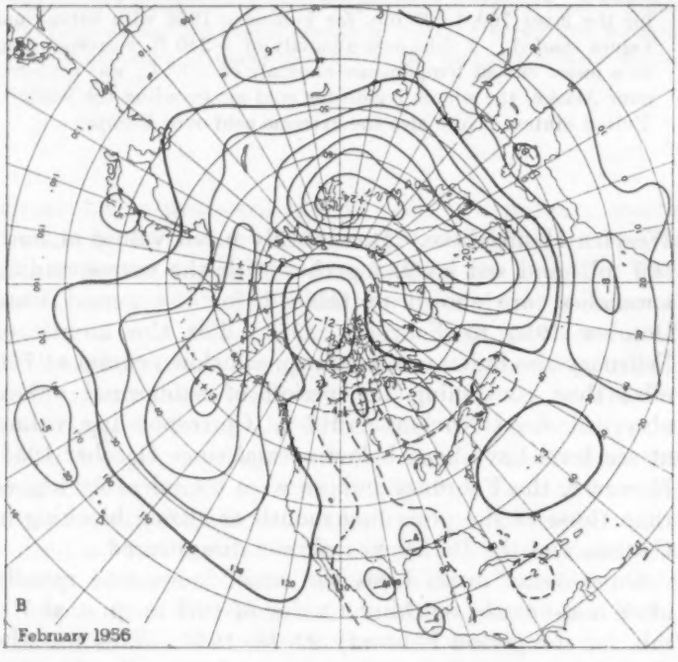

FIGURE 6.—(A) Mean sea level isobars and (B) departures from normal (both in millibars) for February 1956. Solid arrows in (A) indicate primary storm tracks as deduced from a plot of the daily Low positions.

January to February the index at both sea level and 700 mb. increased sharply in the Western Hemisphere, but declined abruptly in the Eastern Hemisphere. This was the culmination of a gradual change in the circulation of the Eastern Hemisphere from a high index, zonal-type pattern in December [2], to a meridional, low-index-type pattern during February. Both 700-mb. and sea level indices were far below normal in February, with a value of −4.1 m. p. s. at sea level indicating strong easterly flow.

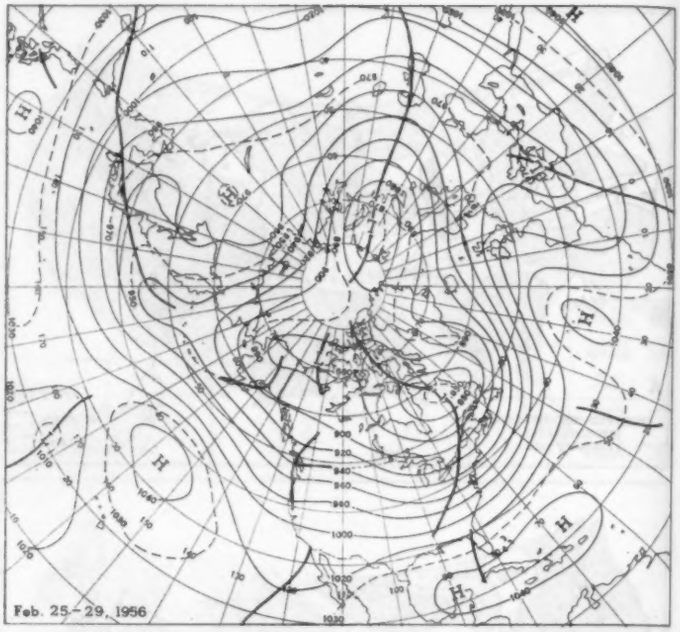

FIGURE 7.—Mean 700-mb. height (tens of feet) for the 5-day period of highest 700-mb. zonal index, February 25–29, 1956. Fast westerly flow prevailed at middle latitudes in most of the Northern Hemisphere.

The change from January [1] was quite pronounced and can best be seen by reference to figure 2. Indicative of this change in pattern is the extensive area of positive anomalous height change from the North Atlantic across northern Eurasia, along with negative changes at lower latitudes. Thus, it would appear that regional considerations are necessary when one attempts to relate the circulation pattern to the hemispheric index, as recently emphasized by Klein [8].

4. ATLANTIC AND EURASIAN BLOCKING

One of the most pronounced and persistent blocking patterns ever to occur in the North Atlantic and Eurasian continent was observed during February 1956. The features commonly associated with blocking were all evident to a rather marked degree on the monthly circulation charts. For example, the jet stream at 700 mb. showed a pronounced split in mid-Atlantic, with one current flowing northward into polar regions, and the other southeastward across North Africa (fig. 8A). Both currents had wind speeds considerably above the normal (fig. 8B). At sea level the Siberian anticyclone was considerably stronger than normal and displaced to the northwest (fig. 6). Surface pressures were much above normal across all of northern Eurasia and the North Atlantic, with greatest departures near the two major blocking centers. Two primary storm tracks were observed, one following the jet stream north of the blocked area, the other paralleling the southern branch of the jet (figs. 6A and 8A). Those systems passing to the north were somewhat weaker than normal for February, while

TABLE 3.—*Maximum intensities of the Eurasian and Atlantic blocking centers at 700 mb. (in tens of feet) and sea level (in millibars) for the overlapping 5-day periods during existence of each block. Identification of a block determined by the presence of a closed anticyclone north of 45° N.*

Period	Eurasian center			Atlantic center		
	700 mb.		Sea level pressure	700 mb.		Sea level pressure
	Height	Anomaly		Height	Anomaly	
Jan. 28–Feb. 1	992	+850	1044			
Feb. 1–5	997	+970	1044	1,021	+300	1037
Feb. 4–8	1,010	+1150	1048	1,032	+710	1038
Feb. 8–12	1,026	+1300	1059	1,025	+920	1035
Feb. 11–15	1,029	+1300	1062	1,002	+680	1028
Feb. 15–19	1,056	+1470	1065	999	+500	1026
Feb. 18–22	1,015	+850	1049	1,013	+950	1033
Feb. 22–26				1,002	+630	1030

those storms following the southern track through the Mediterranean were deeper than normal, reaching their greatest intensity in the mean Low near Italy.

Three separate and distinct blocks appeared on the mean 700-mb. chart (fig. 1), all associated with closed, warm anticyclones. Note the extensive area of positive 700-mb. height anomaly extending almost completely around the Northern Hemisphere at higher latitudes, and the band of negative anomaly at lower latitudes from the Atlantic across Eurasia to the western Pacific. The weakest of these blocks was located in northeastern Siberia and was associated with a height anomaly of +340 ft., while the blocks in the North Atlantic and near Novaya Zemlya were associated with strong ridges and height anomalies of +520 ft. and +750 ft., respectively. The latter is the greatest positive 700-mb. height anomaly ever to occur in Eurasia on a monthly mean chart during our period of record (1948–56).

It is of interest to discuss the two major blocks on a 5-day mean basis. For this purpose blocking was defined as the presence of a closed anticyclone north of 45° N. In table 3 is given the maximum intensity of each blocking center at 700 mb. and sea level, along with the maximum 700-mb. height departure from normal, for the overlapping 5-day periods beginning with the inception of each block. The Eurasian block was the more stable of the two, moving very little while growing steadily to a maximum intensity of 10,560 ft. at 700 mb. and 1065 mb. at sea level, on February 15–19. The associated 700-mb. height anomaly, +1,470 ft., has been exceeded only once in the entire Northern Hemisphere during our period of record (1945–56). That occurred on February 19–23, 1947 when an anomaly of +1,600 ft. was observed in Baffin Bay during another period of pronounced blocking [9]. The intensity of the Atlantic block was more erratic in nature, passing through two cycles on a 5-day mean basis. It disappeared on February 26, while the Eurasian block existed until February 23. The duration of these blocks, 24 days and 27 days, respectively, is considerably longer than the average duration of 16 days for a winter block as noted by Rex [10].

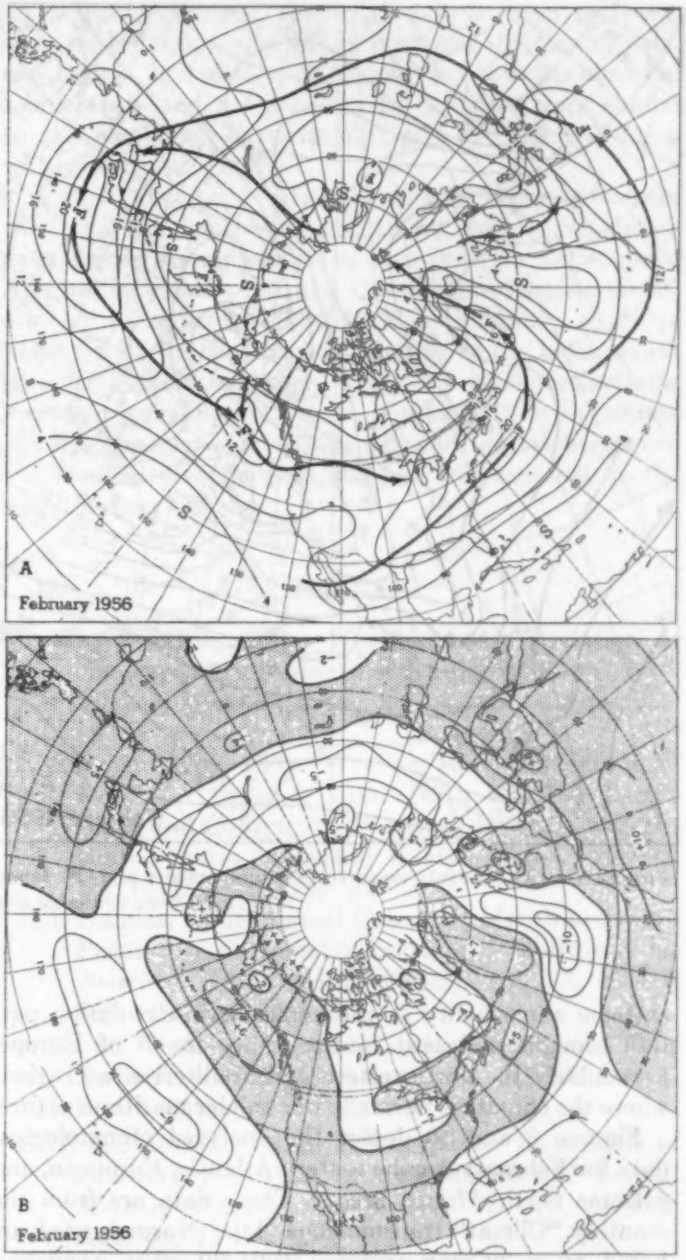

FIGURE 8.—(A) Mean 700-mb. isotachs and (B) departure from normal wind speed (both in meters per second) for February 1956. Solid arrows in (A) indicate position of the primary jet axes. "F" refers to centers of fast wind speeds; "S" to centers of slow winds. Areas of above normal wind speeds in (B) are shaded. Note the strong jet in the western Atlantic and its split into two branches by the North Atlantic block.

5. EUROPEAN WEATHER

Undoubtedly the most outstanding weather item of the month was the persistent and severe cold observed over the entire European Continent. The cold wave, described as the worst of the century in many areas, was closely related to the pronounced blocking in the North Atlantic and Eurasia, described in the previous section. This

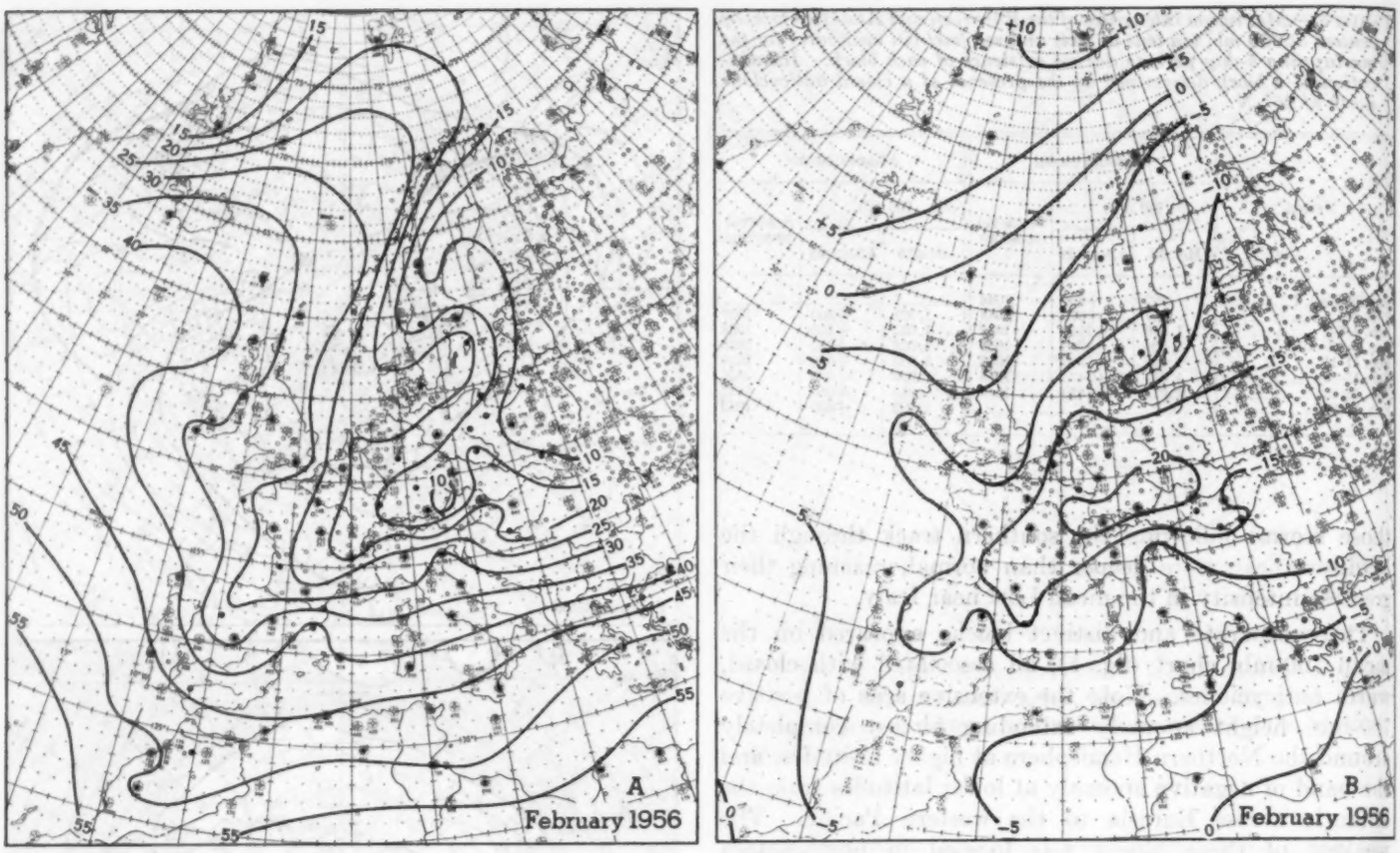

FIGURE 9.—(A) Monthly mean surface temperature and (B) departure from normal (both in °F.) for February 1956. Stations for which data were available are indicated by the solid dots.

extreme abnormality in the hemispheric circulation pattern brought increased continentality to all of Europe, particularly the northwestern and Mediterranean regions where the climate is normally of a milder maritime nature.

Figures 9 and 10 depict the analyzed climatological data for February for the eastern Atlantic, European, and extreme north African areas. These data are from the monthly "Climat" transmissions [11]. Normals used are based on a 30-year average (1901–30 when available) and are computed by the individual stations. They are considered as standard by the World Meteorological Organization. For the stations where normals based on this period or another 30-year period were not available, reference was made to Clayton [12] and Kendrew [13].

Figure 9B shows that temperatures averaged far below normal for the month over all of Europe. Greatest departures were observed in eastern France, southern Germany, Switzerland, and Austria where temperatures were as much as 20° F. below normal. Zurich, Switzerland, reported the greatest anomaly, a mean temperature of 24° F. below normal. In Paris, France a temperature of 9° F. was a record low for the second half of February, while Berlin, Germany had its coldest February 24 (−4° F.) in 125 years. Extreme temperatures of −40° F. were reported from northern Sweden and −45° F. near the Swiss-Italian frontier.

It is well known that easterly flow brings to Europe its coldest winter weather. Thus it is not surprising to find that stronger than normal easterly components prevailed at both sea level (fig. 6) and 700 mb. (fig. 1), across the entire Eurasian Continent. These east winds advected cold continental air masses from a region that is normally very cold during the winter—Russia and the Siberian Plain. In most of this area, temperatures in the layer from the surface to 700 mb. averaged below normal for the month (fig. 5). As examples of this intense cold, Verkhoyansk, in eastern Siberia, recorded one of the world's lowest temperatures (possibly a record) when a minimum of 102° F. below zero was recorded late in January 1956; while Moscow, Russia reported a temperature of −49° F. on January 31 [14]. Figure 5 shows that the center of this anomalously cold air was located in France, where a thickness anomaly of −400 ft. corresponded to a mean virtual temperature of 24° F. below normal.

To the west of the Atlantic block strong southerly flow at middle and lower levels (figs. 1, 6, 8) advected warm maritime air northward, resulting in a pronounced distortion of the mean isotherms (fig. 9). At Spitzbergen the temperature averaged 12° F. above normal for the month. The greatest temperature anomaly was associated with the Eurasian block, where a thickness

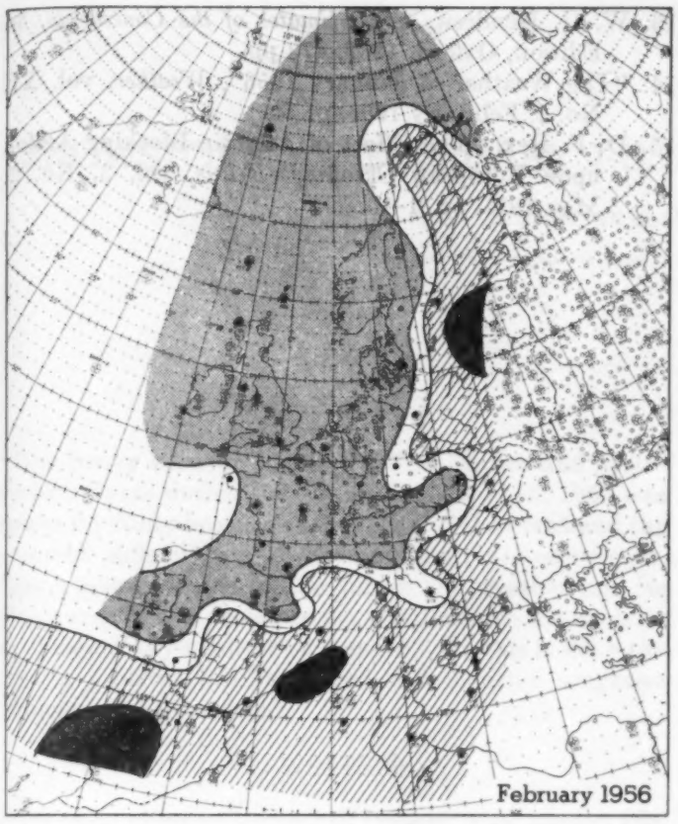

FIGURE 10.—Precipitation anomaly for February 1956. Data used in this analysis were the quintiles of the frequency distribution in which the monthly precipitation totals fell. To simplify the analysis quintiles 1 and 2 were combined into a single below normal class indicated by light shading, while quintiles 4 and 5 were combined into a single above normal class shown by the hatched areas. Unshaded portions are near normal (quintile 3) and darker shaded areas indicate a 30-year record. Stations for which data were available are indicated by the solid dots.

anomaly of +380 ft. in the polar regions corresponds to a mean virtual temperature of 23° F. above normal (fig. 5).

Less than normal precipitation fell in Great Britain and western Europe (fig. 10). This relatively dry weather was related to the prevalence of continental air masses in northeasterly flow, surface and aloft; lack of an adequate moisture source; and a deficiency of cyclonic activity. Greater than normal amounts of precipitation fell in eastern Europe and in regions bordering the Mediterranean Sea, with a few areas reporting the greatest amount for the 30-year period upon which their normal is based. This precipitation, much of it in the form of snow, was associated with the mean trough extending from eastern Europe to northwestern Africa (fig. 1), and with migratory cyclones following the primary storm track through the Mediterranean (fig. 6A). Somewhat weaker storms moving along the track from the North Sea southward produced little precipitation until they deepened over the warm waters of the Mediterranean. Snow covered the French Riviera for the first time in 15 years when a fall of 16 inches occurred, the heaviest in memory. Heavy, near record snows also fell in Portugal, northern Spain, and Italy. It is of interest to point out that the observed temperature and precipitation patterns are very similar to the composite patterns obtained by Rex [15] for a winter block.

A rapid reversal of climatic regimes occurred toward the end of the month as the prevailing easterly circulation gave way to strong westerlies, thus bringing warm, moist Atlantic air masses into the Continent. Heights at 700 mb. fell as much as 1,700 ft. from February 15–19 to February 25–29 near Novaya Zemlya as the block weakened and sank to lower latitudes. Cyclonic activity increased and followed a more normal path in the northeastern Atlantic, and, at month's end, an intense storm with central pressure near 965 mb. was centered on the Scandinavian coast.

REFERENCES

1. W. H. Klein, "The Weather and Circulation of January 1956—A Month with a Record Low Index", *Monthly Weather Review*, vol. 84, No. 1, Jan. 1956, pp. 25–34.
2. J. F. Andrews, "The Weather and Circulation of December 1955—A Month with a Major Pacific Block and Contrasting Extremes of Weather in the United States," *Monthly Weather Review*, vol. 83, No. 12, Dec. 1955, pp. 327–335.
3. J. Namias, "The Annual Course of Month-to-Month Persistence in Climatic Anomalies," *Bulletin of the American Meteorological Society*, vol. 33, No. 7, Sept. 1952, pp. 279–285.
4. U. S. Weather Bureau, *Weekly Weather and Crop Bulletin, National Summary*, vol. XLIII, No. 6, Feb. 6, 1956.
5. H. E. Brown and R. A. Brintzenhofe, "Snowstorm of February 1–5, 1956, in New Mexico and Texas," *Monthly Weather Review*, vol. 84, No. 2, Feb. 1956, pp. 75–85.
6. C. M. Woffinden, "The Weather and Circulation of November 1955—A Month with Pronounced Blocking and Extreme Cold," *Monthly Weather Review*, vol. 83, No. 11, Nov. 1955, pp. 272–278.
7. C. R. Dunn, "The Weather and Circulation of October 1955—A Month with a Double Index Cycle," *Monthly Weather Review*, vol. 83, No. 10, Oct. 1955, pp. 232–237.
8. W. H. Klein, "The Central Role of the Height Anomaly in the Outlook for Long Range Weather Forecasting," *Transactions of the New York Academy of Sciences*, Series II, vol. 18, No. 4, Feb. 1956, pp. 375–387.
9. J. Namias, "Characteristics of the General Circulation over the Northern Hemisphere During the Abnormal Winter of 1946–47," *Monthly Weather Review*, vol. 75, No. 8, Aug. 1947, pp. 145–152.

10. D. F. Rex, "Blocking Action in the Middle Troposphere and its Effect upon Regional Climate," Parts I and II, *Tellus*, vol. 2, Nos. 3 and 4, Aug. and Nov. 1950, pp. 196–211 and 275–301.
11. U. S. Weather Bureau, *Monthly Climatic Data for the World*, vol. 9, No. 2, February 1956.
12. H. H. Clayton, "World Weather Records," *Smithsonian Miscellaneous Collections*, vols. 79, 90, 105, Smithsonian Institution, Washington, D. C., 1927, 1944, 1947.
13. W. G. Kendrew, *The Climates of the Continents*, 3d Edition, Oxford, 1937, 473 pp.
14. "The Weather of January 1956", *Weather*, vol. XI, No. 2, February 1956, p. 54.
15. D. F. Rex, "The Effect of Atlantic Blocking Action upon European Climate," *Tellus*, vol. 3, No. 2, May 1951, pp. 1–16.

SNOWSTORM OF FEBRUARY 1-5, 1956, IN NEW MEXICO AND TEXAS

H. E. BROWN and R. A. BRINTZENHOFE

National Weather Analysis Center, U. S. Weather Bureau, Washington, D. C.

1. INTRODUCTION

The heavy snowfall in eastern New Mexico and northwestern Texas during the period February 1–5, 1956 was chosen for study because of the rarity of the event and the apparent difficulty in forecasting such an occurrence. This article proposes to summarize the weather and its effects and then to associate the weather with the analysis in an essentially qualitative manner. As this is done the forecast problem will be defined and then the prognosis problem will be discussed.

2. WEATHER

The snowstorm which moved through New Mexico and the northwestern part of Texas may be divided into two sections. One was February 1–3 as the snowfall progressed north to south through New Mexico, and the other February 3–5 as the area of the snowfall remained rather stationary over the southeastern corner of New Mexico and part of northwestern Texas.

By 0030 GMT on February 1 rain was falling at Albuquerque and snow was reported through the northern part of the State, through Colorado, and into western Kansas. By 0330 GMT snow was beginning in the Texas Panhandle and was edging farther southward in New Mexico. By 0030 GMT on the 2d it was snowing in Mexico with the largest snowfall in western New Mexico and lesser amounts elsewhere, e. g., 5 inches at El Paso. Over in the Panhandle and the South Plains of northwestern Texas the snowfall was lighter with amounts ranging from a trace to 2 inches. As the snow moved down over the area, cold temperatures (see fig. 1) and winds with gusts of 30–50 knots were reported. The temperatures were generally in the lower 20's and the winds whipped the snow around to reduce the visibilities to near zero; a real blizzard had moved into the country. At this stage of the storm considerable hardship was experienced by people who lived in the vicinity of Albuquerque and southward to El Paso. The snow drifts closed highways and blocked city streets seriously handicapping travel.

By 1230 GMT of the 3d the snow had tapered off over the western part of New Mexico, but in an area roughly bounded by Wink-Lubbock-Amarillo-Tucumcari-Roswell-Wink, snow fell almost continuously until 0630 GMT, February 5. From then on until 0030 GMT, February 6 the snow gradually decreased from west to east. On the 3d the second part of the storm began as the biggest increase of snow was felt in the southeastern part of New Mexico and the snow both there and in Texas was wetter than that which had previously fallen in this area. On the 4th the biggest accumulation of snow was in the Panhandle and South Plains of Texas.

The snow depth broke records of 50 years duration, and the combination of snow, cold, and winds caused blizzard conditions and considerable hardship. At least 18 deaths were attributed directly to the storm. The normal life of the area was completely paralyzed during the storm and there were still transportation difficulties up through February 14. Highway travel was stopped as drifts blocked the roads and even intercity buses suspended operations after several buses were stranded and the passengers rescued by tractor.

At Clovis, N. Mex., the Santa Fe Railroad sent a special one-car train to pick up stranded motorists between Clovis and Hereford, Tex. The personnel at the Clovis Air Force Base did much to relieve the hardships of the stranded

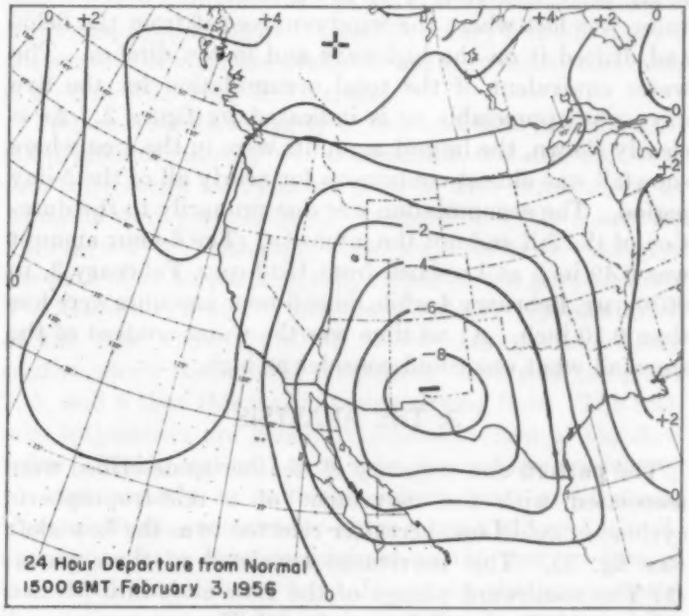

FIGURE 1.—24-hour 1,000–500-mb. departure from normal for 1500 GMT, February 3, 1956. Thickness lines give a good indication of the temperature field. (c. f., Kibler et al. [1]).

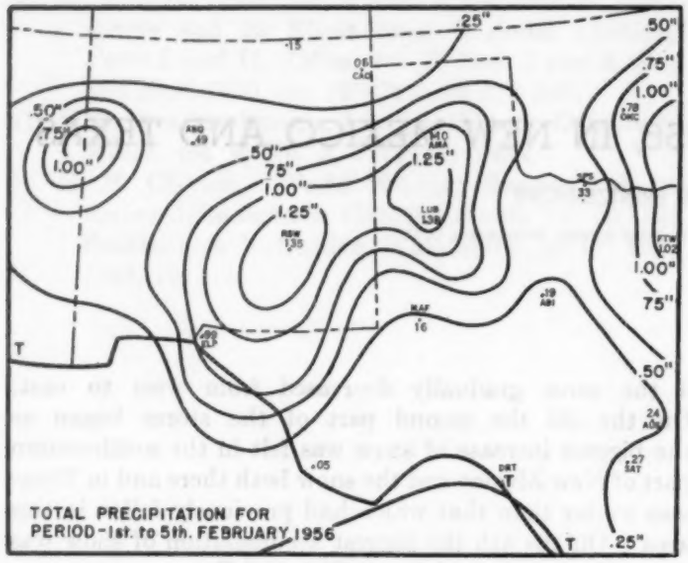

FIGURE 2.—Total-storm isohyetal map for the period February 1–5, 1956.

motorists by bringing them to the base for food and shelter until the highways were opened. A cross-country bus, stalled in a snow drift 9 miles from the Texas border, was without heat or food for its passengers. The driver fought his way through the snowstorm to arrive at the border town of Glenrio, "almost frozen", so he might get aid to the people in this bus. In the metropolitan centers of the region many stores were closed, schools shut down for the day on February 3, and many of the main streets were completely blocked by the accumulation of snow.

The snow gave promise of replenished soil moisture where it lay more uniformly over the ground, but much of its value was lost where the wind removed it from the fields and drifted it on the highways and in the ditches. The water equivalent of the total accumulation for the five days was appreciable as is indicated by figure 2. As is clearly shown, the largest amounts were in the area where snowfall was almost continuous for nearly all of the 5-day period. The accumulation was due primarily to the duration of the fall and not the intensity. The 6-hour amount was 0.49 inch at Lubbock from 1830 GMT, February 3, to 0030 GMT, February 4 while most 6-hour amounts were less than 0.10 inch. At no time was the water content of the snowfall what one could consider as high.

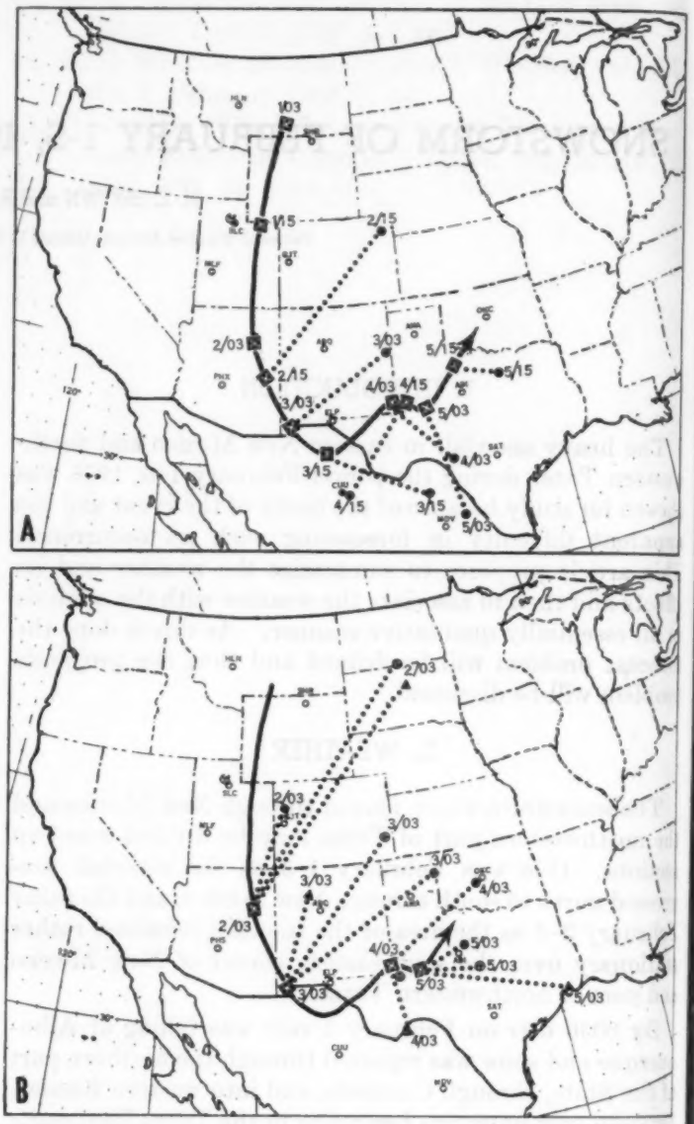

FIGURE 3.—(A) Comparison of the 500-mb. track of the cold Low with the positions as computed by use of the Wilson technique [15]. ⊠ = Observed track. ● = Position as given by the Wilson computation. (B) Comparison of the 500-mb. track of the cold Low with the positions as forecast by various methods. ⊠ Observed 24-hour positions. ● Positions as forecast by the 36-hour baroclinic prognostication (JNWP). ⊗ Positions as forecast by the 36-hour NWAC prognostication. ▲ Positions as forecast by the 48-hour barotropic prognostication (JNWP).

3. THE ANALYSIS

The pattern and sequence of weather as described were associated with the movement of a mid-tropospheric cyclone or cold Low, hereafter referred to as the Low aloft (see fig. 3). This movement consisted of three parts: (1) The southward plunge of the Low aloft into Mexico prior to 1500 GMT, February 3; (2) The movement and stagnation over northwestern Texas, 1500 GMT, February 3 to 0300 GMT, February 5; (3) The acceleration in an east-northeast direction after 0300 GMT, February 5. During part (1) the Low aloft filled some, e. g., the 17,800-ft. contour shrank to the size that the 17,600-ft. contour had earlier; and during part (2) the Low maintained its intensity. As the Low aloft moved southward, it was accompanied by a surface ridge coming southward to the east of the Rockies (fig. 4A). During parts (2) and (3) the surface circulation gradually changed to a more cyclonic flow and by 1230 GMT, February 4 (fig. 4B) the Low aloft nearly reached to the ground. The surface temperatures gradually rose during this weak cyclogenesis.

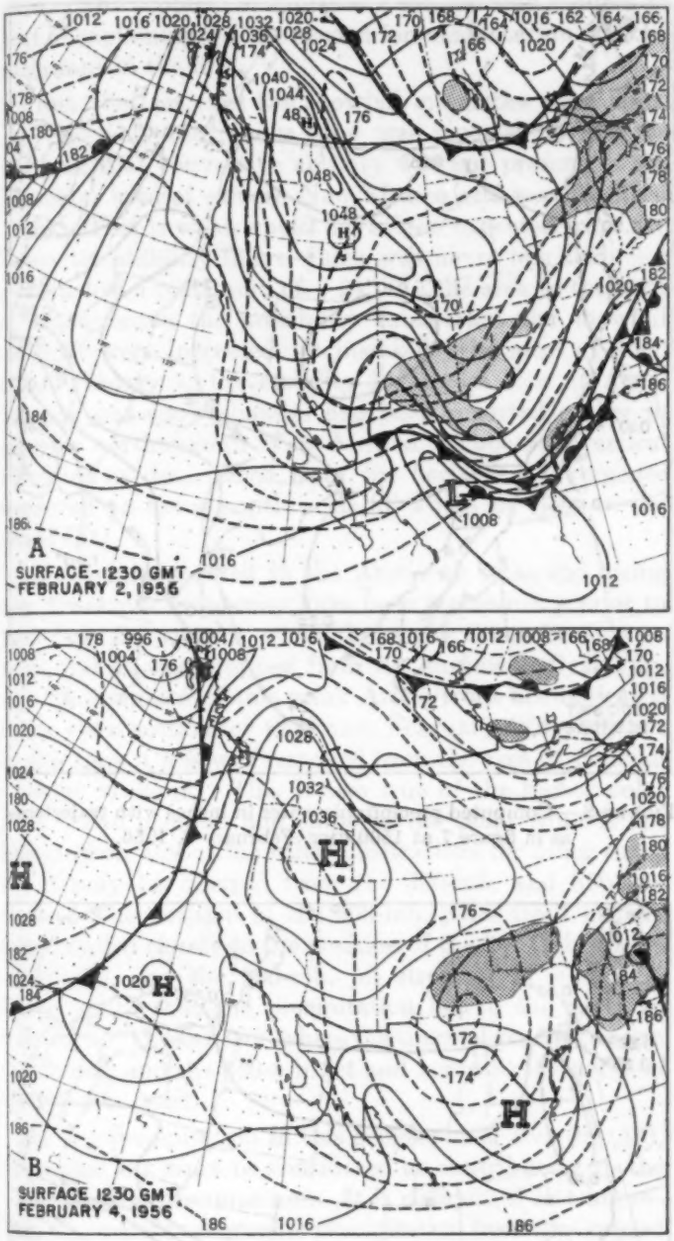

FIGURE 4.—Surface charts with the 1,000–500-mb. thickness (dashed lines) labeled in hundreds of feet. Shading shows areas of active precipitation. (A) 1230 GMT, February 2, 1956 (B) 1230 GMT, February 4, 1956.

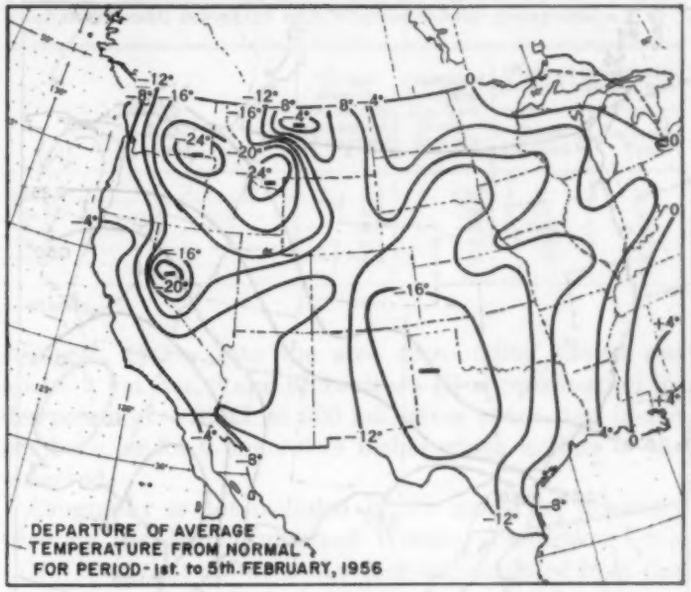

FIGURE 5.—Departure of average temperature from normal (° F.) for the week ending at midnight, local time, on February 5, 1956.

As the first step in examining the association of the weather with the Low aloft, the moisture supply that was available to the area was investigated by charting the precipitable water. By use of a template devised by Showalter [2] the amount of precipitable water in inches was read directly from the plot of the dew point curve on the plotted pseudoadiabatic diagrams. Throughout the period, the amount of precipitable water was rather evenly distributed vertically in all of the soundings in the area, with any appreciable decrease in the amount occurring above 500 mb. All soundings were evaluated from the surface to 400 mb. As would be expected from the cold surface temperatures that prevailed (fig. 5), the amounts of precipitable water were always small. A comparison of the precipitable water charts (figs. 6–9) shows little variation of precipitable water in the area of precipitation being considered here. In fact, the maximum amount of 0.46 inches was available at Amarillo on the 1st, when Amarillo had only a trace of snow. Between February 1 and 2 precipitable water decreased some as drier air came into the area from the north as the Low aloft and the Arctic front pushed southward. From February 3 to February 5 the amount of moisture available was very nearly constant, e. g., 0.24–0.30 inch at Amarillo.

To demonstrate the early drying and then how the constant moisture supply was maintained, 850-mb. and 700-mb. trajectories for 24 hours prior to their termination at Amarillo were plotted on the precipitable water charts for February 2–4. Although these trajectories do not give the path of an air particle, they suffice for the purpose here. The trajectories at 700 mb. are generally representative of the flow above 7,000 ft. which was predominantly southwesterly throughout the period. It is seen in figures 7, 8, and 9 that this was always a drying flow. The 850-mb. trajectories are generally representative of the flow below 7,000 ft. and with time they changed from northerly to more easterly so as to come from more moist areas. The relatively constant moisture supply above 7,000 ft. appears to have been maintained by the upward flow of moisture from the lower level. It appears that the increase in snow amounts on February 4 cannot be accounted for by just an increase in the moisture supply.

Since the freezing level throughout the period was at the ground, it was probable that condensation would result in

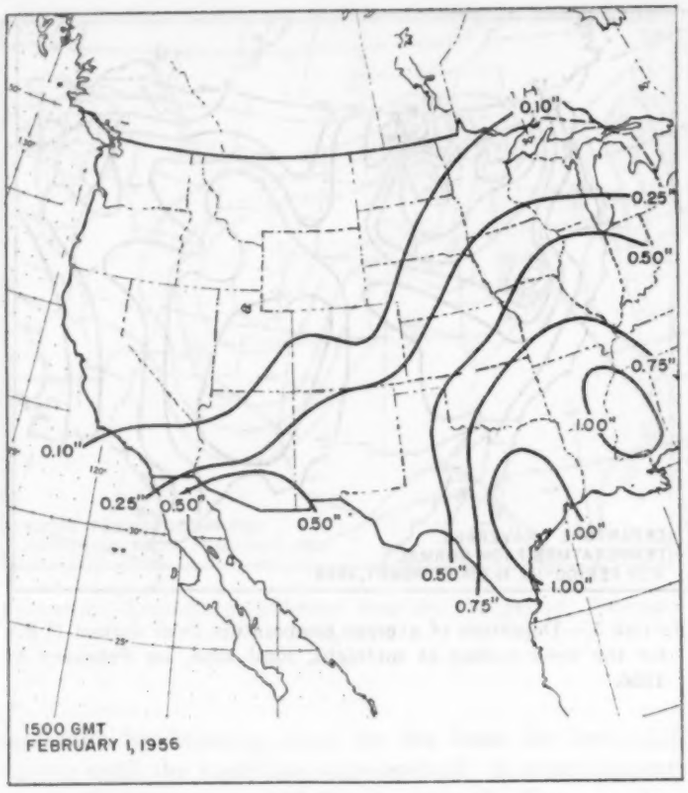

FIGURE 6.—Computed precipitable water in inches at 1500 GMT' February 1, 1956.

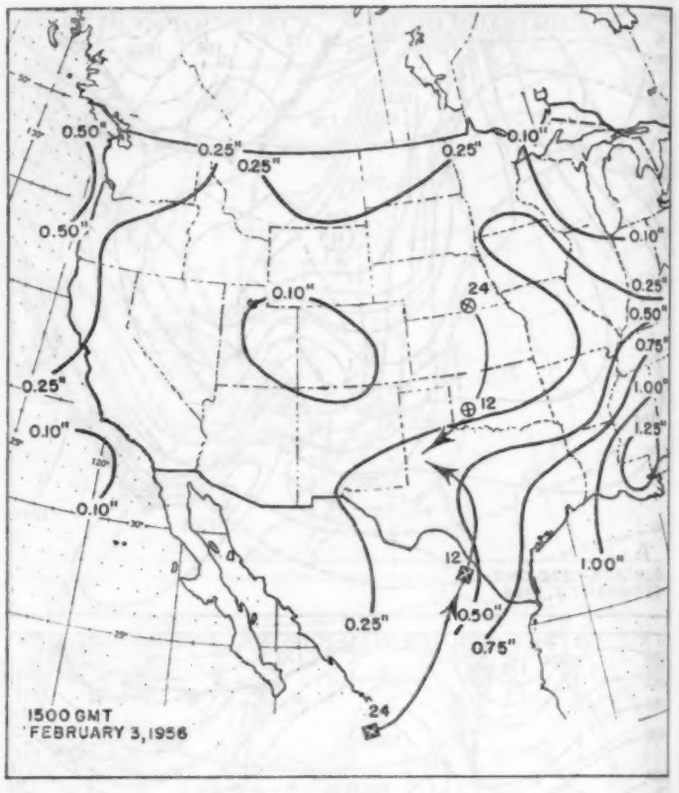

FIGURE 8.—Computed precipitable water in inches with trajectories as in figure 7 at 1500 GMT, February 3, 1956.

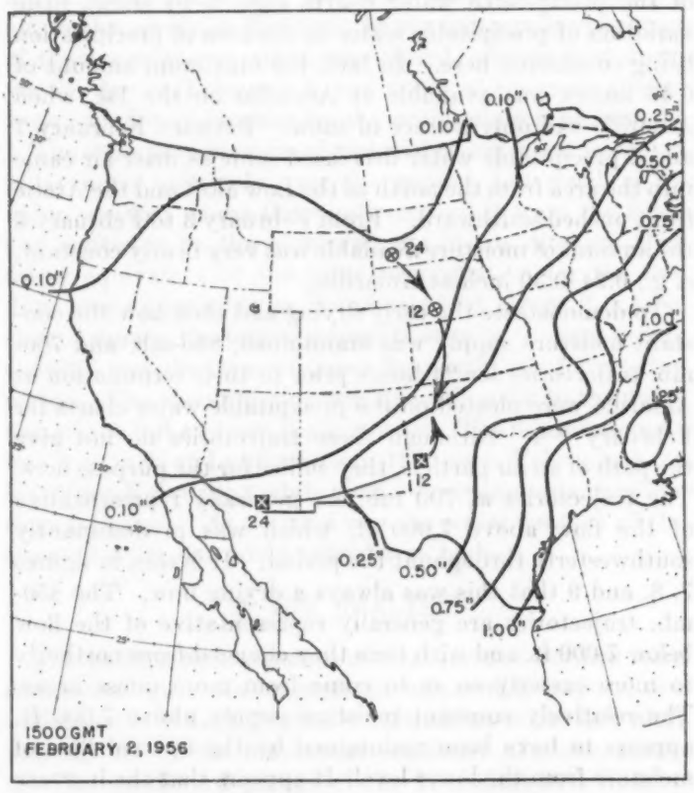

FIGURE 7.—Computed precipitable water in inches with ⊗ trajectories for the 850-mb. flow and ⊠ trajectories for the 700-mb. flow for 24 hours previous to termination at Amarillo at 1500 GMT, February 2, 1956.

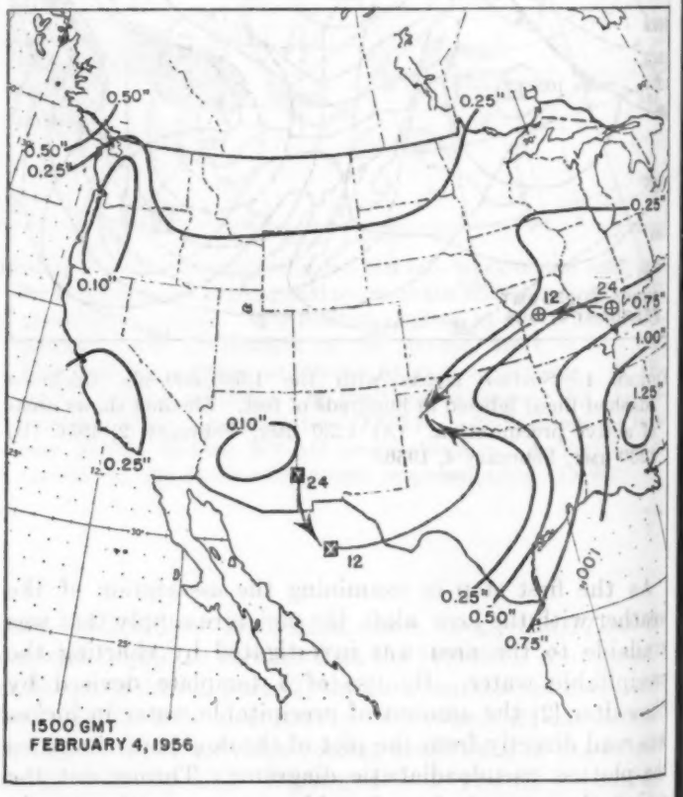

FIGURE 9.—Computed precipitable water in inches with trajectories as in figure 7 at 1500 GMT, February 4, 1956.

snow. The problem of explaining the snowfall reduces to that of explaining the lift needed for condensation and the variations in the lift.

From the fact that the snowfall intensities were light, and that only continuous snow was reported, it may be assumed that convective activity was not present in the particular area of eastern New Mexico and northwestern Texas. This is what would have been expected from the Showalter stability index which was never less than +9 and reached a maximum of +24. In the area to the west of Albuquerque the possibility exists that the snowfall amounts were increased by instability because at 1500 GMT, February 1, the stability index was zero at Albuquerque and snow showers had been reported earlier in extreme northwestern New Mexico. Thus the vertical velocities as determined from the horizontal divergence measured on the synoptic scale [3] would be close to the actual lift.

All precipitation fell in the Arctic air mass and lifting over the Arctic front may have been a possibility prior to 1230 GMT, February 2, when the Arctic front became so weak that it was dropped from the surface analysis (fig. 4). The remains of this weak Arctic front are indicated on the cross section for 1230 GMT, February 4 (fig. 10) but by this time it was well removed from the area of snowfall north of Midland. This is also true of the higher polar front. The position and slope of the polar front is not indicated on any of the other illustrations for other times but it may be inferred from the 500-mb. and 300-mb. charts. The position of the 500-mb. polar front usually corresponded closely to the position of the 20° C. isotherm at 500-mb. and the 300-mb. jet stream. It is seen in figures 11–15 that the precipitation fell to the north of both the 20° C. isotherm, where the thermal gradient began to increase, and the 300-mb. jet and hence to the north of the 500-mb. front.

For any precipitation in this geographical area (fig. 16), orographic lift must be considered as contributing to the total observed precipitation. It is difficult, if not impossible, to separate orographic precipitation from that caused by meteorological factors (see L. C. W. Bonacina [4]). For example, it is frequently observed that with surface isobars indicating upslope flow to the east of the Rockies, the actual winds blow at an angle greater than that required by frictional considerations and that the winds actually follow the topographic contours rather than the isobars. To have the wind more closely follow the isobaric contours and hence blow upslope, it appears that a meteorological mechanism is needed. On February 1 and 2, there was very little orographic lift as the low-level flow was very nearly parallel to the topographic contours. But on February 3, the upslope flow increased as the wind speeds increased and as the flow became more nearly normal to the topographic contours. The upslope flow reached a maximum on the 4th and decreased on the 5th to nearly the same as on the 3d. This trend agrees well with the trend in precipitation amounts given in table 1. The

TABLE 1.—*Computed vertical velocities and calculated 6-hour precipitation amounts compared with observed 6-hour precipitation*

1500 GMT	Vertical velocity 700–400 mb. cm. sec.$^{-1}$ (+ upward)	Calculated precipitation for 6 hours (inches)	Observed precipitation (inches) 1230–1830 GMT	
			Clovis, N. Mex.	Lubbock, Tex.
Feb. 1	2.7	0.00	T	T
Feb. 2	1.5	.04	(1)	T
Feb. 3	5.0	.03	0.05	0.02
Feb. 4	3.8	.00	.19	.06
Feb. 5	−1.5	.00	.02	.04

[1] Missing.

strongest upflow into the area surrounding Clovis was about 2 cm. sec.$^{-1}$ and Showalter's [5] approximation for dewpoints of −8° C. at 900 mb. gives about 0.04 inches per hour, or for 6 hours 0.24 inches which is close to the observed.

Orography is not included in the model [6] presently used by the Joint Numerical Weather Prediction Unit, (JNWP) so that the vertical velocities calculated from this model do not include the initial vertical velocities that are due to upslope over the terrain. The vertical velocities calculated by JNWP were used to calculate precipitation with the hope that any precipitation not accounted for would be due to upslope. Of course, a discrepancy be-

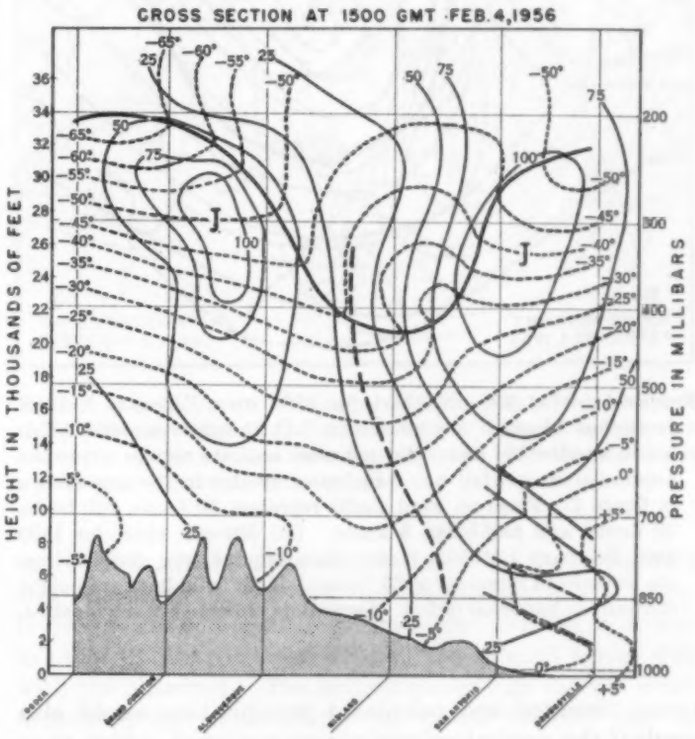

FIGURE 10.—Southeast-northwest vertical cross-section through the cold Low at 1500 GMT, February 4, 1956. Double heavy solid line is the polar front, single heavy solid line is the tropopause, double heavy dashed line is the Arctic front, and the single heavy dashed line is the vertical line of the Low. Lighter dashed lines are isotherms in ° C. and the lighter solid lines are isotachs for every 25 knots.

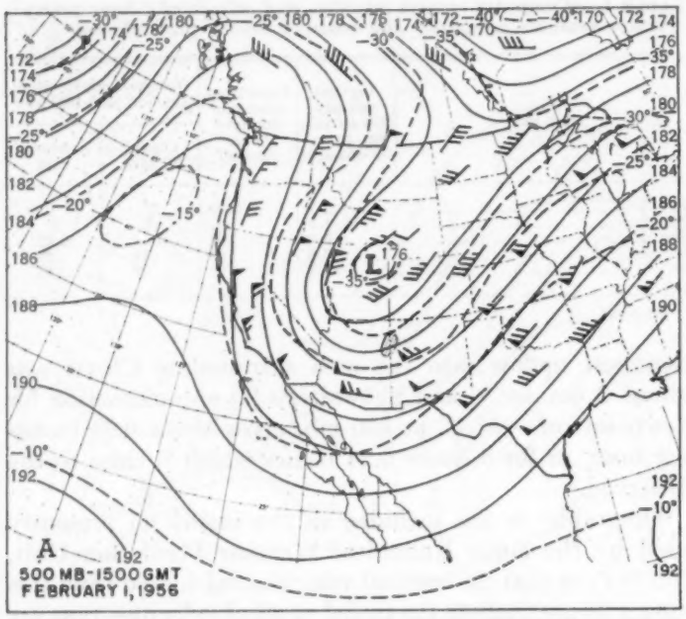

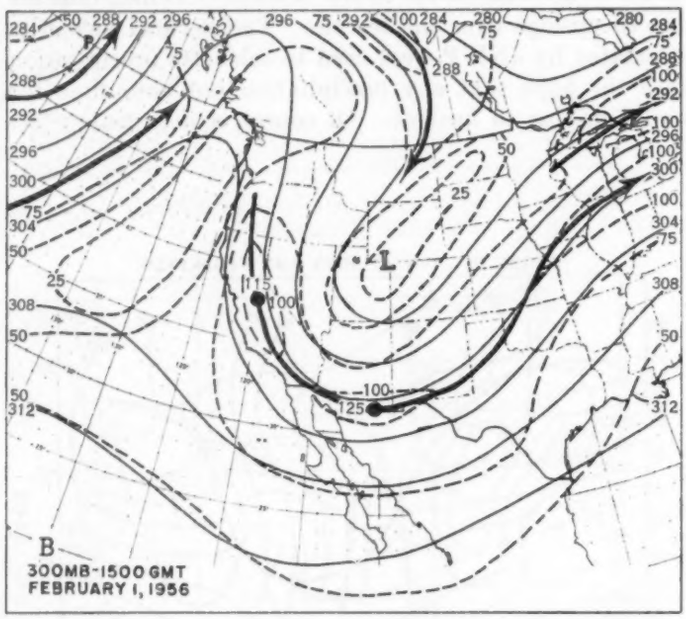

FIGURE 11.—(A) 500-mb. chart for 1500 GMT, February 1, 1956. Isotherms (dashed) are labeled in ° C.; height contours (solid) are in hundreds of feet. Shaded areas indicate regions where the accumulated snowfall was 6 inches or greater in the area shown in figure 2. Flags on wind shafts represent 50 knots, full barbs 10 knots, and half-barbs 5 knots. (B) 300-mb. chart for 1500 GMT, February 1, 1956. Heavy lines are the jets, dashed lines are isotachs in intervals of 25 knots. Light solid lines are height contours in hundreds of feet. Large dots indicate isotach maxima.

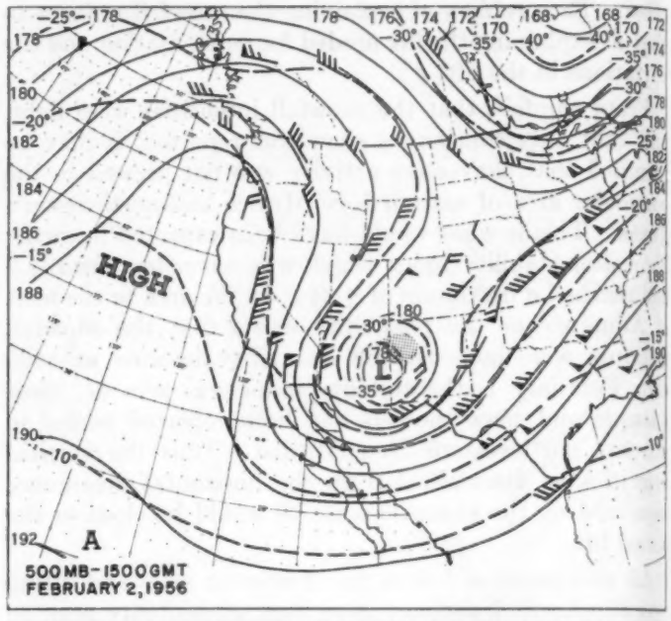

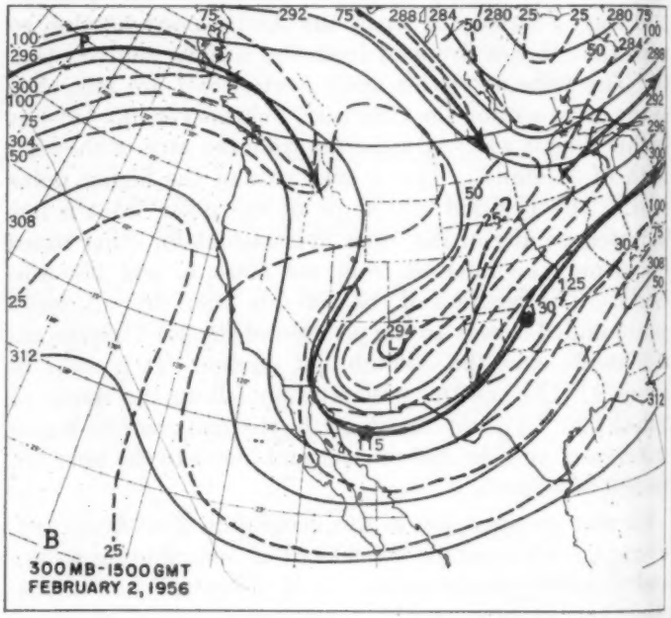

FIGURE 12.—1500 GMT, February 2, 1956. (A) 500-mb. chart. (B) 300-mb. chart.

tween observed and calculated precipitation would also result if the vertical velocities were too small, which they would be if potential instability was present or if the distance between grid points used by JNWP was too great [3]. For this case these two considerations are not believed to have affected the calculations.

The vertical velocities for the layer 900–700 mb. and 700–400 mb. were computed from the 1500 GMT data by JNWP as part of the initial analysis preparatory to the baroclinic prognosis and they include any lift that might be described as due to frontal lifting. For the calculations it might be better to use the vertical velocities for smaller layers, which might be estimated if the level of least divergence were known, but as it was not, the calculations are for just the two layers. The vertical velocities used were those over Clovis, N. Mex., which is in the center of the triangle formed by Amarillo, Albuquerque, and Midland (fig. 16), whose raob soundings were averaged to give the temperatures and dewpoint temperatures necessary for the calculations. The method of Thompson and Collins [7] which incorporates Fulks' [8] formula for rate of

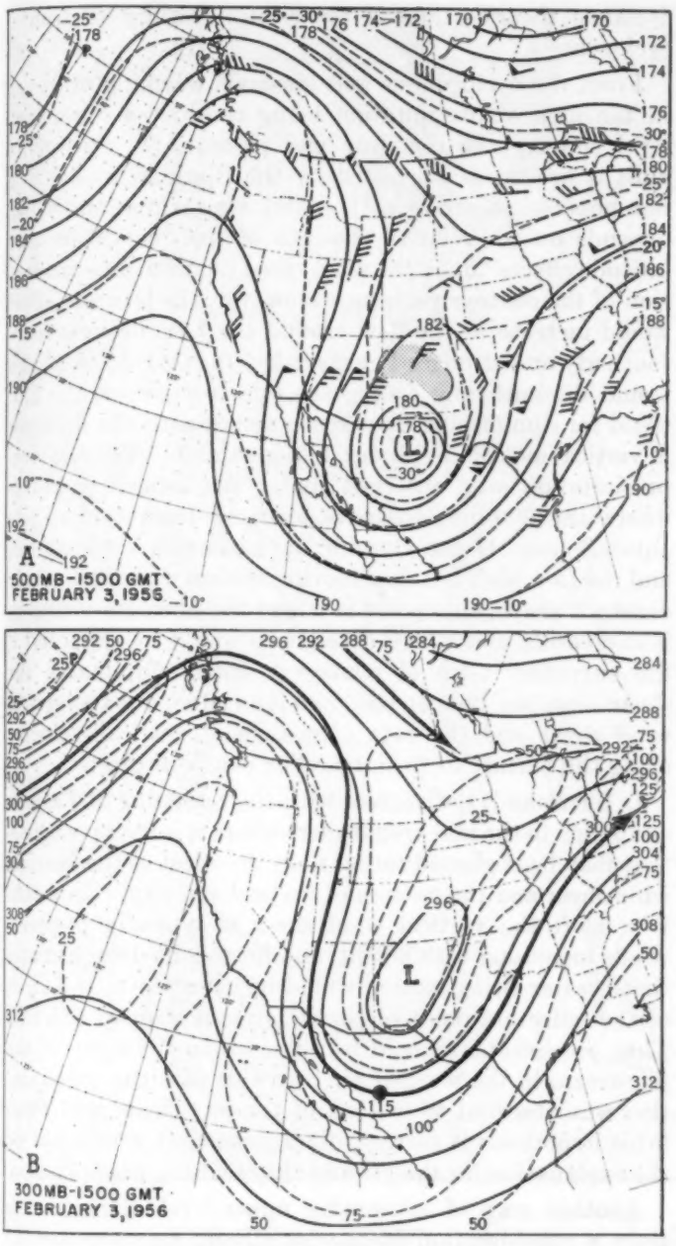

FIGURE 13.—1500 GMT, February 3, 1956. (A) 500-mb. chart. (B) 300-mb. chart.

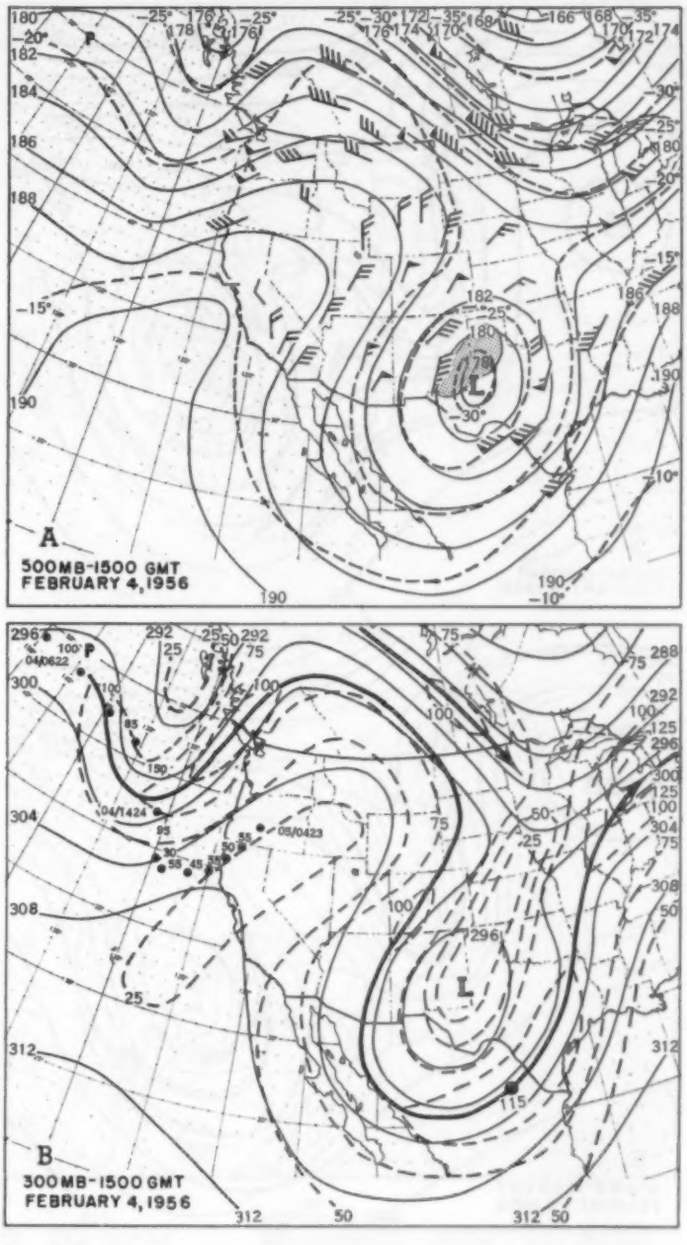

FIGURE 14.—1500 GMT, February 4, 1956. (A) 500-mb. chart. (B) 300-mb. chart. Small dots show path of transosonde with average speed in knots between positions. 04/1424 position is most nearly synoptic with the chart.

precipitation was used. The precipitation was calculated for a 6-hour period, rather than for the 12-hour period used by Thompson and Collins, under the arbitrary assumption that the calculated vertical velocities and averaged raobs for 1500 GMT were representative of the period 1230–1830 GMT for which precipitation amounts are available. The calculated precipitation amounts are representative of the area near the center of the triangle. The amounts at Clovis which is in the center may not be representative of this area so the amounts at Lubbock, Tex., were also included.

In none of the resulting calculations did the lower layer contribute to the precipitation as the velocity was not sufficient to lift the air to saturation. Also on February 1 and February 4 and 5 the vertical velocity in the upper layer was not sufficient to produce precipitation as is seen in table 1. On the 3d, the calculated amount agrees well with the observed. The largest amount on the 4th is not accounted for. Combining the initial velocity due to orography and the higher-level velocity from JNWP might come close to accounting for even the greatest intensity of snowfall observed.

For this type of circulation, the distribution of divergence is not clear from empirical studies or from dynamical reasoning. J. Bjerknes [9] says, ". . . and also the rain in the front half of a cold trough or a cold vortex are

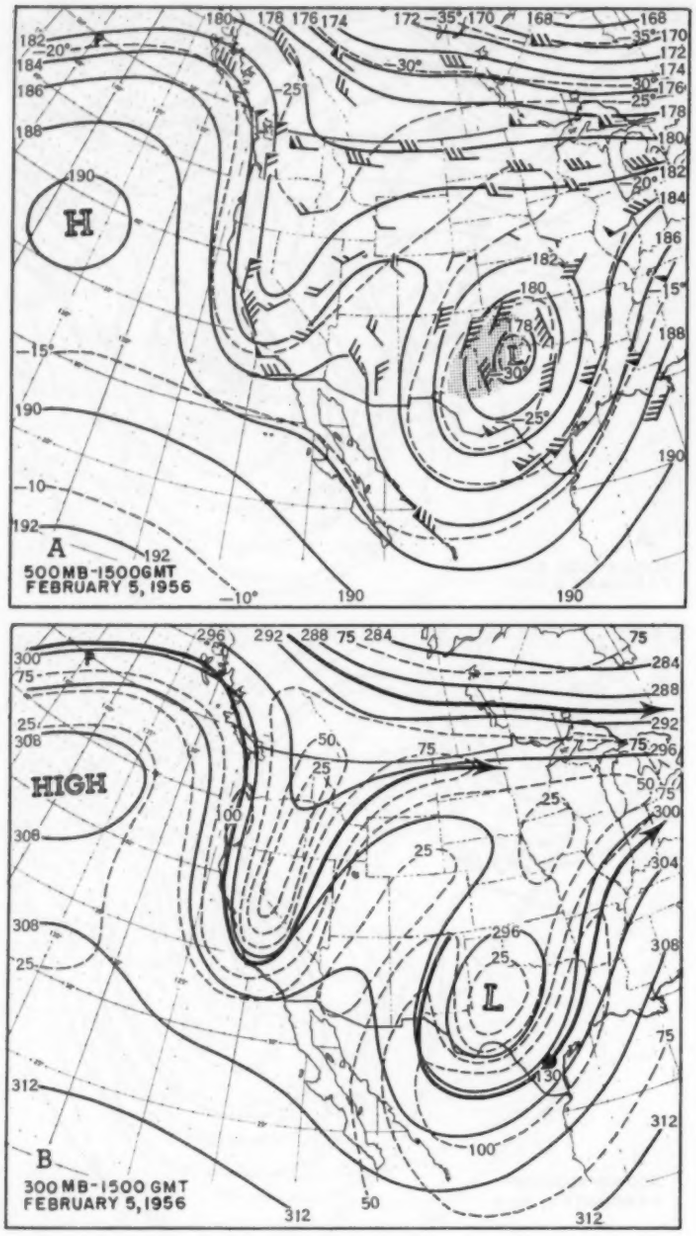

FIGURE 15.—1500 GMT, February 5, 1956. (A) 500-mb. chart. (B) 300-mb. chart.

probably to be explained by the general upward motion shown in Fig. 1." Figure 1 is his well-known model for the distribution of divergence above a frontal wave with the short wave trough in the westerlies above the surface wave. Palmén [10] states that cold upper Lows can be considered as a further development of the upper trough in the Bjerknes model. He also says that the mid-tropospheric Low has the structure characteristic of the fully occluded frontal cyclone although it is the result of processes other than the occlusion of wave-shaped frontal perturbations. J. Bjerknes has this to say of the fully occluded cyclone: "This sketch of the last part of the life cycle of cyclones is even less intimately related to exact dynamic theories than is the existing theory of frontal cyclogenesis."

From the cyclogenesis and low-level warming observed in the area of precipitation being considered here, low-level convergence certainly was present. If divergence aloft is needed as suggested by the Bjerknes model it is not possible to arrive at the first approximation, which depends on the relative strength of the "curvature and latitude effects" upon the wind speed [9], from an examination of the contour pattern. However, the latitude effect would increase as the flow around the Low became more southerly and stronger February 1–5 (figs. 11–15) and this would diminish any divergence due to curvature. This trend for diminishing divergence agrees with the decrease in vertical motion, February 3–5, in table 1. The heaviest precipitation was observed under the inflection points where the 300-mb. contours changed from cyclonic to anticyclonic. If the contour approximates a streamline and the Low aloft is a slow moving system with a relatively constant shape, this point is where the absolute vorticity is decreasing and where divergence would be expected if the curvature term of relative vorticity dominates the shear term (see Palmén [10]) and if an effect due to vertical wind shear and the rate of change of vertical velocity along the normal to the streamline can be neglected.

L. Sherman [11] disagrees with the reasoning of Palmén as applied to the mid-troposphere where it is the divergence that may be neglected rather than the effect of the vertical wind shear and the pattern of vertical velocity. In a cold Low aloft the vertical wind shear is typically positive, winds increasing with height, and for this he demonstrates that greater rising motion would be expected to the right of the inflection point of the jet stream than to the left. Thus precipitation would be observed to the right of the jet stream in the warmer air. In this case the precipitation was observed to the left of the jet stream and thus, if his hypothesis is correct, divergence aloft would not be the explanation for the lift and the resulting precipitation.

Another way of estimating upper-level divergence is from a consideration of the jet stream as suggested by Riehl et al. [12]. This effect must be thought of as being superimposed upon the divergence as estimated from the contours as a complete theoretical treatment combining the two effects is not available (see Bjerknes [9]). Around an isotach maximum along a straight jet, divergence is found in the front left quadrant and in the rear right, but Beebe and Bates [13] have pointed out that for a cyclonically curved jet one can be sure of divergence only in the front left quadrant. Inspection of the 300-mb. charts shows that on February 1, the precipitation area (fig. 11) was under the front left quadrant of the isotach maximum of the cyclonically curved jet stream. By 0300 GMT, February 2 (not shown) the jet maximum approached Amarillo and by 1500 GMT, February 2 (fig. 12) the area was under the left rear quadrant where for a cyclonically curved jet stream one can be sure of convergence, and hence the upward vertical motion and the precipitation

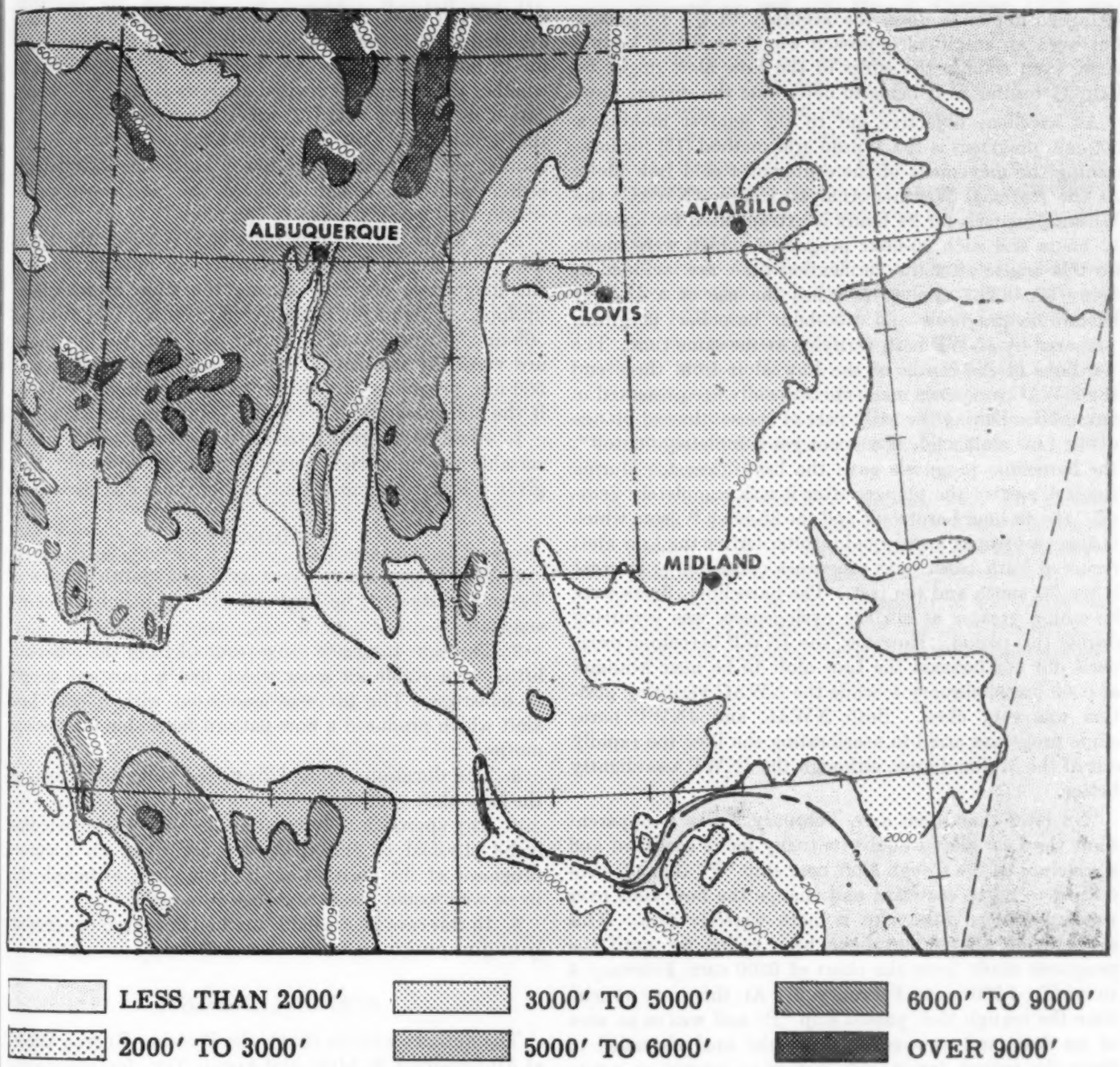

FIGURE 16.—Topographic map of the region affected by the storm of February 1–5, 1956.

should decrease. This change checks with a decrease in the calculated vertical velocities of February 1–2, in table 1. By 1500 GMT, February 3 (fig. 13), another isotach maximum had rotated around the Low so that once again the precipitation area was under the front left quadrant and the vertical velocities again increased (table 1.) The precipitation area remained in this quadrant February 4 and 5 (figs. 14 and 15).

Teweles [14] in a test relating this concept to precipitation, found that "on the eastern slope of the Rockies when precipitation occurs with upslope flow (easterly winds at low levels), there is no apparent association with any of these high-level synoptic patterns." However, in this case the high-level pattern may at least have been a contributing factor.

4. THE PROGNOSIS

It seems inconceivable that any forecast could be made for the heavy snowfall without knowledge of the movement of the Low aloft, particularly its 12-hour stagnation near Midland. A direct physical approach makes very

stringent demands upon the accuracy of the prognosis, but even an empirical approach would need this knowledge, even though the effect of the Low aloft might be indirect insofar as it helps to determine the surface flow.

An excellent objective aid to the analyst making a 500-mb. prognosis is the Wilson grid method [15] for forecasting the movement of the center of a cold Low aloft. At the National Weather Analysis Center (NWAC) the Wilson prognosis for 24 hours is extrapolated for another 12 hours and such 36-hour prognoses, which were made for this article after the verification time, are included in figure 3A. The analyst also has the use of a 48-hour barotropic prognosis and a 36-hour baroclinic prognosis prepared by JNWP both verifying at the same time. The positions of the center of the Low aloft from these and the NWAC prognosis made operationally are presented in figure 3B. During the early part of the southward plunge of the Low aloft while it was not yet completely "cutoff", the baroclinic prognosis gave the best forecast. During the last part of the plunge, after it was completely "cutoff," the 48-hour barotropic and the 36-hour Wilson, which is also barotropic, gave equal results. After the Low aloft recurved both barotropic prognoses consistently forecast it too far south and too fast. The baroclinic effects were becoming greater as surface cyclogenesis was occurring during this period. However, the JNWP baroclinic prognosis did not forecast the Low aloft to be near Midland at 0300 GMT, February 4, while the NWAC verifying position was very close. Both NWAC and JNWP baroclinic prognoses erred in accelerating the Low too rapidly out of the Midland area, although the JNWP was slightly better.

No later than 1500 GMT, February 3 was it apparent that the Low aloft would eventually move eastward and accelerate as the trough aloft near ship "P" (fig. 13) continued to move eastward and change the flow aloft over western United States to a more westerly flow. This acceleration should not have been called for until the prognosis made from the chart of 0300 GMT, February 4 to verify 1500 GMT, February 5. At this very crucial time the trough aloft passed ship "P" and was in an area of no data and as a consequence the analysis failed to show the trough far enough east or as intense as it was shown to be by subsequent events. On the 300-mb. chart for 1500 GMT, February 5 (fig. 15B) note the intensity of the trough as compared to 1500 GMT, February 4 (fig. 14B) and note also the 100-knot isotach maximum in the northwest flow on the 5th as compared to a 50-knot plus maximum on the 4th. It might be argued that the trough had intensified in this period if it were not for experimental data not available in time for the original analysis. Part of the track of a balloon flying at constant pressure, a transosonde [16], is given on the 300-mb. chart for 1500 GMT, February 4 (fig. 14B). From this it is seen that at this time the trough was deeper than analyzed and the 100-knot northwest winds already existed. This might well have prompted the analyst to forecast the acceleration even sooner increasing the prognosis error especially after the Low moved rapidly northeastward for 12 hours after 1500 GMT, February 3. Regardless of whether the original or revised analysis is used, the application of Henry's rule [17] gives good results. That is that a cold Low aloft in the southwestern United States should not be forecast to move until the katallobaric center with the trough aloft to the northwest comes within 1200 nautical miles of the Low.

None of the surface prognoses of NWAC or the 1,000-mb. prognoses of JNWP forecasted an upslope wind of the magnitude observed during the time of maximum upslope. This might be expected from the fact that the 500-mb. prognoses were in error and that the prognoses are vertically consistent. Of course, even with a poor 500-mb. prognosis the surface prognosis might be better if the thickness prognosis had a compensating error.

It would be of great interest to see if any other models suitable for numerical weather prediction would have given a better prognosis than any of those discussed here.

5. SUMMARY

1. The heavy snow cover over the South Plains of Texas was due to the long duration of a light-intensity snowfall.

2. The light-intensity snow resulted from the adiabatic lifting of a stable air mass which had a constant supply of moisture. The lift was associated with a cold Low aloft which produced a flow pattern favorable for upslope motion.

3. The duration resulted from the slow movement of the Low aloft over the area.

4. Any approach to forecasting the snow cover, whether it be physical or empirical, depends upon an accurate prognosis of the position of the Low aloft, although this in no way would insure a perfect forecast.

5. In this case no available method appeared consistently to give prognoses which were sufficiently accurate.

ACKNOWLEDGMENTS

The authors wish to thank the Weather Bureau Offices at Albuquerque, N. Mex., and Austin, Tex., for information furnished, and the staff members of NWAC for reviewing the article.

REFERENCES

1. C. L. Kibler, C. M. Lennahan, and R. H. Martin, "Temperature Forecasting As an Implicit Feature in Prognostic Charts—A Case Study for January 23–31, 1955," *Monthly Weather Review*, vol. 83, No. 1, January 1955, pp. 23–30.
2. A. K. Showalter, "Precipitable Water Template," *Bulletin of the American Meteorological Society*, vol. 35, No. 3, March 1954, pp. 129–131.
3. H. Landers, "On the Magnitude of Divergence and Vorticity," *Journal of Meteorology*, vol. 13, No. 1, February 1956, pp. 121–122.

4. L. C. W. Bonacina, "Orographic Rainfall and Its Place in the Hydrology of the Globe," *Quarterly Journal Royal Meteorological Society*, vol. 71, 1945, pp. 41–55.
5. A. K. Showalter, "Rate of Precipitation from Pseudo-Adiabatically Ascending Air," *Monthly Weather Review*, vol. 72, No. 1, January 1944, p. 1.
6. J. G. Charney and N. A. Phillips, "Numerical Integration of the Quasi-geostrophic Equations for Barotropic and Simple Baroclinic Flows," *Journal of Meteorology*, vol. 10, No. 2, April 1953, pp. 71–99.
7. J. C. Thompson and G. O. Collins, "A Generalized Study of Precipitation Forecasting. Part 1: Computation of Precipitation from the Fields of Moisture and Wind," *Monthly Weather Review*, vol. 81, No. 4, April 1953, pp. 91–100.
8. J. R. Fulks, "Rate of Precipitation from Adiabatically Ascending Air," *Monthly Weather Review*, vol. 63, No. 10, October 1935, pp. 291–294.
9. J. Bjerknes, "Extratropical Cyclones," *Compendium of Meteorology*, American Meteorological Society, Boston, 1951, pp. 577–598.
10. E. Palmén, "The Aerology of Extratropical Disturbances," *Compendium of Meteorology*, American Meteorological Society, Boston, 1951, pp. 599–620.
11. L. Sherman, "Estimates of the Vertical Velocity Based on the Vorticity Equation," *Journal of Meteorology*, vol. 10, No. 5, October 1953, pp. 399–400.
12. H. Riehl, K. S. Norquest, and A. L. Sugg, "A Quantitative Method for the Prediction of Rainfall Patterns," *Journal of Meteorology*, vol. 9, No. 5, October 1952, pp. 291–298.
13. R. G. Beebe and F. C. Bates, "A Mechanism for Assisting in the Release of Convective Instability," *Monthly Weather Review*, vol. 83, No. 1, January 1955, pp. 1–10.
14. S. Teweles, "A Test of the Relationship Between Precipitation and Synoptic Patterns at 200 and 300-Millibars," *Journal of Meteorology*, vol. 10, No. 6, December 1953, pp. 450–456.
15. H. P. Wilson, "A Test of a Grid Method of Forecasting the Motion of Lows at 500-mb. in Arctic Regions," Cir. 2539 TEC 194, Meteorological Division, Department of Transport, Canada, October 4, 1954.
16. A. D. Anderson and H. J. Masterbrook, "The Transosonde—A New Meteorological Data Gathering System," *NRL Report* 4649, Naval Research Laboratory, Washington, D. C., November 3, 1955.
17. W. K. Henry, On the Movement of the Southwest Low, thesis for the degree of Master of Science, University of Chicago, September, 1949 (unpublished).

U. S. GOVERNMENT PRINTING OFFICE: 1956

Chart I. A. Average Temperature (°F.) at Surface, February 1956.

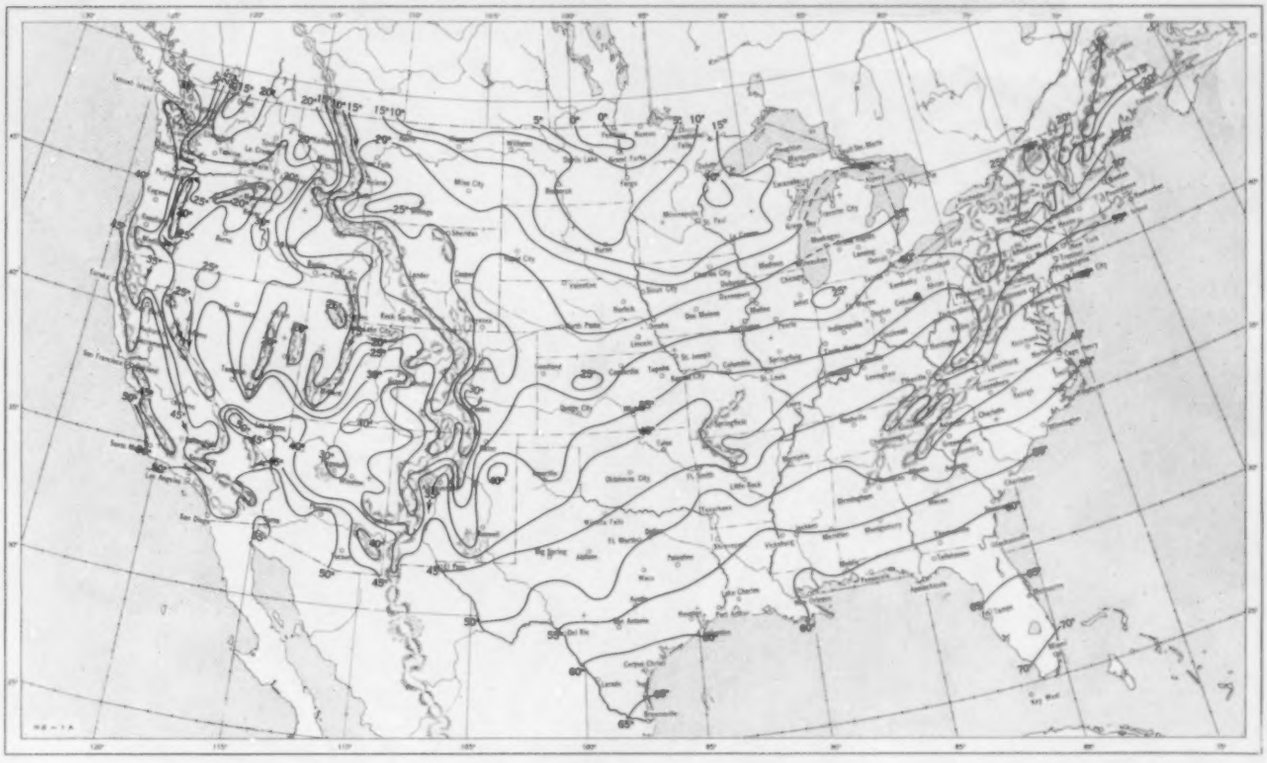

B. Departure of Average Temperature from Normal (°F.), February 1956.

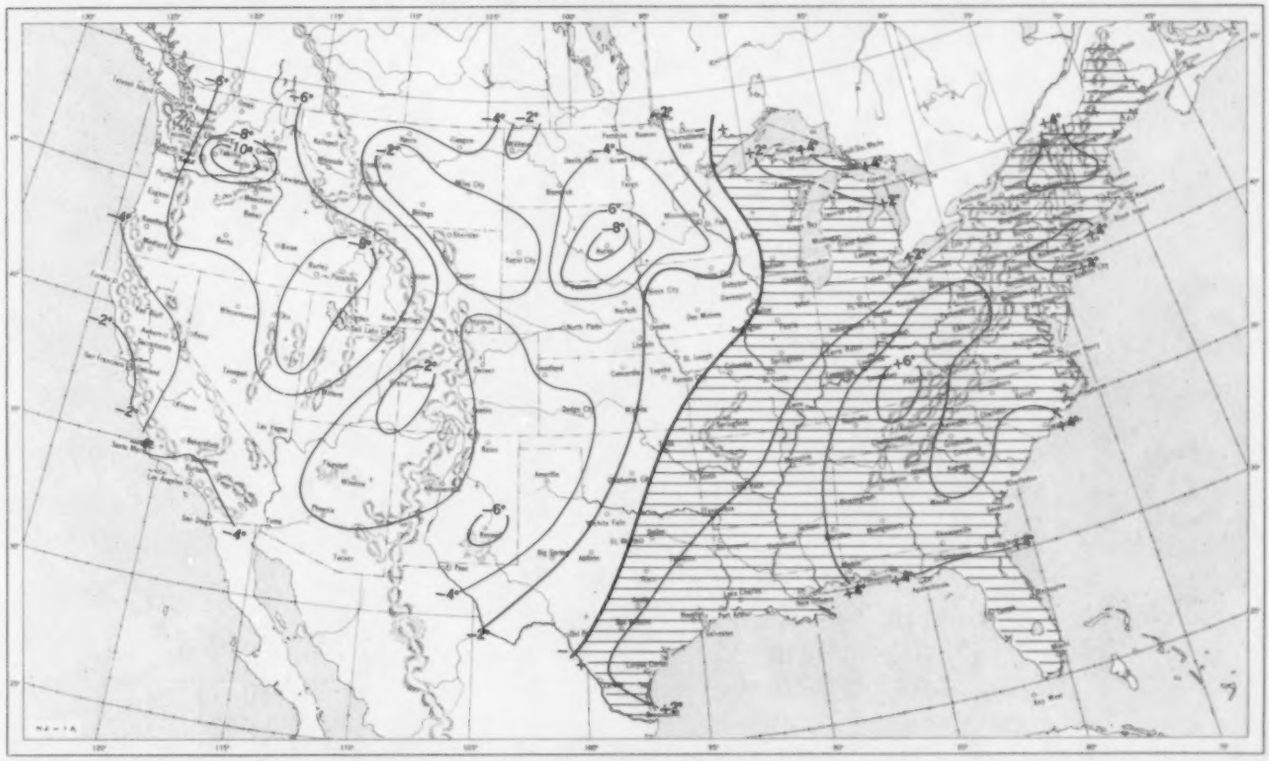

A. Based on reports from 800 Weather Bureau and cooperative stations. The monthly average is half the sum of the monthly average maximum and monthly average minimum, which are the average of the daily maxima and daily minima, respectively.
B. Normal average monthly temperatures are computed for Weather Bureau stations having at least 10 years of record.

Chart II. Total Precipitation (Inches), February 1956.

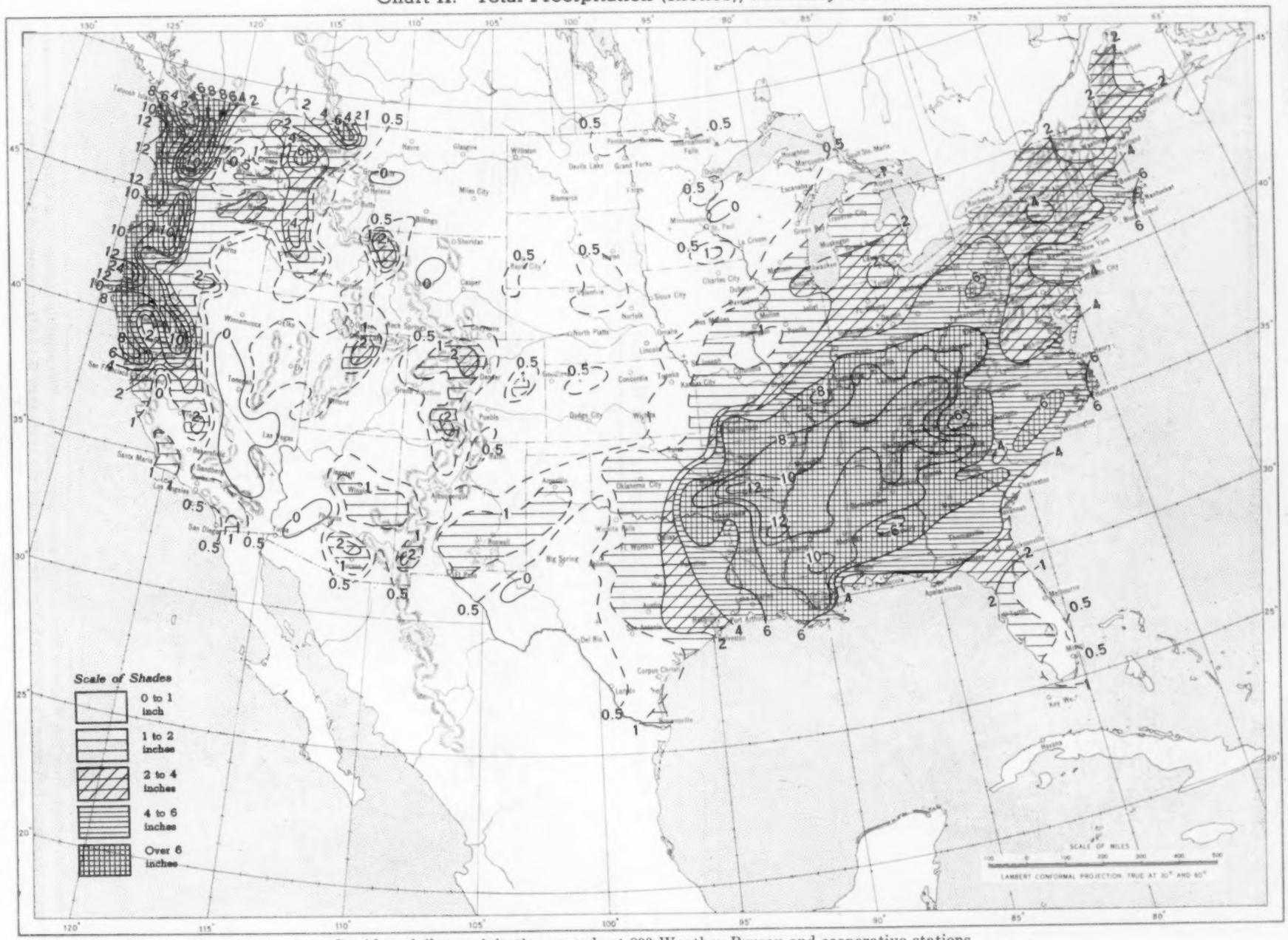
Scale of Shades
0 to 1 inch
1 to 2 inches
2 to 4 inches
4 to 6 inches
Over 6 inches
SCALE OF MILES
LAMBERT CONFORMAL PROJECTION TRUE AT 30° AND 60°

Based on daily precipitation records at 800 Weather Bureau and cooperative stations.

Chart III. A. Departure of Precipitation from Normal (Inches), February 1956.

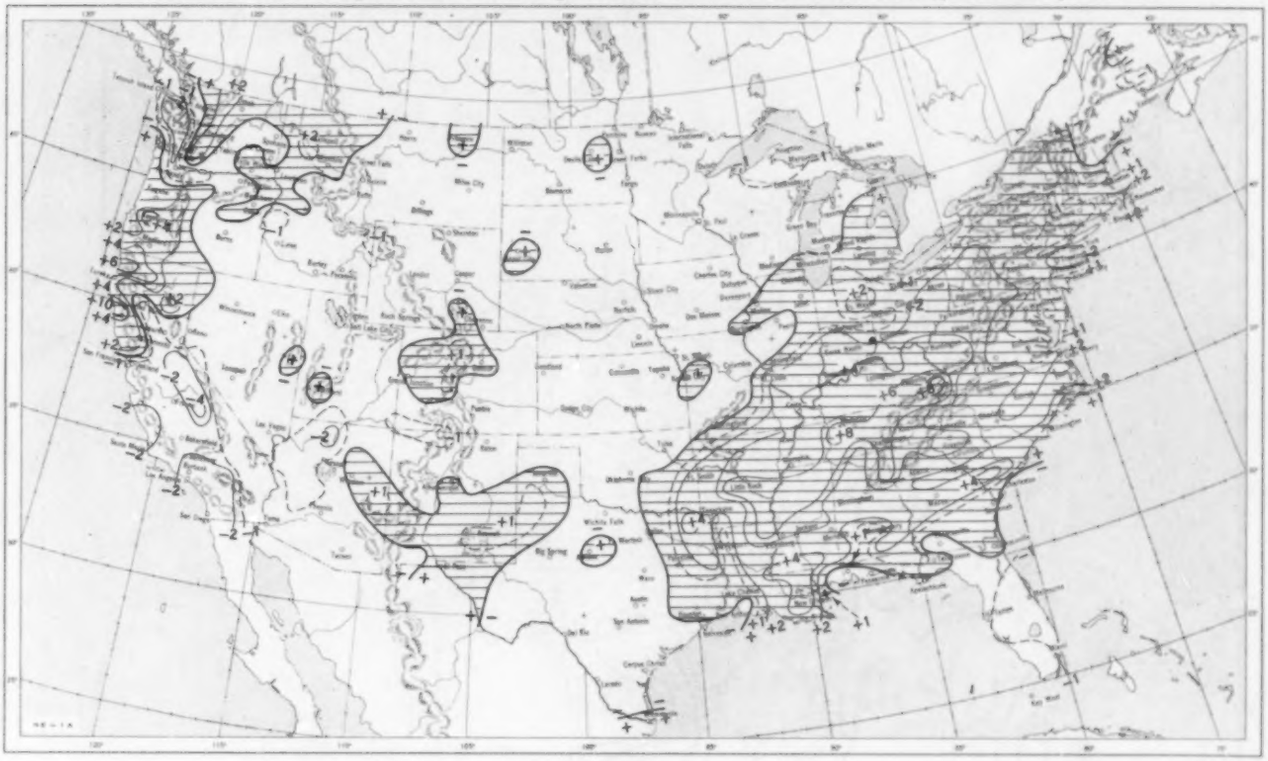

B. Percentage of Normal Precipitation, February 1956.

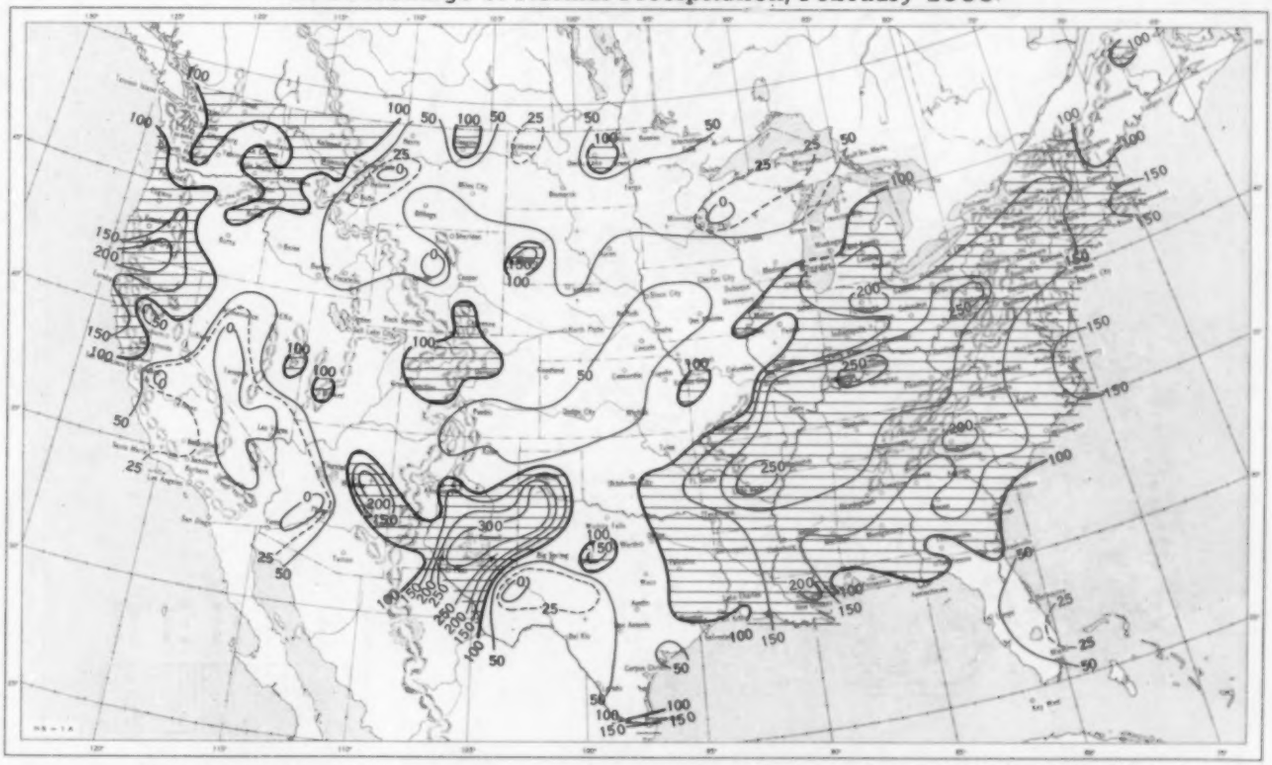

Normal monthly precipitation amounts are computed for stations having at least 10 years of record.

Chart IV. Total Snowfall (Inches), February 1956.

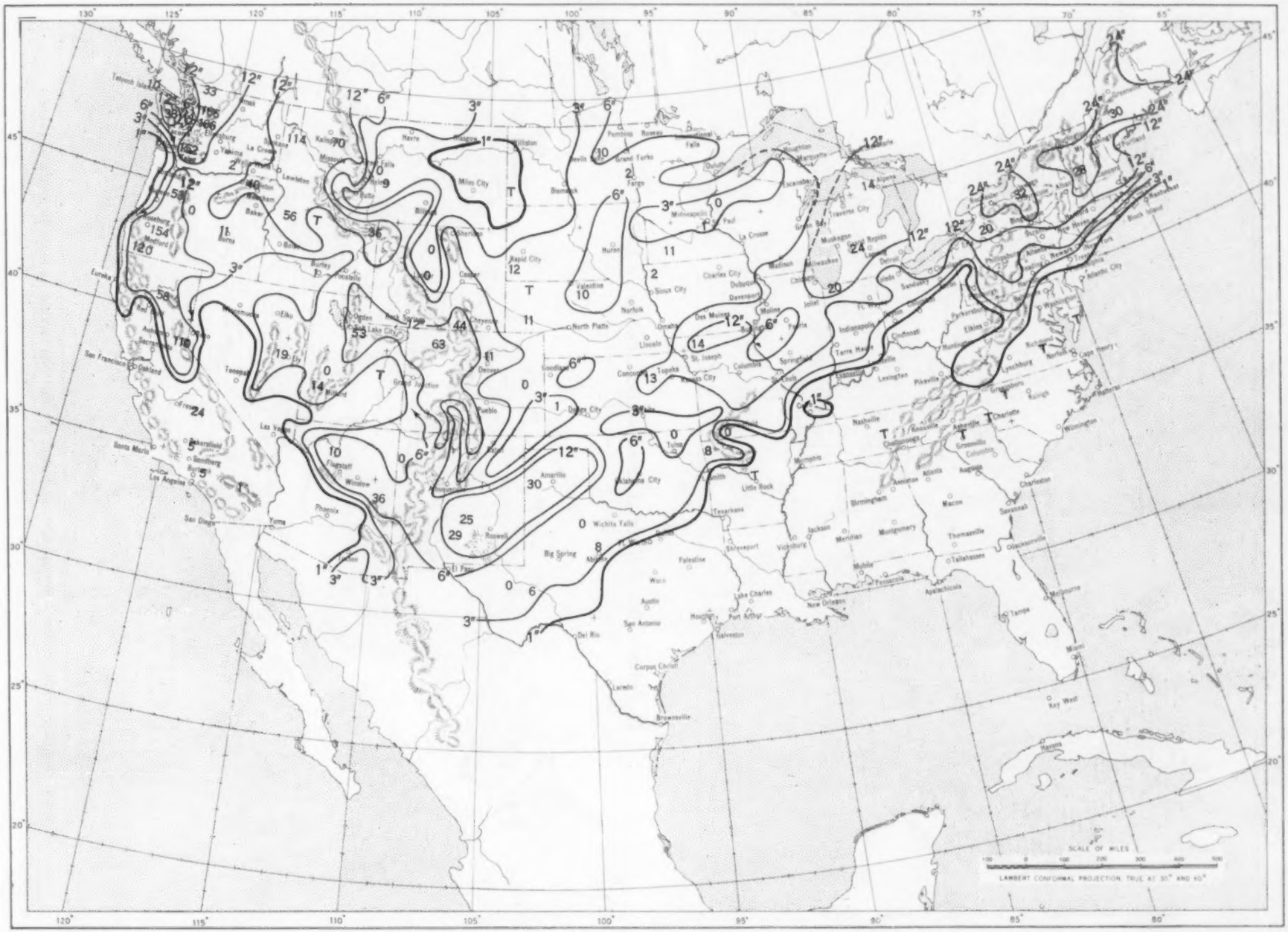

This is the total of unmelted snowfall recorded during the month at Weather Bureau and cooperative stations. This chart and Chart V are published only for the months of November through April although of course there is some snow at higher elevations, particularly in the far West, earlier and later in the year.

Chart V. A. Percentage of Normal Snowfall, February 1956.

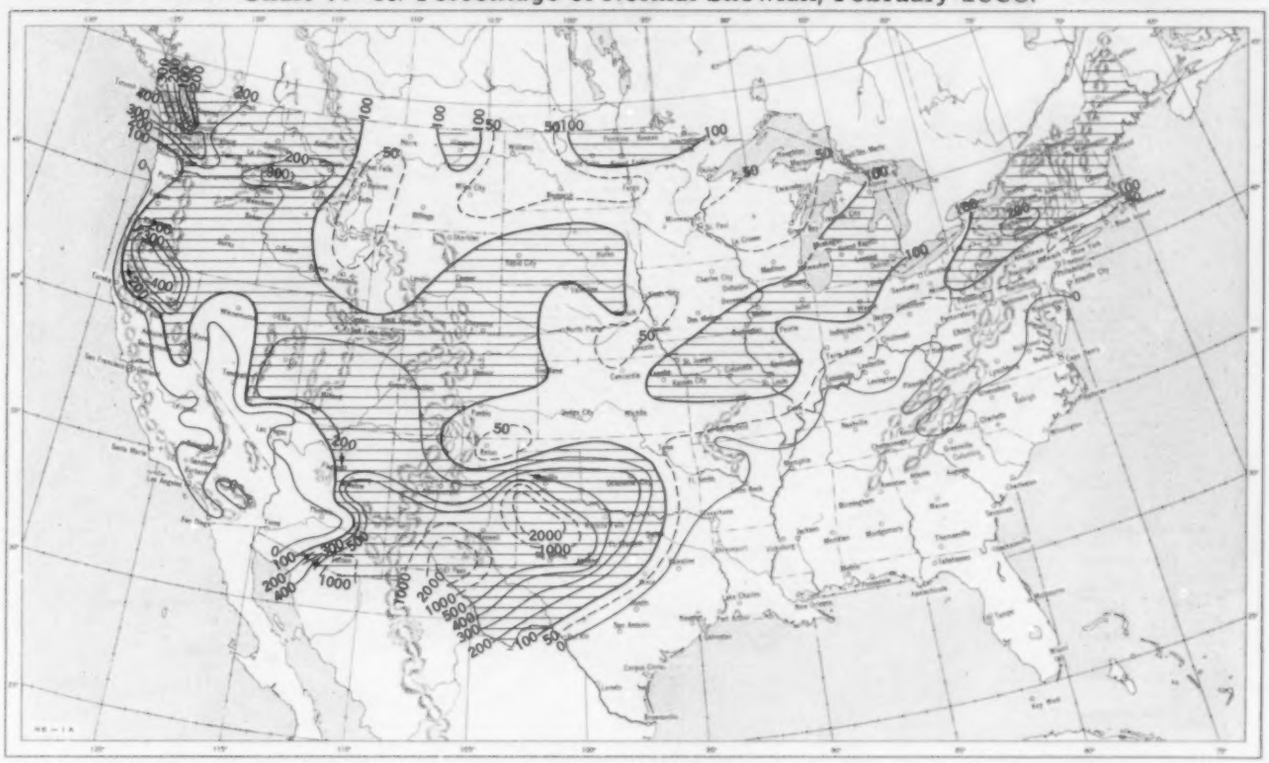

B. Depth of Snow on Ground (Inches). 7:30 a. m. E. S. T., February 27, 1956.

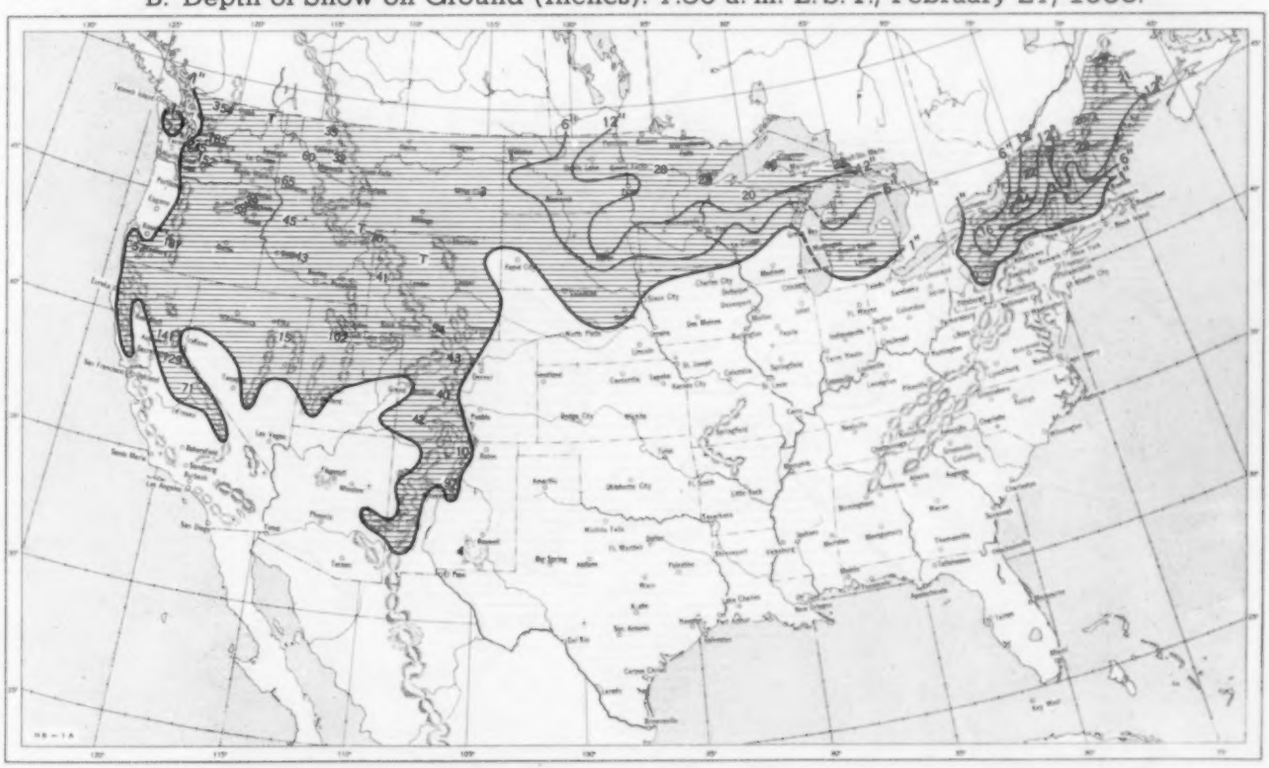

A. Amount of normal monthly snowfall is computed for Weather Bureau stations having at least 10 years of record.
B. Shows depth currently on ground at 7:30 a. m. E. S. T., of the Tuesday nearest the end of the month. It is based on reports from Weather Bureau and cooperative stations. Dashed line shows greatest southern extent of snowcover during month.

Chart VI. A. Percentage of Sky Cover Between Sunrise and Sunset, February 1956.

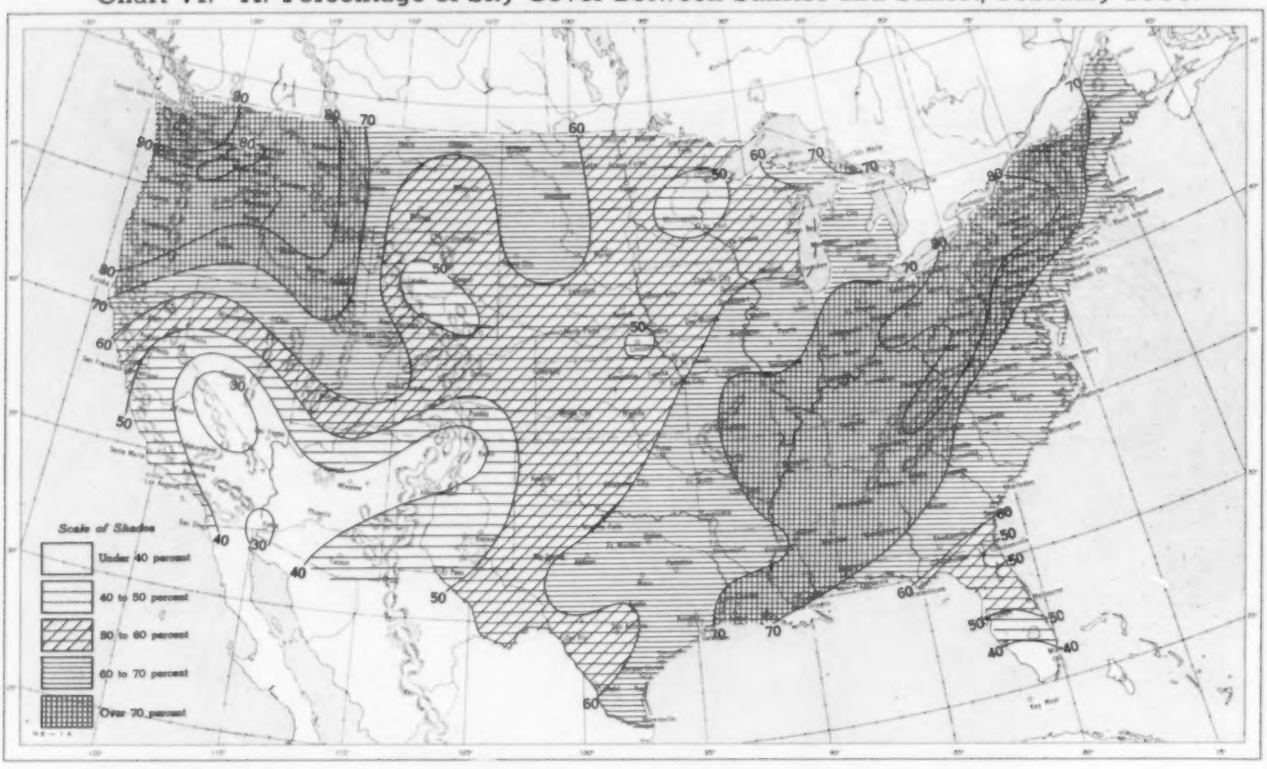

B. Percentage of Normal Sky Cover Between Sunrise and Sunset, February 1956.

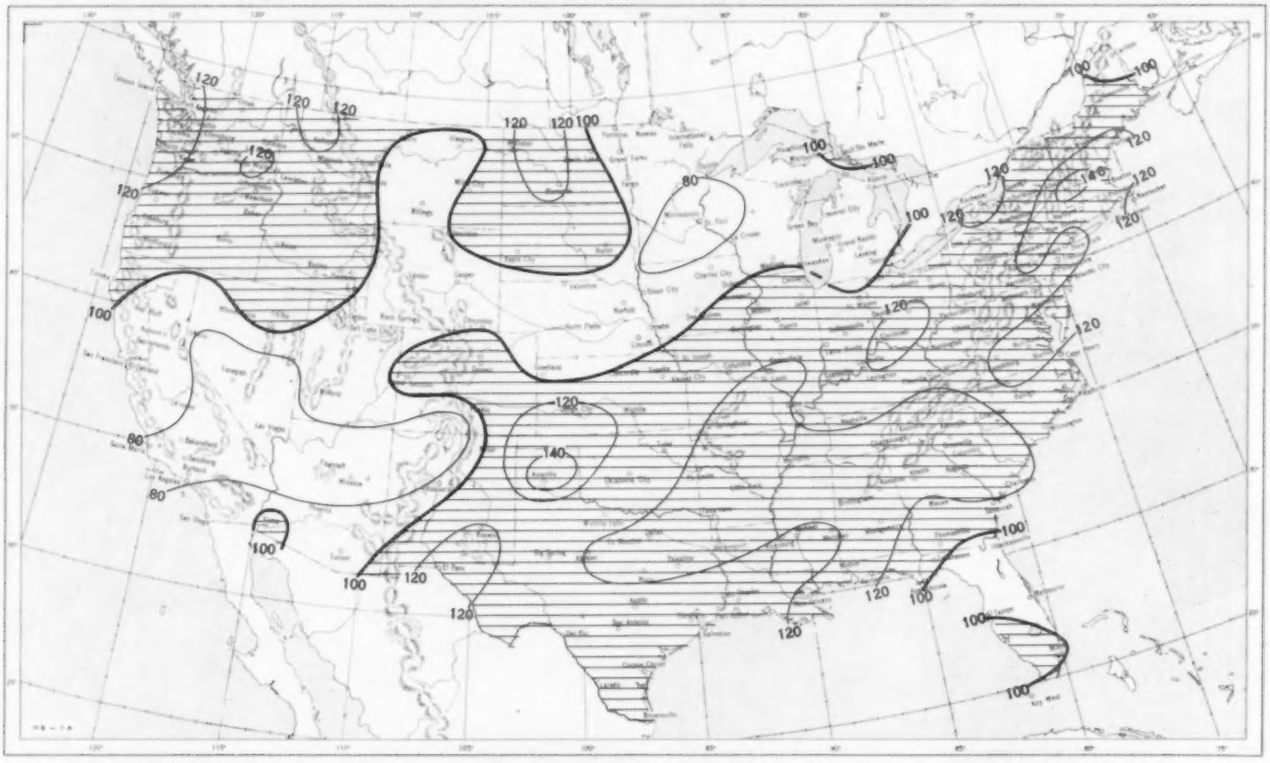

A. In addition to cloudiness, sky cover includes obscuration of the sky by fog, smoke, snow, etc. Chart based on visual observations made hourly at Weather Bureau stations and averaged over the month. B. Computations of normal amount of sky cover are made for stations having at least 10 years of record.

Chart VII. A. Percentage of Possible Sunshine, February 1956.

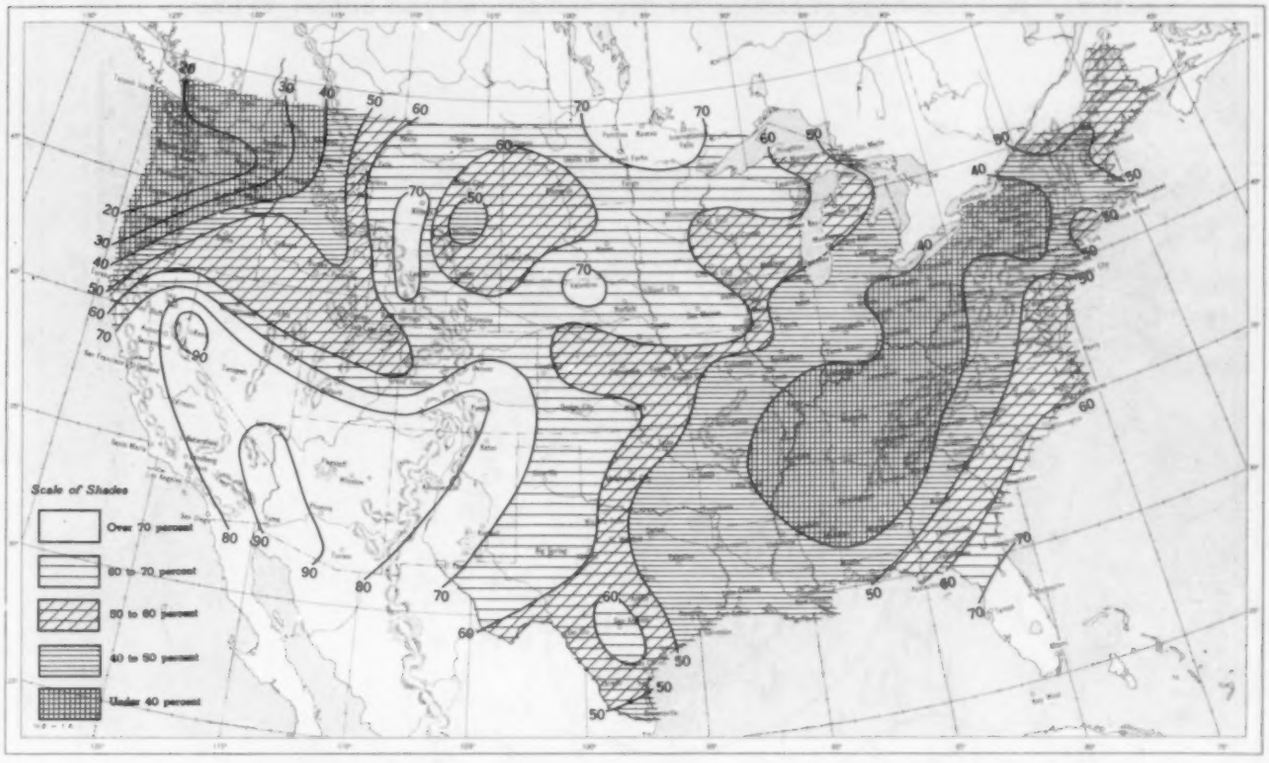

B. Percentage of Normal Sunshine, February 1956.

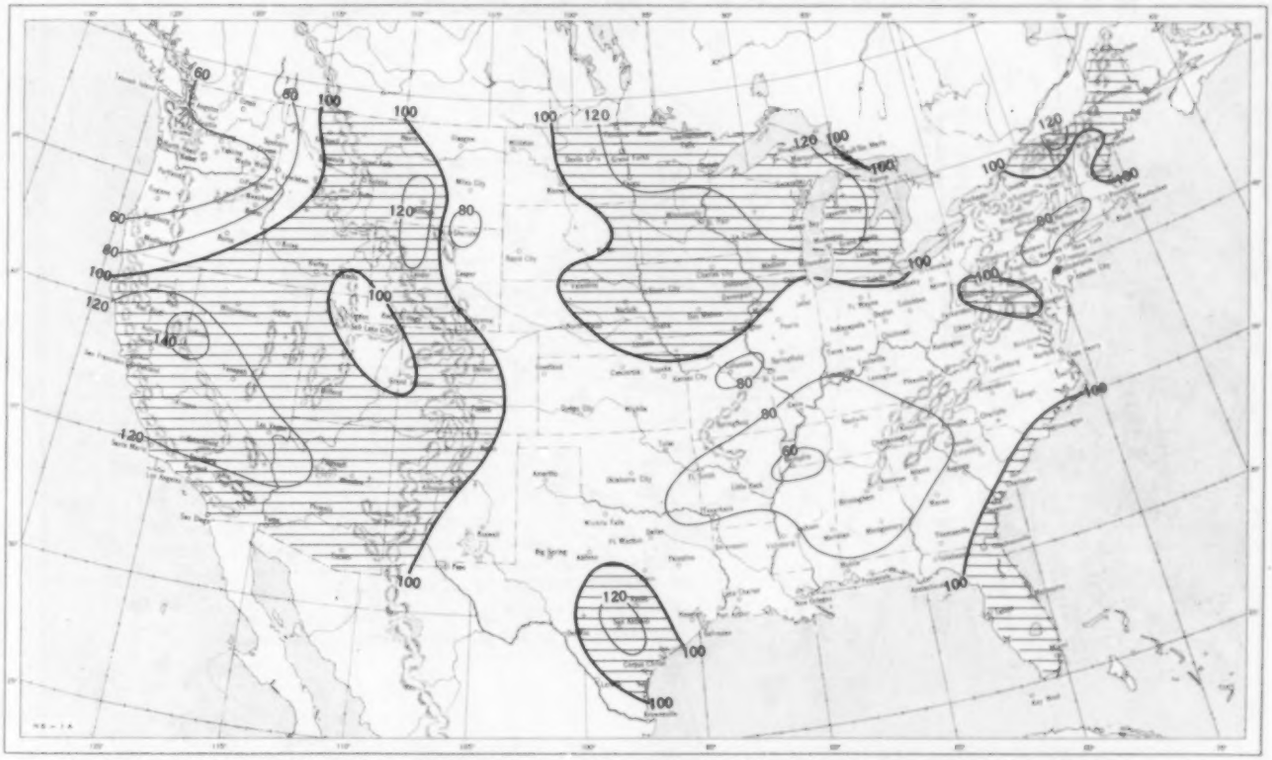

A. Computed from total number of hours of observed sunshine in relation to total number of possible hours of sunshine during month. B. Normals are computed for stations having at least 10 years of record.

Chart VIII. Average Daily Values of Solar Radiation, Direct + Diffuse, February 1956. Inset: Percentage of Mean Daily Solar Radiation, February 1956. (Mean based on period 1951-55.)

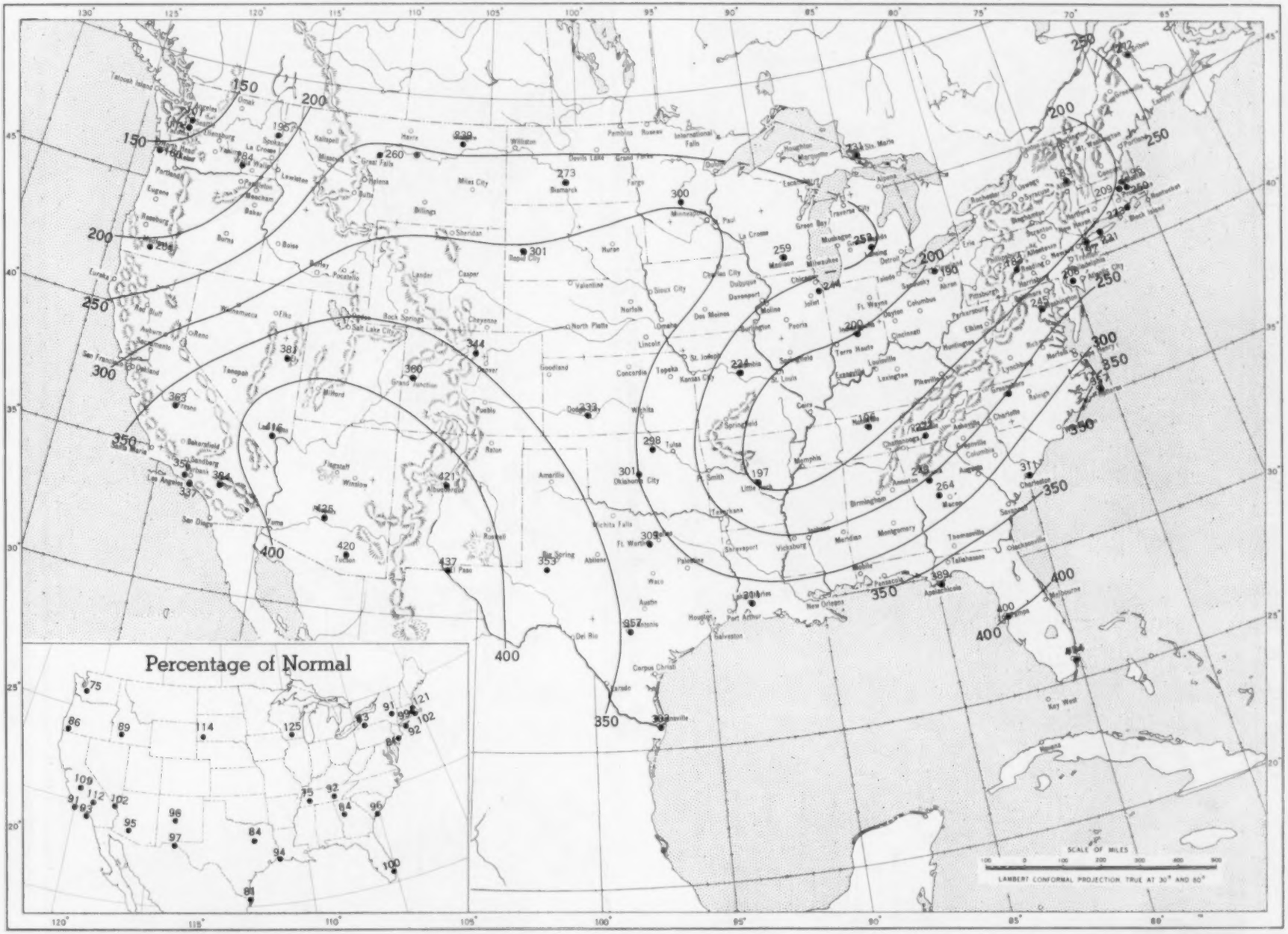

Chart shows mean daily solar radiation, direct + diffuse, received on a horizontal surface in langleys (1 langley = 1 gm. cal. cm. $^{-2}$). Basic data for isolines are shown on chart. Further estimates are obtained from supplementary data for which limits of accuracy are wider than for those data shown.

Chart IX. Tracks of Centers of Anticyclones at

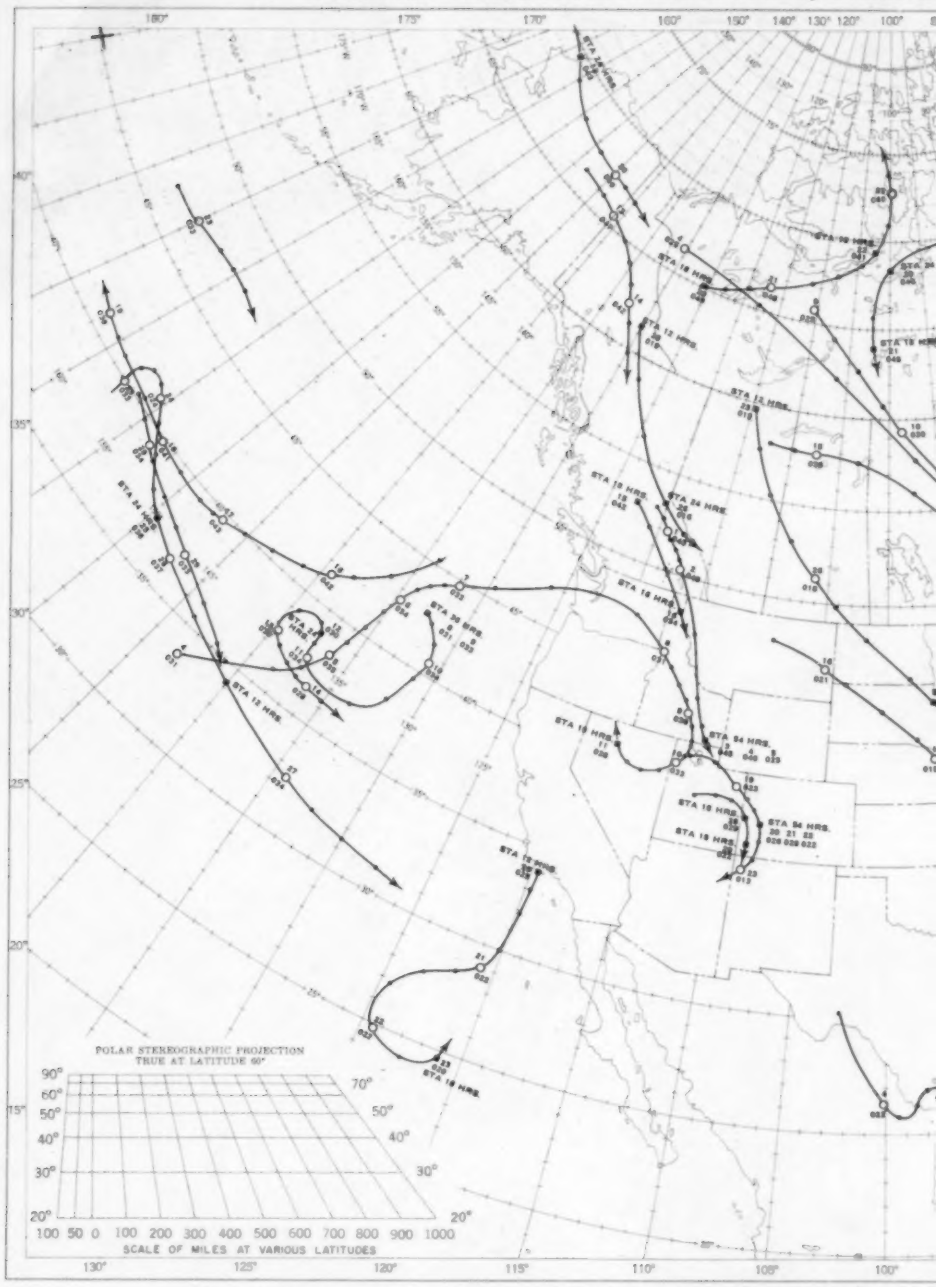

Circle indicates position of center at 7:30 a. m. E. S. T. Figure above ci
Dots indicate intervening 6-hourly positions. Squares indicate position
indicates reformation at new position. Only those centers which

ones at Sea Level, February 1956. (Corrected)

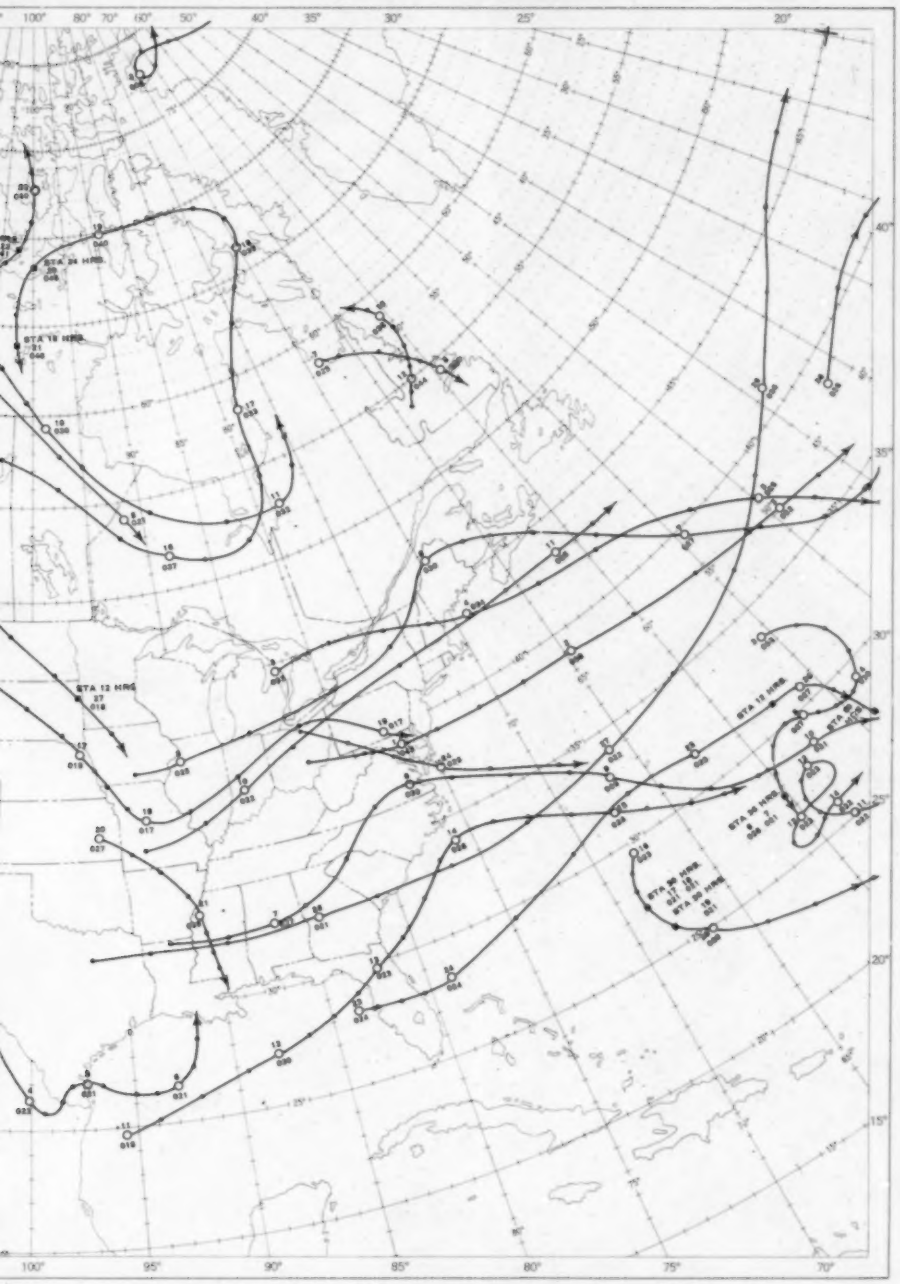

above circle indicates date, figure below, pressure to nearest millibar. position of stationary center for period shown. Dashed line in track ers which could be identified for 24 hours or more are included.

Sea Level, February 1956. (Corrected)

F. See Chart IX for explanation of symbols.

FEBRUARY 1956 M. W. R.

LXXXIV—25

Chart X. Tracks of Centers of Cyclones at Sea L

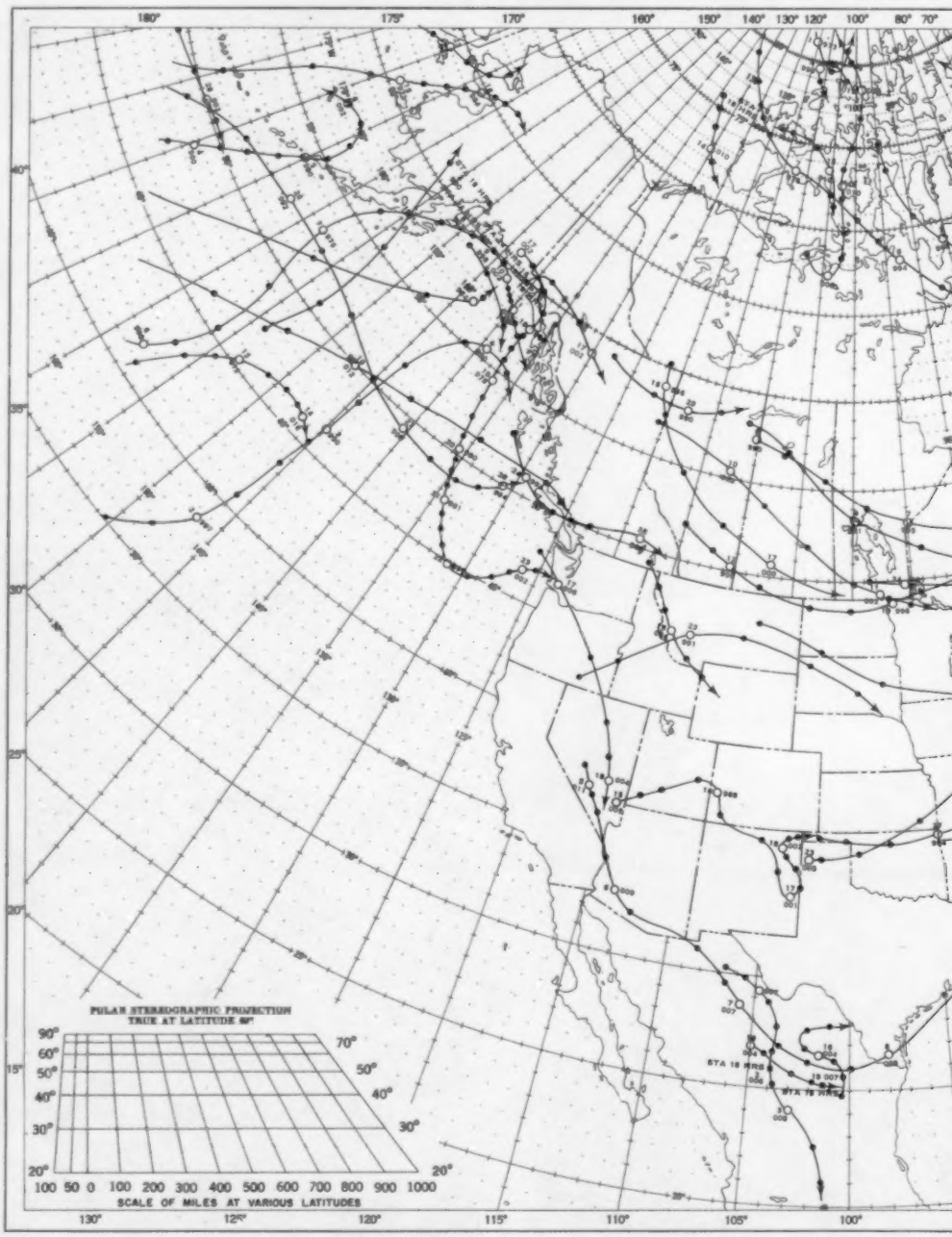

Circle indicates position of center at 7:30 a. m. E. S. T. See

Chart IX. Tracks of Centers of Anticyclones at S

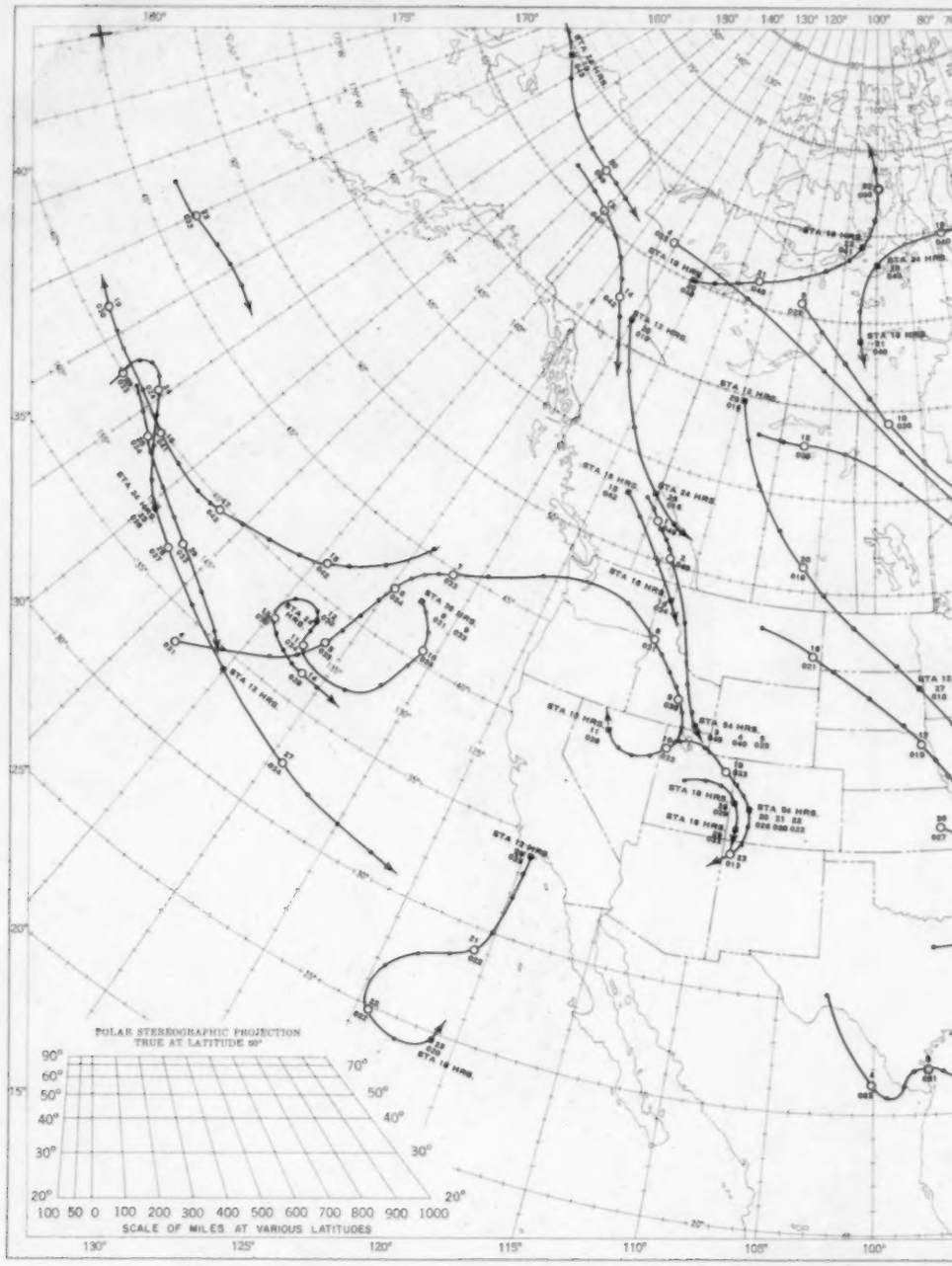
POLAR STEREOGRAPHIC PROJECTION
TRUE AT LATITUDE 60°
90° 60° 50° 40° 30° 20°
70° 50° 40° 30° 20°
100 50 0 100 200 300 400 500 600 700 800 900 1000
SCALE OF MILES AT VARIOUS LATITUDES

Circle indicates position of center at 7:30 a. m. E. S. T. Figure above circl
Dots indicate intervening 6-hourly positions. Squares indicate position of
indicates reformation at new position. Only those centers which c

...es at Sea Level, February 1956. (Corrected)

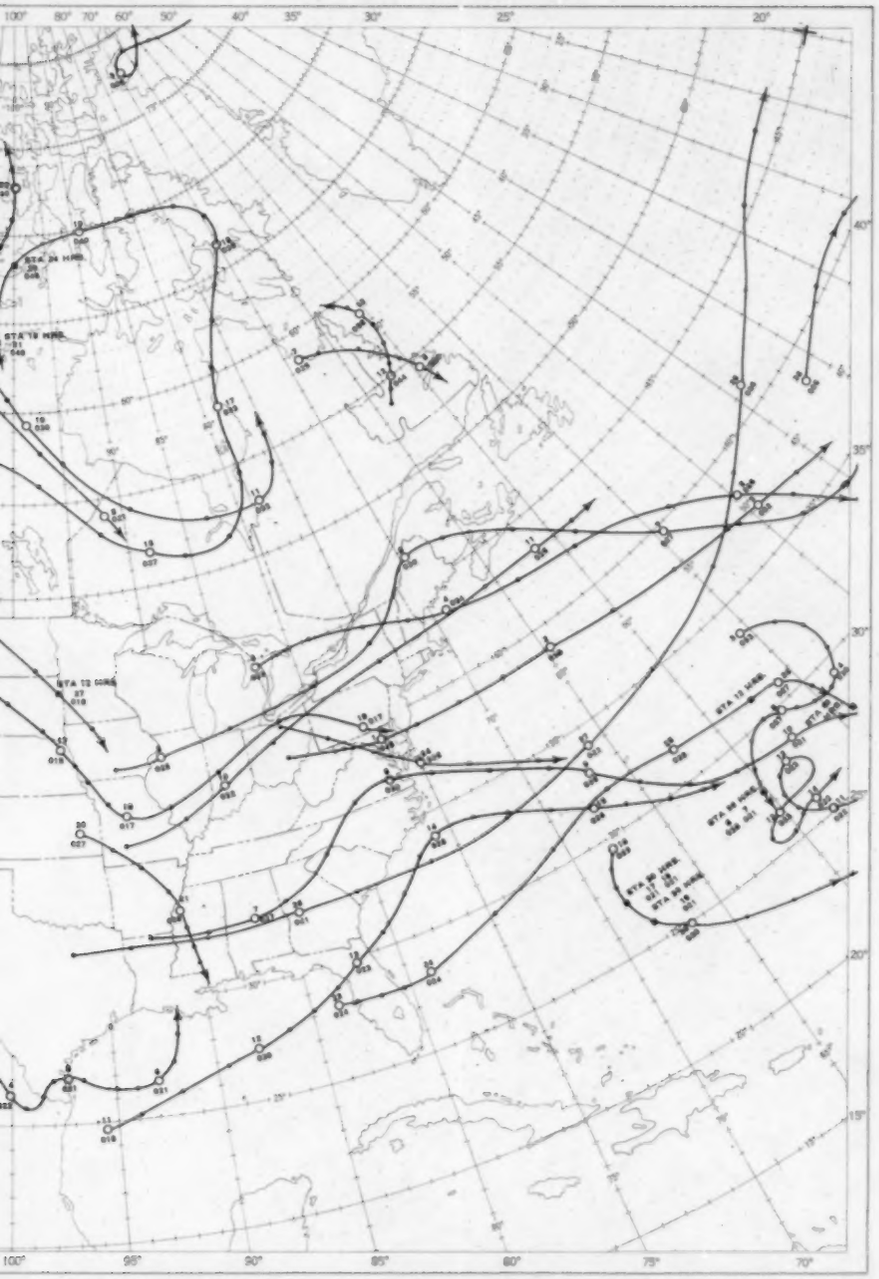

...bove circle indicates date, figure below, pressure to nearest millibar.
...osition of stationary center for period shown. Dashed line in track
...s which could be identified for 24 hours or more are included.

Chart X. Tracks of Centers of Cyclones at Sea

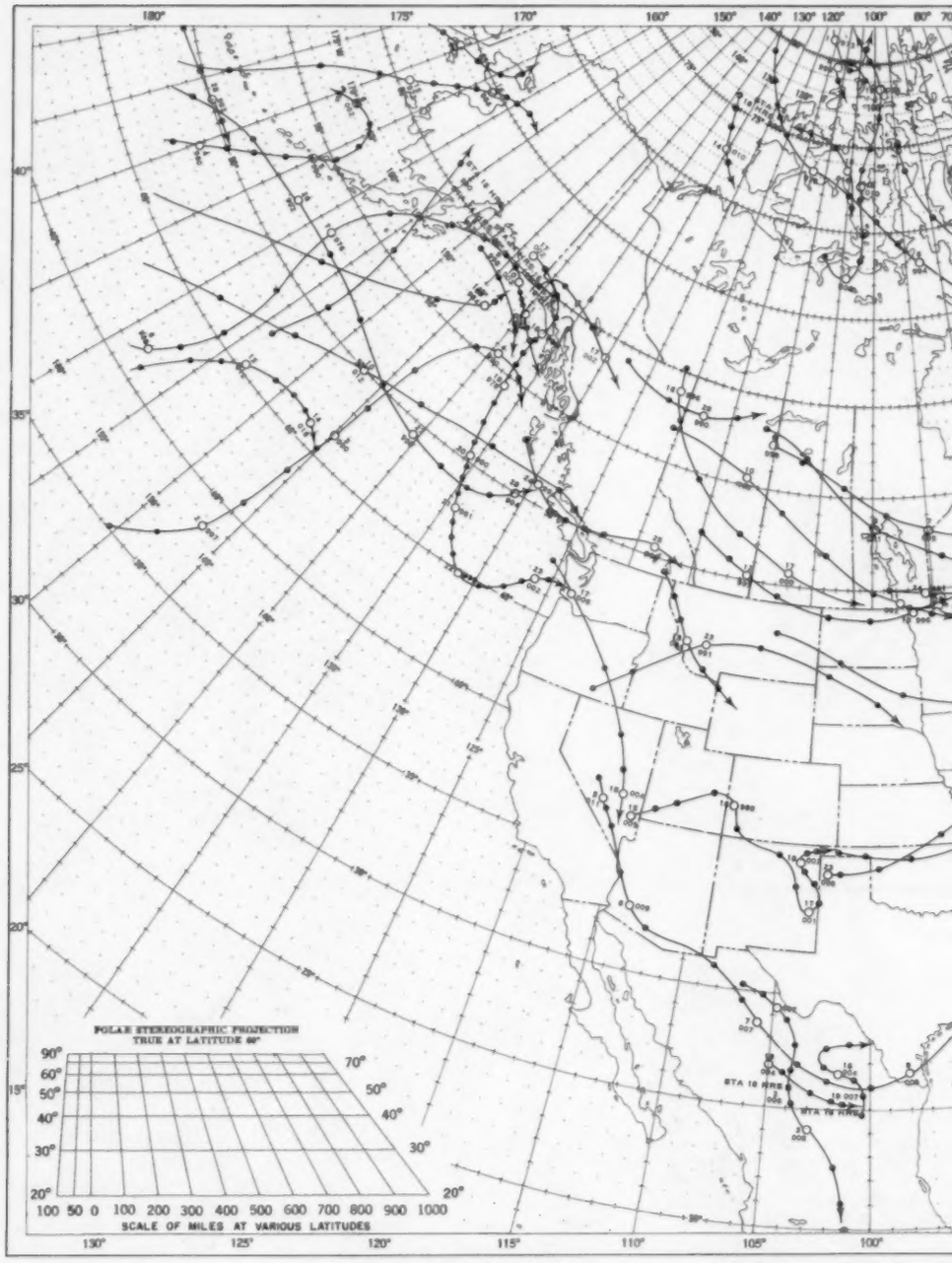
POLAR STEREOGRAPHIC PROJECTION
TRUE AT LATITUDE 60°
90° 60° 50° 40° 30° 20°
70° 50° 40° 30° 20°
100 50 0 100 200 300 400 500 600 700 800 900 1000
SCALE OF MILES AT VARIOUS LATITUDES

Circle indicates position of center at 7:30 a. m. E. S. T. S

at Sea Level, February 1956. (Corrected)

S. T. See Chart IX for explanation of symbols.

Chart IX. Tracks of Centers of Anticyclones at Sea Level, February 1956.

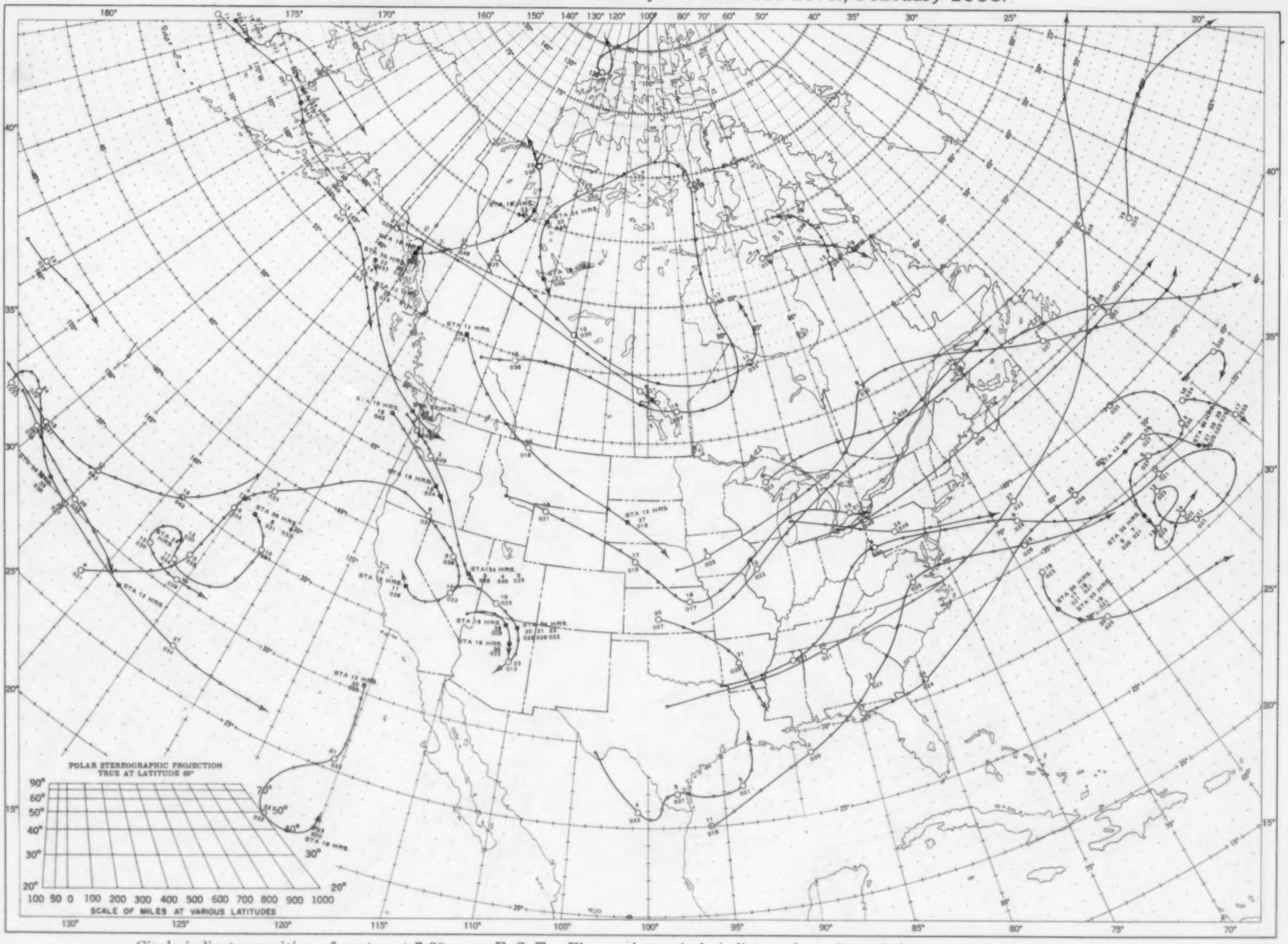
POLAR STEREOGRAPHIC PROJECTION
TRUE AT LATITUDE 60°
90° 60° 50° 40° 30° 20°
100 50 0 100 200 300 400 500 600 700 800 900 1000
SCALE OF MILES AT VARIOUS LATITUDES

Circle indicates position of center at 7:30 a. m. E. S. T. Figure above circle indicates date, figure below, pressure to nearest millibar. Dots indicate intervening 6-hourly positions. Squares indicate position of stationary center for period shown. Dashed line in track indicates reformation at new position. Only those centers which could be identified for 24 hours or more are included.

Chart X. Tracks of Centers of Cyclones at Sea Level, February 1956.

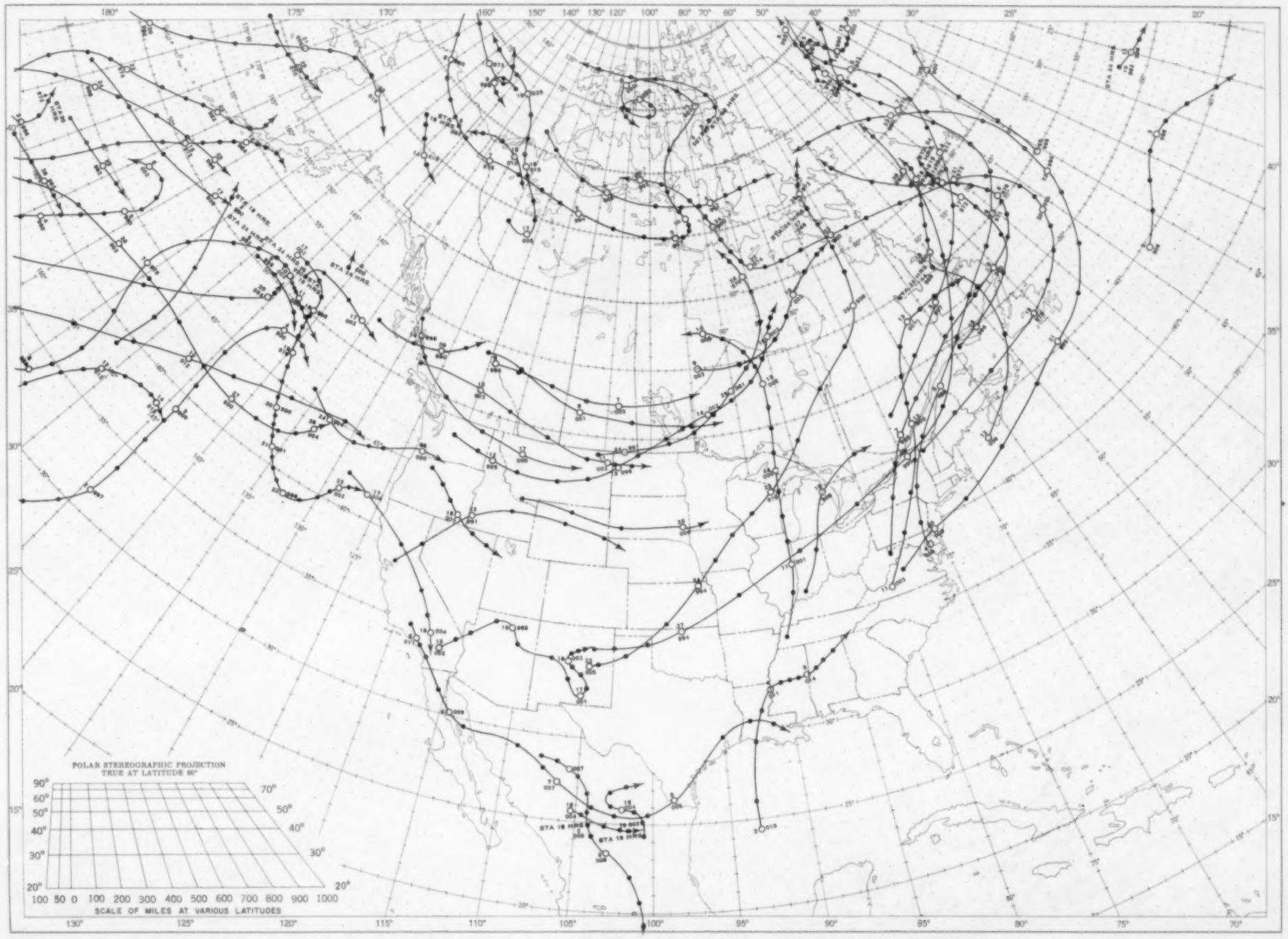
POLAR STEREOGRAPHIC PROJECTION
TRUE AT LATITUDE 60°
SCALE OF MILES AT VARIOUS LATITUDES
100 50 0 100 200 300 400 500 600 700 800 900 1000

Circle indicates position of center at 7:30 a. m. E. S. T. See Chart IX for explanation of symbols.

Chart XI. Average Sea Level Pressure (mb.) and Surface Windroses, February 1956. Inset: Departure of Average Pressure (mb.) from Normal, February 1956.

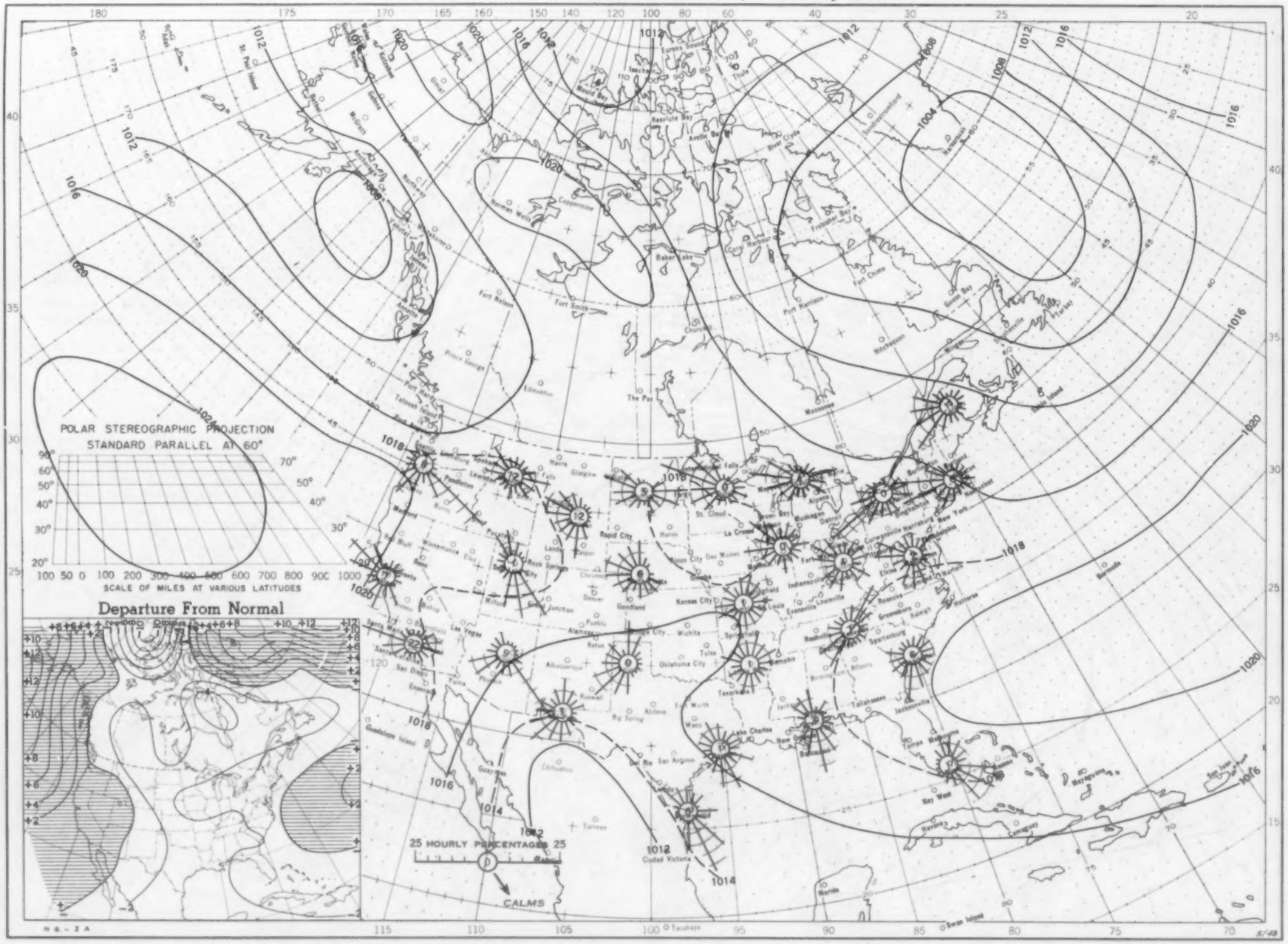

Average sea level pressures are obtained from the averages of the 7:30 a. m. and 7:30 p. m. E. S. T. readings. Windroses show percentage of time wind blew from 16 compass points or was calm during the month. Pressure normals are computed for stations having at least 10 years of record and for 10° intersections in a diamond grid based on readings from the Historical Weather Maps (1899-1939) for the 20 years of most complete data coverage prior to 1940.

Chart XII. Average Dynamic Height in Geopotential Meters (1 g.p.m. = 0.98 dynamic meters) of the 850-mb. Pressure Surface, Average Temperature in °C. at 850 mb., and Resultant Winds at 1500 Meters (m.s.l.), February 1956.

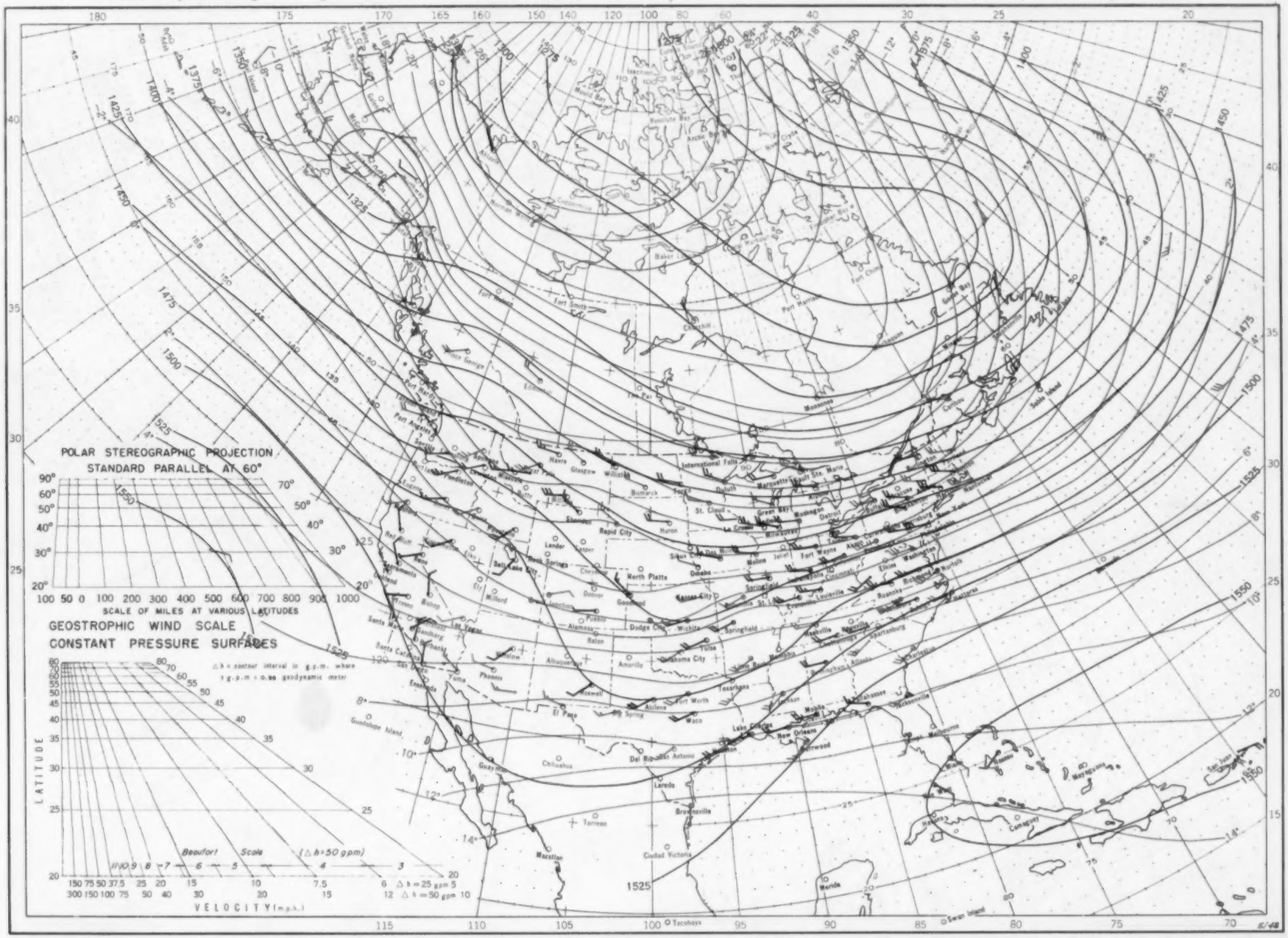

Contour lines and isotherms based on radiosonde observations at 0300 G. M. T. Winds shown in black are based on pilot balloon observations at 2100 G. M. T.; those shown in red are based on rawins taken at 0300 G. M. T. Wind barbs indicate wind speed on the Beaufort scale.

Chart XIII. Average Dynamic Height in Geopotential Meters (1 g.p.m.. = 0.98 dynamic meters) of the 700-mb. Pressure Surface, Average Temperature in °C. at 700 mb., and Resultant Winds at 3000 Meters (m.s.l.), February 1956.

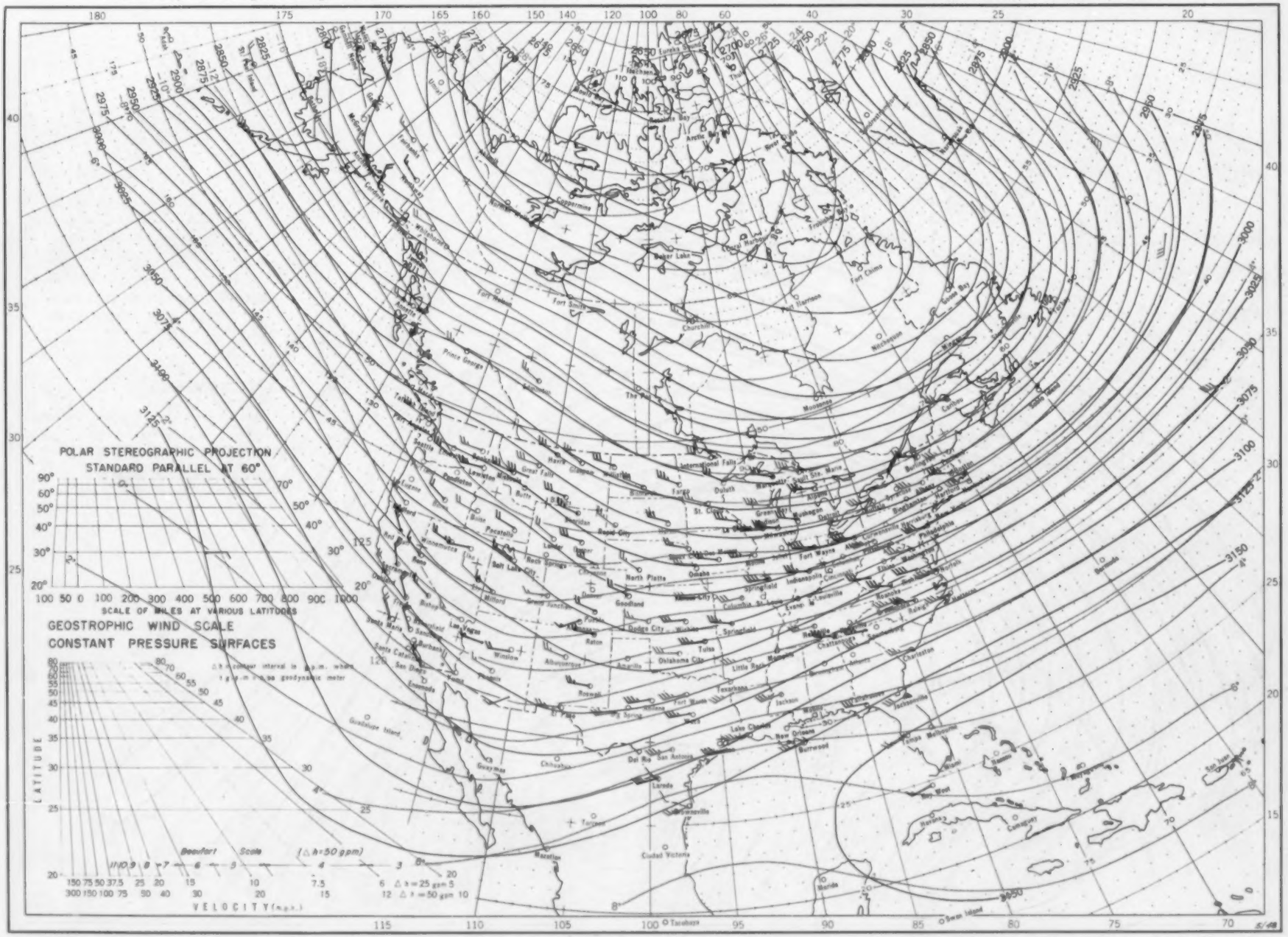

Contour lines and isotherms based on radiosonde observations at 0300 G. M. T. Winds shown in black are based on pilot balloon observations at 2100 G. M. T.; those shown in red are based on rawins taken at 0300 G. M. T. Wind barbs indicate wind speed on the Beaufort scale.

Chart XIV. Average Dynamic Height in Geopotential Meters (1 g.p.m. = 0.98 dynamic meters) of the 500-mb. Pressure Surface, Average Temperature in °C. at 500 mb., and Resultant Winds at 5000 Meters (m.s.l.), February 1956.

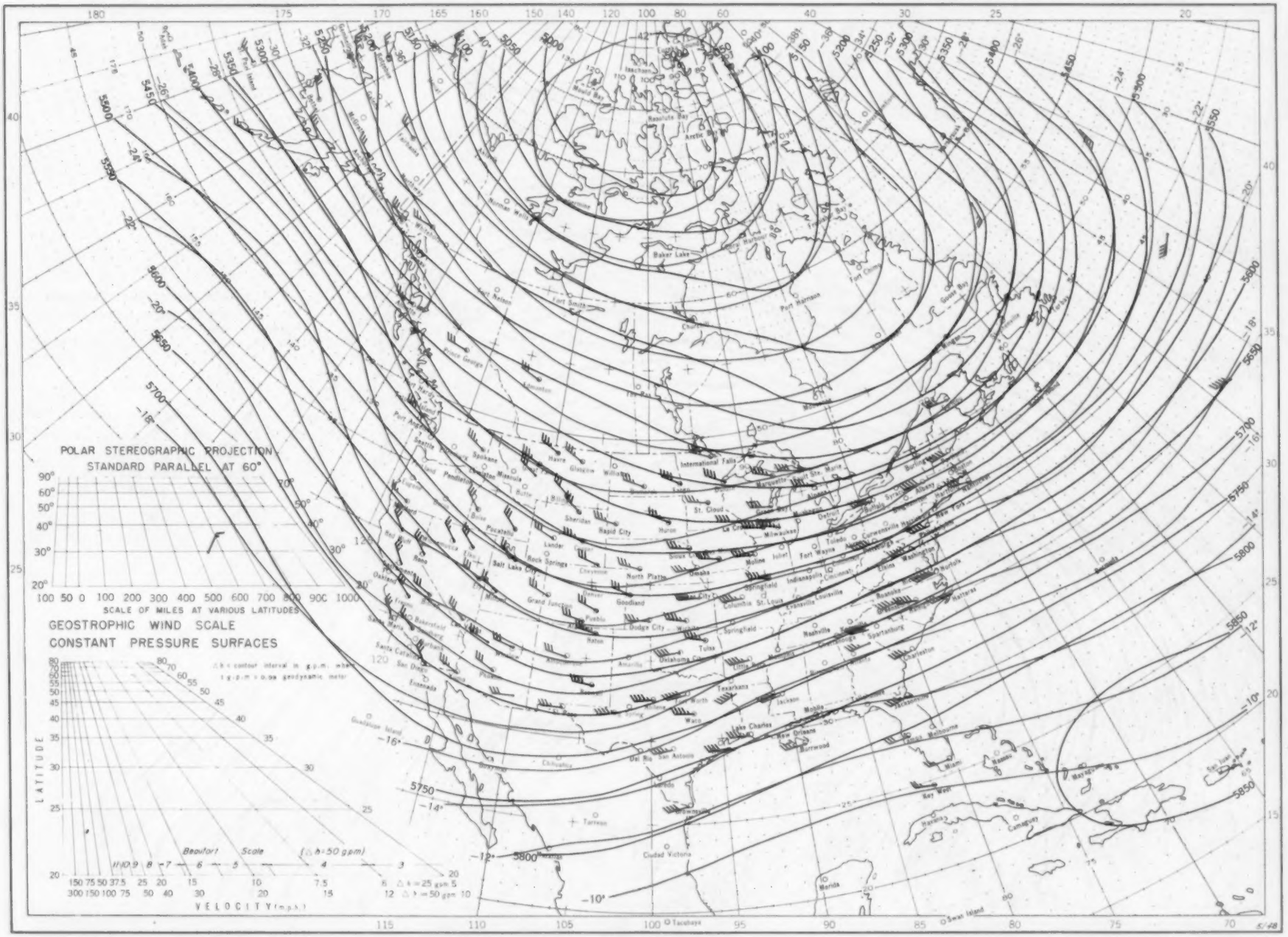

Contour lines and isotherms based on radiosonde observations at 0300 G. M. T. those shown in red are based on rawins at 0300 G. M. T. Winds shown in black are based on pilot balloon observations at 2100 G. M. T.; Wind barbs indicate wind speed on the Beaufort scale.

Chart XV. Average Dynamic Height in Geopotential Meters (1 g.p.m. = 0.98 dynamic meters) of the 300-mb. Pressure Surface, Average Temperature in °C. at 300 mb., and Resultant Winds at 10,000 Meters (m.s.l.), February 1956.

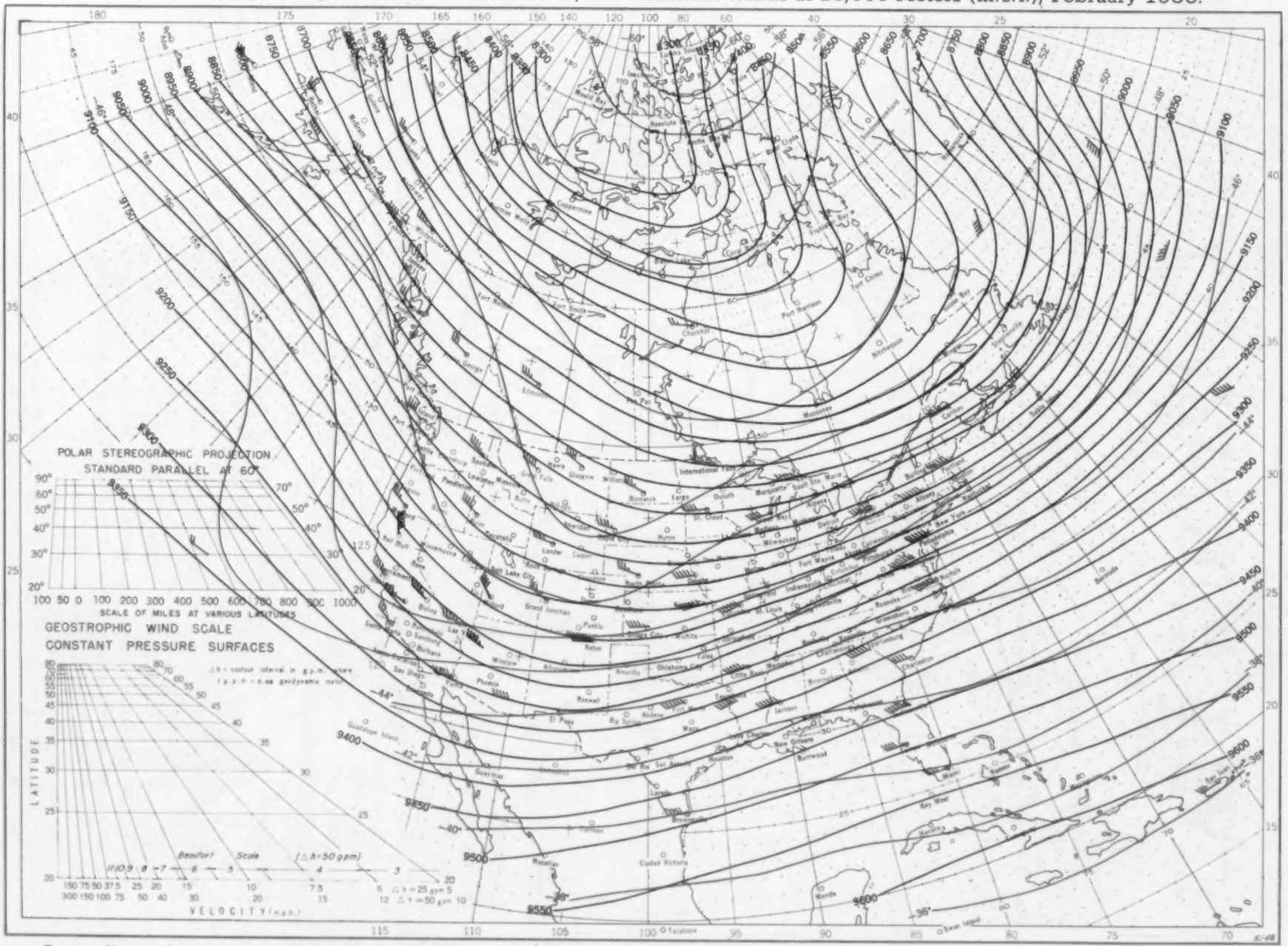

Contour lines and isotherms based on radiosonde observations at 0300 G. M. T. Winds shown in black are based on pilot balloon observations at 2100 G. M. T.; those shown in red are based on rawins at 0300 G. M. T. Wind barbs indicate wind speed on the Beaufort scale.